ISSN 2249-4278

Journal of Advances in Applied Computational Mechanics and Engineering

Volume No. 13

Issue No. 2

May - August 2025

ENRICHED PUBLICATIONS PVT.LTD

JE - 18,Gupta Colony, Khirki Extn,
Malviya Nagar, New Delhi - 110017.
E- Mail: info@enrichedpublication.com
Phone :- +91-8877340707

ISSN 2249-4278

Journal of Advances in Applied Computational Mechanics and Engineering

Aims and Scope

Journal of Advances in Applied Computational Mechanics & Engineering is a research journal, which publishes top-level work from all areas of theoretical and applied mechanics including theoretical, computational, and experimental aspects, as well as theoretical modeling, methods of analysis and instrumentation. It includes basic disciplineoriented areas such as dynamics, continuum mechanics, solid and fluid mechanics, structures, heat transfer, tribology, geomechanics, and biomechanics, as well as inter-disciplinary subjects such as new numerical and computational techniques, systems control technology, engineering design tools, manufacturing technology, materials and energy technology, and environmental engineering.

ISSN 2249-4278

Journal of Advances in Applied Computational Mechanics and Engineering

ISSN 2249-4278

Journal of Advances in Applied Computational Mechanics and Engineering

(Volume No. 13, Issue No. 2, May- August 2025)

Contents

Sr. No.	Articles / Authors Name	Pg. No.
1	Numerical Investigation on Flow-Field Characteristics towards Removal of Free-Water by A Separator with Coalescing Plates *– Xiangdong Qi, Hongqi Zhang2, Xitong Sun and Zhihua Wang*	1 - 22
2	The Electromagnetic Scattering Problem by a Cylindrical Doubly Connected Domain at Oblique Incidence: An Inverse Problem *– Leonidas Mindrinos*	23 - 29
3	A Conformable Inverse Problem with Constant Delay *– Auwalu Sa'idu and Hikmet Koyunbakan*	30 - 42
4	On the G'/G Expansion Method Applied to (2+1)-Dimensional Asymmetric-Nizhnik-Novikov-Veselov Equation *- S.M. Mabrouk and A.S. Rashed*	43 - 54
5	Fuzzy Rough Subgroups on Approximation Space *- Nurettin Bağırmaz*	55 - 60

ISSN 2249-4278

Numerical Investigation on Flow-Field Characteristics towards Removal of Free-Water by A Separator with Coalescing Plates

Xiangdong Qi, Hongqi Zhang, Xitong Sun1, and Zhihua Wang

1Key Laboratory for Enhanced Oil & Gas Recovery of the Ministry of Education, Northeast Petroleum University, Daqing 163318, China

2Oil Recovery Plant No. 2, PetroChina Daqing Oilfield Company Limited, Daqing 163414, China

3 Jilin Branch of China Aviation Fuel Company Limited, Changchun 130500, China

Abstract:

The produced water-containing polymer brings new challenges to oil-water separation in oilfield production, yet separators with coalescing plates to remove free water have been playing an active role. In this paper, the flow-field characteristics of polymerladen produced water in a separator with coalescing plates are analyzed using computerized mathematical methods to investigate the effects with a water content of 55%, 70%, and 85%, flow rate of 3500 m3/d, 4800 m3/d, and 6000 m3/d, and duration time of 20 min, 40 min, and 60 min on flow-field properties and separating efficiency are studied. The results show that the separating efficiency is positively correlated with water content and duration time, and duration time has the greatest improvement to the separating efficiency, but the enhancement of flow rate may reduce the separating efficiency. It is also observed that the separation efficiency of free-water reached 70.9% and the water content at the oil outlet of the separator reached 20.4% at a duration time of 60 min, when the contained polymer concentration and water content in the oil-water mixture are 500 mg/L and 70%, respectively.

1. Introduction

With the intensive exploitation of oilfields, a variety of measures such as water flooding and chemical agents have been widely used, thus crude oil production and economic benefits have been guaranteed [1-3]. Subsequently, the prevalence of impurities such as water, sediment, and polymers are commonly present in the produced water from oil wells, respectively, the transportation and utilization of crude oil are affected and threats to the environment may increase [4-5]. Furthermore, the oil-water interfacial stability is affected by components such as polymer and asphaltene in produced water, which brings new challenges to the treatment of produced water [5-7]. Typically, water and crude oil mixture need to be separated and treated in the oilfield to achieve compliance with refining and commercial requirements [8-10].

The existent form of water in crude oil is not fixed, so the difficulty of separation and treatment will continue to change. Free water is separated from oil in a short time by gravity sedimentation at room temperature, on the contrary, some amount of water will form a stable emulsion with crude oil, which is difficult to separate by gravity sedimentation [11, 12]. In industry, the process of separating free water and then treating oil-water emulsion has been applied on a certain scale [13]. Therefore, efficient separation of free water from emulsion is important.

Although free water is usually separated by gravity, there are differences in specific treatment equipment and methods [12-14]. At the same time, the separation effect will also change significantly. For example, wang et al. [15] simulated a separator with a bi-directional corrugated plate structure, which can obtain higher separating efficiency when the oil concentration is 30% to 60% and the flow rate of the inlet is 13 L/min ~ 133 L/min. Moreover, lower oil concentrations allow the selection of larger inlet flow rates within the appropriate range. Almarouf et al. [16] arranged a series of inclined multi-arc coalescing plates in the oil-water separator and proposed that the geometrical characteristics of the separator govern the separation effect between oil and water. Under the conditions of longer duration time and higher water content, the separation effect between oil and water will be enhanced, and the processing temperature and degree of oil shedding are linear. Kim et al. [17] simulated the influence of mesh size on the separation of an oil-water mixture under different pressure gradients, and the narrow pores can improve interfacial resistance and viscous dissipation, which help prevent oil infiltration by consuming oil inertia. From the point of coalescence and breakup of droplets, Yuan et al. [18] considered that droplets with smaller surface tension are suitable for lower separation speed, and separating efficiency can be enhanced by controlling the shape and spacing of wave plates, on the contrary, the speed of droplets with larger surface tension is a convenient way to increase the separating efficiency. Oruç et al. [19] experimentally studied the separating of mixtures at different temperatures, taking into account the corrugated plate spacing, shape, and angle, and obtained the highest value of separating efficiency. Yayla et al. [20, 21] investigated the influence of the Reynolds Number and the configuration of the coalescing plate on the oil-water separation. They found that the Reynolds Number of the oil-water mixture was inversely related to the separating efficiency. When the hole shape of the coalescing plate is elliptical and rectangular, the size of the hole does not affect separating efficiency. Moreover, when the distance of the coalescing plate is 12 mm and the Reynolds Number is 18, the separating efficiency is the highest for a cylinder with an aperture of 15 mm. In general, the various methods of removal of free water have the same goal, that is, by creating good conditions, oil and water rely on density difference and by the gravity to separate, and liquid separation plate and coalescing plate plays an irreplaceable role in this segment.

However, the properties of produced water are constantly changing when the polymer continues to exist, and the adaptability of the traditional separator to an oil-water mixture containing polymer is reduced, thus the separation effect of free-water has not reached the expected goal [13, 14, 22]. On the other hand, the separator with coalescing plates is widely used as the free-water separation equipment in oilfields, and the separation effect of oil-water mixtures containing polymers also lacks systematic evaluation.

Therefore, the suitability of oil-water mixtures containing polymers in separators with coalescing plates should be understood. The flow-field characteristics of the separation are concentrated reflections of the removal effect of free water, which is also inevitably affected by factors such as water content, flow rate, and duration time. Meanwhile, the separation effect of an oil-water mixture containing polymer in the separator provides a reference for the optimization of the separator structure.

In this paper, a Φ3600 mm×16000 mm separator with coalescing plates is built for mathematical simulation. The EULERIAN model and RNG k-ε model are applied to simulate the flow-field characteristics in the separator, and the role of steady flow and coalescence unit is shown. The separation of free water with the effect of water content, flow rate, and duration time of oil-water mixture containing polymer is studied by combining qualitative and quantitative methods. The flow-field change of the separator is further discussed by detecting the pressure field, flow field, and oil phase concentration distribution, furthermore, the oil-water separation effect is also evaluated.

2. Methodology

2.1. Modeling of Separator with Coalescing Plates

In the process of oil-water separation in Daqing Oilfield (China), a horizontal settling separator is mainly used to separate free water, and its model is Φ 3600 mm×16000 mm separator with coalescing plates, which has been widely used. Therefore, a physical model with an equal proportion to the separator is established.

The separation of oil and water depends on the steady flow unit and coalescence unit in the separator. As shown in Fig. (1a), the liquid separation plate is used as a steady flow unit, and the coalescing plate is used as a coalescence unit. The goal of oil-water separation can be achieved through these units. This is because the flow field becomes stable within the unit area, the oil droplets rise upward and the water phase settles downward.

Therefore, during the numerical simulation, the structure of the separator is reasonably simplified, the auxiliary components such as the oil tank and the base inside the separator are omitted, and the components such as the manhole and safety valve group outside the separator are not considered. As shown in Fig. (1b), a simplified physical model of the separator is constructed, and the coalescing plate is arranged horizontally. The main structural dimensions of the separator can be obtained from Table 1.

Table 1: Structure size data of separator with coalescing plates.

Structural Parameters	Size	Structural Parameters	Size
Total volume of separator (m^3)	160	Oil phase outlet diameter (mm)	300
Length of elliptical heads at both ends of separator(mm)	500	Water phase outlet diameter (mm)	300
Total length of separator (mm)	16000	Distance from inlet to liquid separation plate (mm)	2100
Inlet diameter (mm)	300	Distance from inlet to the center of coalescing plate (mm)	9100
Length of coalescing plate (mm)	8000	Coalescing plate spacing (mm)	150
Thickness of liquid separation plate (mm)	20	Thickness of coalescing plate (mm)	20
Hole diameter of liquid separation plate (mm)	230	Opening ratio of liquid separation plate (%)	15

In the process of removing free water by using the separator, the oil-water mixture enters the inside of the separator in a tangential direction through the inlet, and the initial steady flow is realized by the liquid separation plate and then enters the coalescence unit. At this time, the lower density of the oil makes it rise and coalesce to the bottom surface of the coalescing plate, in turn, the higher density of the water makes it settle to the upper surface of the coalescing plate. The liquid in the coalescing plate will be continuously promoted from the entrance. Subsequently, the oil flows out from the oil outlet at the upper right end, and water flows out from the water outlet at the lower right end, and the separation of free water is realized.

2.2. Mathematical Model for Simulation of Coalescence-Separation

Before selecting the mathematical model, the temperature and pressure characteristics of the free-water separator are considered, and the energy exchange can be neglected.

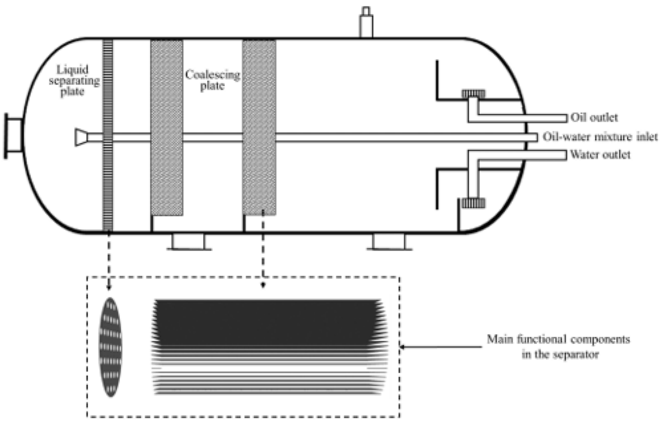

(a) Structure diagram of separator

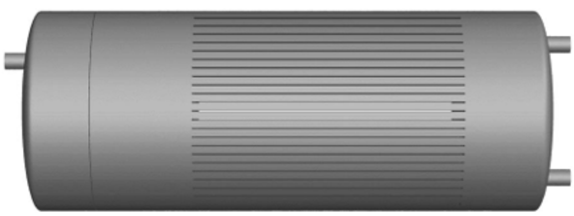

(b) Simplified physical model of separator

Figure 1: Main structure and modeling of Φ3600 mm×16000 mm separator with coalescing plates.

Continuity equation [23, 24]:

$$\frac{\partial(\rho u_x)}{\partial x} + \frac{\partial(\rho u_y)}{\partial y} + \frac{\partial(\rho u_z)}{\partial z} + \frac{\partial \rho}{\partial t} = 0 \tag{1}$$

Momentum equation [25, 26]:

$$\begin{cases} \dfrac{\partial(\rho_m v_m)}{\partial t} + \nabla\,(\rho_m v_m v_m) = [\mu_m(\nabla v_m + \nabla_v^T)] + \nabla\,(\sum_{j=1}^{2} \alpha_j \rho_j v_{dr,j}^2) + \rho_m g + F - \nabla p \\ v_{dr,j} = v_j - v_m \\ \mu_m = \sum_{j=1}^{n} \alpha_j \mu_j \\ \nabla p = \dfrac{\partial p}{\partial x} + \dfrac{\partial p}{\partial y} + \dfrac{\partial p}{\partial z} \end{cases} \tag{2}$$

where $\rho_m$is the density of the oil-water mixture, kg/m^3; v_m is the mass average velocity of the oil-water mixture, m/s; μ_m is the dynamic viscosity of the mixture, Pa·s; α_j is the volume fraction of phase *j*, %; ρ_j is the density of phase j, kg/m^3; $v_{dr,j}$ is the drift velocity of phase j, m/s; F is the external force, N; v_j is the mass velocity of phase j, m/s; μ_j is the dynamic viscosity of phase j, Pa·s ; *p* is the pressure shared by all phases, Pa.

The equation for the volume fraction of the oil phase can be derived from the continuity equation as follows:

$$\frac{\partial(\alpha_k \rho_k)}{\partial t} + \nabla\,(\alpha_k \rho_k v_m) + \nabla(\alpha_k \rho_k v_{dr,k}) = 0 \tag{3}$$

Where $v_{dr,k}$is the drift velocity of phase *k*, m/s; α_k is the volume fraction of phase *k*, %; ρ_k is the density of phase *k*, kg/m^3."

In the simulation of oil-water separating, the flow pattern of the oil-water mixture in the separator should be determined before simulation. The identification of the flow pattern can be quantitatively distinguished by the Reynolds Number. Laminar flow has a small Reynolds Number and high viscous forces in the flow field. In contrast, the turbulent flow has a large Reynolds Number, high inertial forces in the flow field, an extremely unstable flow state, and a relatively disordered flow field [27, 28].

Reynolds Number can determine the flow state of the oil-water mixture in the separator, which can be obtained from Eq. (4) [25, 29].

$$Re = \frac{\rho_m v d_c}{\mu} \tag{4}$$

Where $Re$is the Reynolds Number of the oil-water mixture in the separator; ρ_m is the density of the mixture, kg/m^3; v is the average velocity of the mixture in the separator, m/s; d_c is the equivalent diameter of separator, mm; μ is the dynamic viscosity of mixture in the separator, Pa·s.

The density of the oil-water mixture can be calculated according to Eq. (5).

$$\rho_m = \rho_o(1-\psi) + \rho_w \psi \tag{5}$$

Where $\rho_o$is the density of oil, kg/m^3; ρ_w is the density of water, kg/m^3; ψ is the water content of the mixture, %.

The basic structural characteristics of separators with coalescing plates are considered. Reynolds Number is calculated by Eq. (4) and (5), then the flow pattern is identified. After the analysis and calculation of the working conditions of a treatment station in an oilfield, the free-water separation process is defined as a turbulent flow pattern. Therefore, the widely used and applicable RNG *k*-*ε* model is used for simulation [30, 31].

Moreover, oil and water phase volume fractions are extracted to quantitatively characterize the oil-water separation effect after the calculation runs stably, and the free-water separation efficiency of the oil-water mixture in the separator can be calculated according to Eq. (6).

$$\eta = \frac{\varphi_1 - \varphi_2}{\varphi_1} \tag{6}$$

where $\eta$is the separation efficiency of free-water, %; φ_1 is water phase volume fraction at the inlet, %; φ_2 is water phase volume fraction at the oil outlet, %.

2.3. Solving Process

Based on the established physical model of the separator, the finite volume method is used to solve it, dividing the calculation area of the physical model into non-repeating control volumes (grids), integrating the conservationtype differential equations to be solved in any control volume and a certain time interval over space and time, and specifically completing the application of the algorithm in the model by the commercial software FLUENT.

The grid type is generally divided into structured grid and unstructured grid. Among them, the unstructured grid has good adaptability to complex models [32]. Fluent Meshing is used to generate an unstructured grid after the structure of the separator is considered. Since the liquid separation plate and the coalescing plate are the main implementation areas of the separation function, they are reasonably encrypted. In addition, grid independence verification is accomplished by encrypting the number of grids in the computational domain, and the separator outlet velocity variation is observed at different grid numbers. The relative error of the simulation results decreases with increasing the number of grids, and the grid convergence can be considered when the error is lower than 5%, and finally, the physical model with the grid number 5086345 is used for the formal simulation calculation, and the meshing of the separator is shown in Fig. (2).

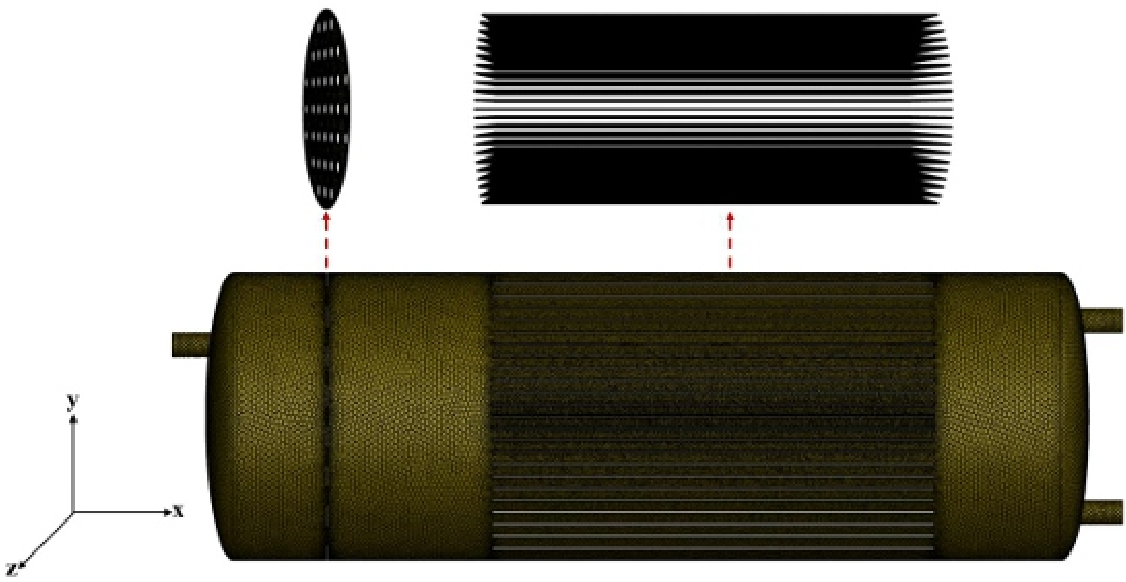

Figure 2: Meshing of Φ3600 mm×16000 mm separator with coalescing plates.

In the FLUENT software, the wall is set to a static state by considering the influence of the viscosity of the wall of the separator. After a given inlet velocity, the outlet boundary of both water and oil is set to

"Outflow". Similarly, the steady flow unit and coalescence unit play an important role. For a clearer understanding of the separation effect and obtaining the separation flow-field characteristics inside the separator, the mixture composed of oil and water is considered to be incompressible fluids in the simulation process. The temperature inside the separator has been kept constant so that heat exchange has been ignored.

The parameters selected for the simulation calculations are determined according to the physical properties of the oil-water mixture in the Daqing oilfield, as shown in Table 2. Due to the mutual motion between the oil and water phases, a non-constant calculation of the simulation process is chosen for "Phase Coupled Simple" [33].

Table 2: Basic calculation parameters of oil - water separation simulation.

Calculation Parameters	Value
Concentration of polymer in oil-water mixture (mg/L)	500
Water phase density (kg/m^3)	1000
Oil phase density (kg/m^3)	845
Oil phase viscosity (mPa·s)	56
Oil-water interfacial tension (N/m)	0.03
Separation temperature (°C)	38
Initial height of oil-water interface (m)	2.5
Contact angle of upper surface of coalescing plate (°)	20
Contact angle of lower surface of coalescing plate (°)	150

3. Results and Discussion

In the operation of a separator, the separation flow field characteristics can be represented by pressure, velocity, streamline, and volume fraction of the phase [15, 17, 21]. Thus, the distribution characteristics of the pressure field, velocity field, and concentration field, as well as the streamlined distribution characteristics inside the separator are observed and analyzed, and the oil-water separation effect of the separator is evaluated. Furthermore, the water content and flow rate are selected based on the nature of the oil-water mixture provided by Daqing Oilfield, while the duration time of the oil-water mixture in the separator is determined by actual process experience. For better quantitative analysis, pressure, and oil phase volume distributions are observed on the separator z=0 profile, and correlation data are extracted parallel to the separator profile and every 0.1 m in the Y direction under conditions relative to the outlet boundary.

3.1. Flow-Field Characteristics of the Separator

Oil-water mixture with a water content of 70%, containing a polymer concentration of 500 mg/L, and a flow rate of 4800 m3/d is selected as a case after the physical properties of the produced water are analyzed. The flowfield characteristics of oil-water separation are further revealed by calculation results. The important role of the stability of the working pressure inside the separator on the separation performance is considered, and the distribution of the pressure field in the separator is shown in Fig. (3a). The uniform decrease of the pressure distribution in the separator from bottom to top can be observed, and the maximum pressure difference is about 3.3 kPa, which confirms separator has good operation stability.

As shown in Fig. (3b), velocity vector distribution in the separator is extracted, and the flow-field distribution during the separation process is more intuitively reflected. The oil-water mixture enters the interior from the left inlet of the separator, and the flow field of the separator is impacted by the maximum flow rate. However, the distribution of the flow rate change uniformly after passing through the steady flow of the liquid-separating plate. Meanwhile, the flow field in the separator tends to be stable, and the role of the liquid separation plate as a steady flow unit is demonstrated.

Fig. (3c) shows the streamlined distribution characteristics inside the separator. Similarly, the streamline is the most intuitive manifestation of separation flow-field characteristics during the separation of free water. It can be found that the high flow rate of the inlet brings significant disturbance to the streamline in the inlet area, and the chaotic state of the streamline can be observed. However, the streamline distribution tends to be stable as a whole, after passing through the coalescence area.

The separating effect of the separator is shown in Fig. (3d), and the change in the volume fraction of oil is the main manifestation. The stratification of the oil/water interface inside the separator exists, however, the stratification of the oil and water interface is more chaotic before entering the coalescence area. The stratification of the oil/water interface is transformed into a clear form after passing through the coalescing plate, the higher oil phase volume fraction area is thickened, and the lower oil phase volume fraction area is continuously thinned.

3.2. Effect of Water Content on Flow-Field Characteristics

The interfering factors of the flow-field characteristics and separation effect in the separator are taken as research objectives. Initially, the effect of water content is explored based on flow-field characteristics in the separator, and the control variable method is used, that is, the contained polymer concentration and flow rate of the oil-water mixture remain unchanged. Then, three kinds of oil-water mixture with a water content of 55%, 70%, and 85% are simulated and analyzed after the production, and research data are referred to.

3.2.1. Pressure Field Distribution and Pressure Drop Characteristics

Pressure field distribution in the separator is compared and analyzed in Fig. (4). The pressure field distribution of the mixture under the three kinds of water content is the same during the separation process, respectively, when the contained polymer concentration and flow rate are 500 mg/L and 4800 m3/d. The pressure drop of the cross-section increases slightly, and pressure field distribution in the

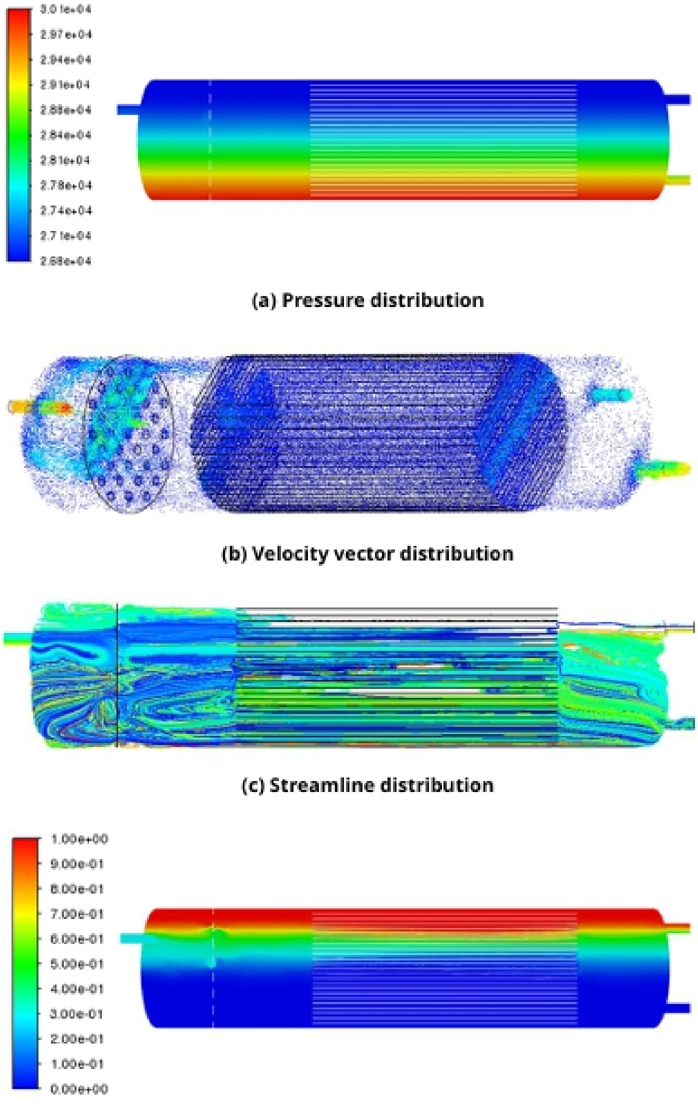

(a) Pressure distribution

(b) Velocity vector distribution

(c) Streamline distribution

(d) Distribution of oil phase volume fraction

Figure 3: Flow-field characteristics in separator with the water content of 70%, the contained polymer concentration of 500 mg/L, and the flow rate of 4800 m^3/d.

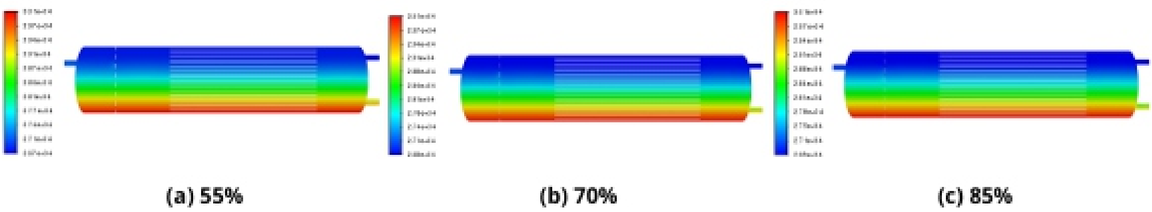

(a) 55% **(b) 70%** **(c) 85%**

Figure 4: Pressure distribution in separator with water content of 55%, 70% and 80%. (z=0)

As shown in Fig. (5), pressure field distribution of the e-separation process is further quantitatively described, and then the characteristic of pressure drop is drawn. The pressure drop changes of the free-water separation process with different water content are similar, and the average increase of pressure

(

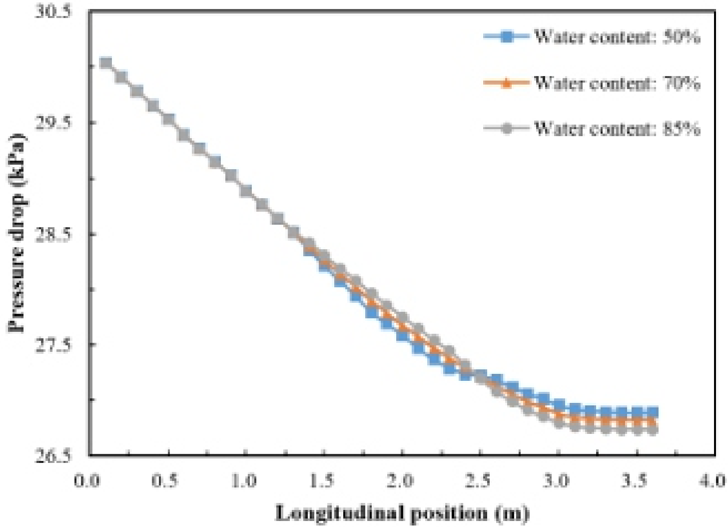

Figure 5: Characteristics of pressure drop in separator with water content of 55%, 70% and 80%.

3.2.2. Streamline Distribution Characteristics

As shown in Fig. (6), the streamlined distribution of an oil-water mixture with three kinds of water content in a separator with coalescing plates is shown. There is a ' gap ' in the streamlining of the oil-water mixture with 55% water content during the separation process, respectively, the stability of the internal flow field of the separator may be reduced. The dispersion performance of the fluid is more significant when the water content increases from 55% to 70% and 85%, and the phenomenon is

(

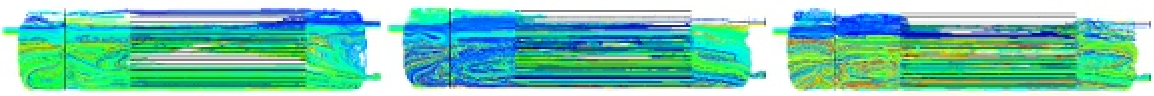

(a) 55% **(b) 70%** **(c) 85%**

Figure 6: Streamline distribution in separator with water content of 55%, 70% and 80%. (z=0).

3.2.3. Oil Phase Concentration Distribution Characteristics

As shown in Fig. (7) and Fig. (8), the oil/water interface characteristics of the mixture with different water contents in the separator are compared and analyzed, and the oil volume fraction is extracted. The oil-water interface stratification changes to fuzzy with the increase in water content. Overall, the distribution of the oil phase volume ratio in the separator is more regular. The maximum and minimum values of the oil phase volume ratio are obtained when the water content is 85% and 55%, respectively, when the longitudinal position is below

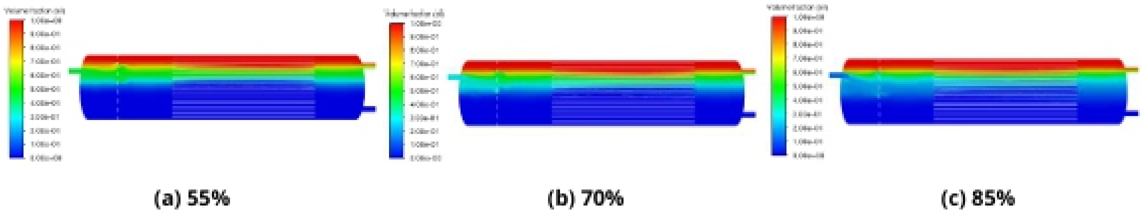

Figure 7: Distribution of oil phase volume fraction in separator with water content of 55%, 70% and 80%. (z=0).

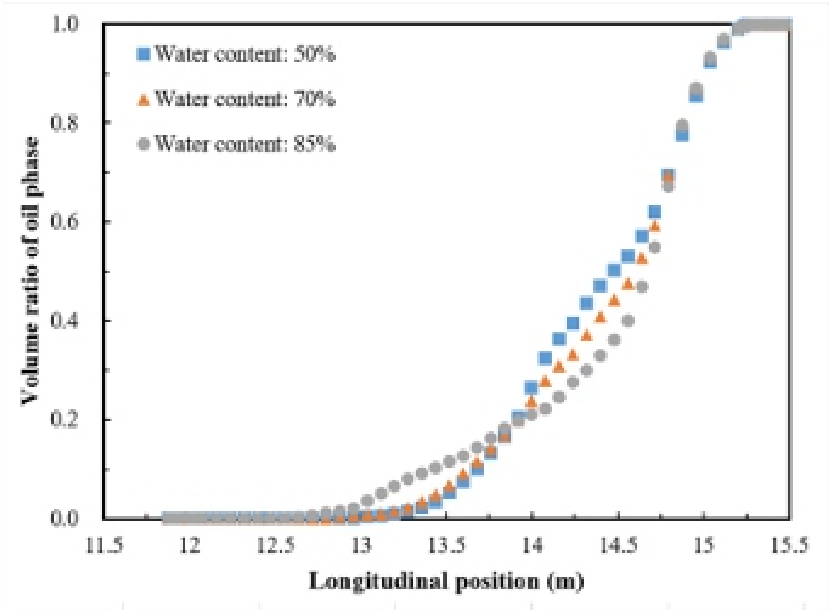

Figure 8: The volume ratio of oil phase in separator with water +content of 55%, 70% and 80%.

2m. On the contrary, the maximum and minimum values of the oil phase volume ratio are obtained when the water content is 55% and 85%, respectively, when the longitudinal position is in the range of 2m and 3m. However, the oil phase volume ratio after separation with a water content of 85% is higher than that with a water content of 55% and 70%, respectively, when the longitudinal position is above 3m.

3.3. Effect of Flow Rate on Flow-Field Characteristics

The effect of flow rate on the flow-field characteristics and separating efficiency is studied, and the pressure field, streamline, and oil phase volume fraction distribution are also analyzed. Similarly, the contained polymer concentration and water content of the mixture are kept at 500 mg/L and 70%, respectively, when flow rates of 3500 m3/d, 4800 m3/d, and 6000 m3/d are simulated and analyzed.

3.3.1. Pressure Field Distribution and Pressure Drop Characteristics

As shown in Fig. (9), the distribution of the pressure field in the separator is extracted with different flow rates. The pressure field in the mixture separating is the same, and the pressure field distribution in the separator is steady, but the pressure drop decreases slightly with the enhancement of the flow rate. Further, pressure field distribution in the separation process of free water affected by flow rate is quantitatively described. The characteristic of pressure drop in the separator is shown in Fig. (10), and pressure drop changes of the three kinds of flow rate are coincident. The steady state of the pressure change characteristics during the operation of a separator with coalescing plates is displayed, and the fluctuation of the flow rate does not bring a significant impact on the pressure field in the separator.

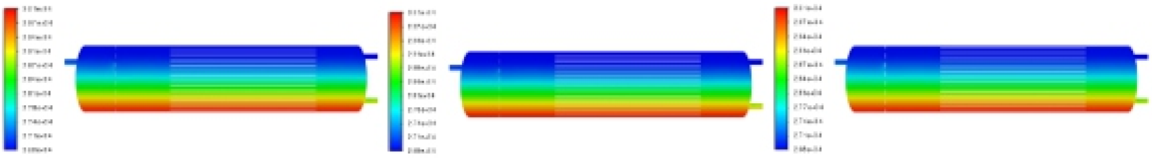

(a) 3500 m^3/d (b) 4800 m^3/d (c) 6000 m^3/d

Figure 9: Pressure distribution in separator with flow rate of 3500 m^3/d, 4800 m^3/d and 6000 m^3/d. (z=0).

3.3.2. Streamline Distribution Characteristics

As shown in Fig. (11), the flow field in the separator is displayed from another perspective, and the streamline in the separator with the flow rate of 3500 m3/d, 4800 m3/d, and 6000 m3/d are analyzed, respectively, when the contained polymer concentration and water content of the oil-water mixture are 500 mg/L and 70%. There are many ' gaps ' between +-the streamlines in the separated flow field when the flow rate is 3500m3/d. The ' gap ' in the separator is filled, and the phenomenon of eddy current begins to appear and developed, respectively, when the flow rate increased from 3500 m3/d to 4800 m3/d and 6000 m3/d. Eventually, it can be observed in Fig. (11c) that the flow field is no longer smooth.

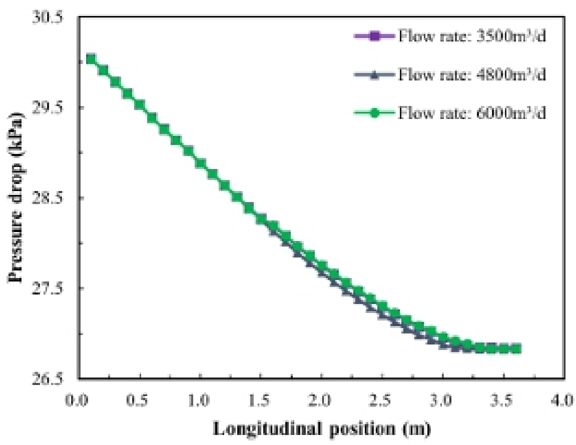

Figure 10: Characteristics of pressure drop in separator with flow rate of 3500 m^3/d, 4800 m^3/d and 6000 m^3/d.

(a) 3500 m^3/d (b) 4800 m^3/d (c) 6000 m^3/d

Figure 11: Streamline distribution in separator with flow rate of 3500 m^3/d, 4800 m^3/d and 6000 m^3/d. (z=0).

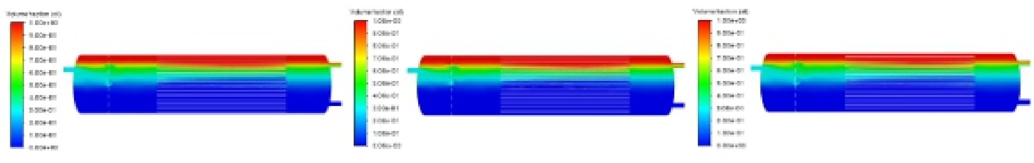

Figure 12: Distribution of oil phase volume fraction in separator with flow rate of 3500 m^3/d, 4800 m^3/d and 6000 m^3/d. (z=0).

3.3.3. Oil Phase Concentration Distribution Characteristics

As shown in Fig. (12), Oil phase concentration distribution in the separator under the effect of different flow rates is obtained, and the oil/water interface state and variation characteristics in the separator are observed. Overall, the oil/water interface in the separator is relatively flat with different flow rates. Higher oil phase concentration distribution gradually becomes thicker, and lower oil phase concentration distribution gradually becomes thinner, respectively, when the flow rate enhances from 3500 m3/d to 4800 m3/d. The difference is that higher oil phase concentration distribution becomes thinner and lower oil phase concentration distribution becomes thicker, respectively, when the flow rate increases from 4800 m3/d to 6000 m3/d, in addition, the change of oil phase concentration distribution is affected by streamlined distribution characteristics is further verified. As shown in Fig. (13), the volume ratio of oil in an e-separator with different flow rates is extracted for quantitative analysis. The volume ratio of oil is the highest for a flow rate is 6000 m3/d, and the smallest for a flow rate is 4800 m3/d, respectively, when the longitudinal position of the separator is below 2.4 m. However, the volume ratio of the oil phase is the highest for a flow rate is 4800 m3/d for the separator longitudinal position above

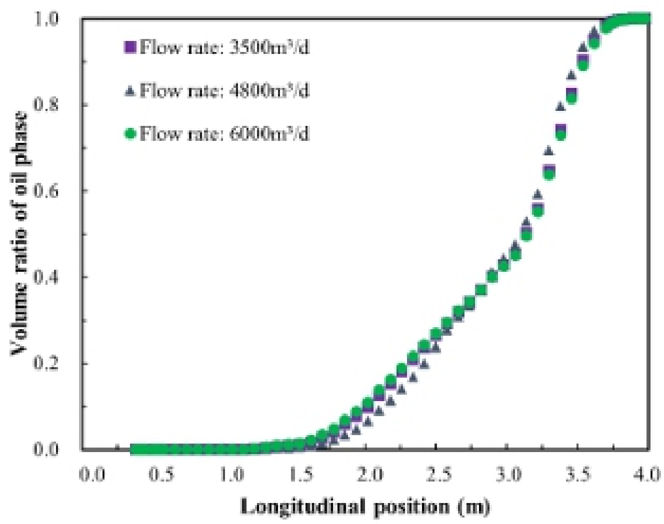

Figure 13: The volume ratio of oil phase in separator with flow rate of 3500 m^3/d, 4800 m^3/d and 6000 m^3/d.

3.4. Effect of Duration Time on Flow-Field Characteristics

Eventually, the influence of duration time on the separation flow-field characteristics and separation effect is studied after understanding the effect of water content and flow rate. The duration time of the oil-water mixture in the separator is changed when the contained polymer concentration and water content of the oil-water mixture are 500 mg/L and 70%. In this study, three kinds of duration time about 20 min, 40 min, and 60 min are simulated and selected.

3.4.1. Pressure Field Distribution and Pressure Drop Characteristics

As shown in Fig. (14), there is a significant difference in the distribution of the pressure field in the separator when the duration time chosen is 20 min, 40 min, and 60 min. The pressure drop in the separator increases with the extension of the duration time, and pressure loss is reduced, which may be due to the reduction of the flow rate in unit time, and the longer duration time makes the pressure drop in the separator increase.

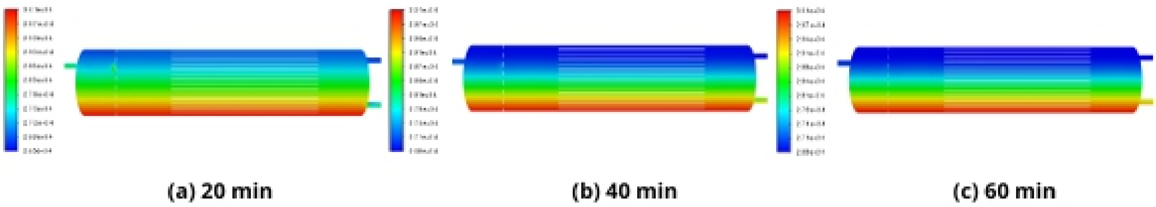

Figure 14: Pressure distribution in separator with duration time of 20 min, 40 min and 60 min. (z=0).

As shown in Fig. (15), the pressure field distribution of the free-water separating process in the separator is quantitatively described by the pressure drop characteristic. The pressure drop increases significantly after 60 min duration time, respectively, when the vertical position of the separator is above 1m and compared with other duration times, and the consistency of pressure distribution and pressure drop characteristics is confirmed.

3.4.2. Streamline Distribution Characteristics

As shown in Fig. (16), the streamlined characteristics of the oil-water mixture in a separator with coalescing plates are similar, respectively, when the duration time is 20 min, 40 min, and 60 min. However, there are obvious phenomena of ' eddy current 'in many places in the separator, when the duration time is 20 min. In Fig. (16c), the phenomenon of ' eddy current ' is greatly reduced, and the stability of the separation flow field is continuously improved for a duration time of 60 min. The separation effect of free water can be improved with an extension of duration time.

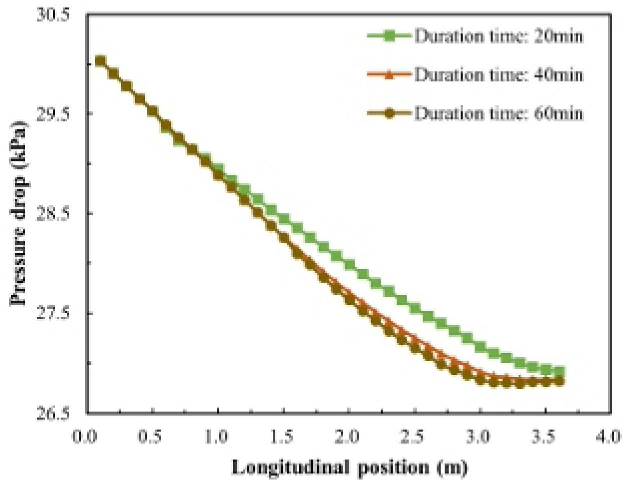

Figure 15: Characteristics of pressure drop in separator with duration time of 20 min, 40 min and 60 min.

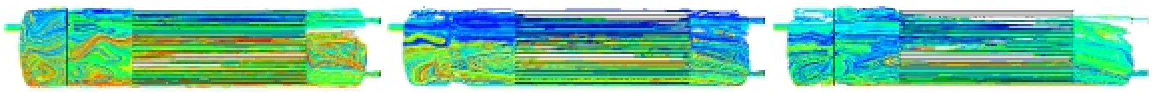

(a) 20 min (b) 40 min (c) 60 min

Figure 16: Streamline distribution in separator with duration time of 20 min, 40 min and 60 min. (z=0)

3.4.3. Oil Phase Concentration Distribution Characteristics

As shown in Fig. (17), there are obvious differences in the distribution of oil phase volume in the separator with the influence of duration time. The oil/water interface in Fig. (17a) is irregular when the duration time is 20 min. After the duration time is extended, the oil/water interface changes from chaos to clarity, and the stratification becomes more and more obvious, respectively, and the concentration distribution areas of higher and lower oil phases become thicker and thinner.

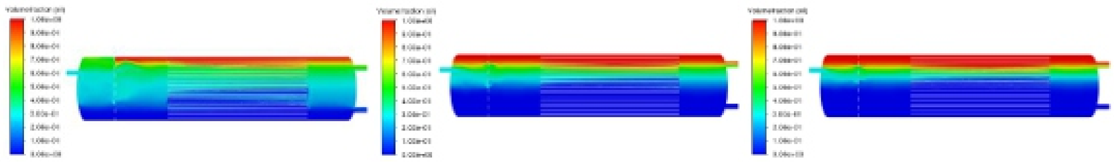

(a) 20 min (b) 40 min (c) 60 min

Figure 17: Distribution of oil phase volume fraction in separator with duration time of 20 min, 40 min and 60 min. (z=0).

As shown in Fig. (18), the oil phase volume proportion in the separator with a duration time of 40 min and 60 min is relatively regular. The proportion with a duration time of 40 min is higher than that with a duration time of 60 min for a vertical position of the separator is below 2.4 m. On the contrary, the volume fraction is the highest when the duration time is 60 min for the area with a longitudinal position of more than 2.4 m. In contrast, the volume proportion in the upper half and lower half of the separator is low and high, respectively, when the duration time is 20 min. It is further proved that extending the duration time can promote the effect of oil and water separation.

3.5. Oil-Water Separation Performance

Oil-water separation is the ultimate goal of the separator, and the quality of the oil phase in the oil outlet should be guaranteed. The water content in oil should be lower than the specified value of the process flow and the water content of the oil outlet should not exceed 30% [22, 34]. Therefore, the effects of water content, flow rate, and duration time on the separation of free water by a separator with coalescing plates are quantitatively characterized, respectively, and the volume fractions of oil and water are extracted. As shown in Fig. (19), the separating performance is mainly reflected by the water content of the oil outlet and the removal rate of free water, and the oil-water separation effect under different water content, flow rate, and duration time is compared and analyzed.

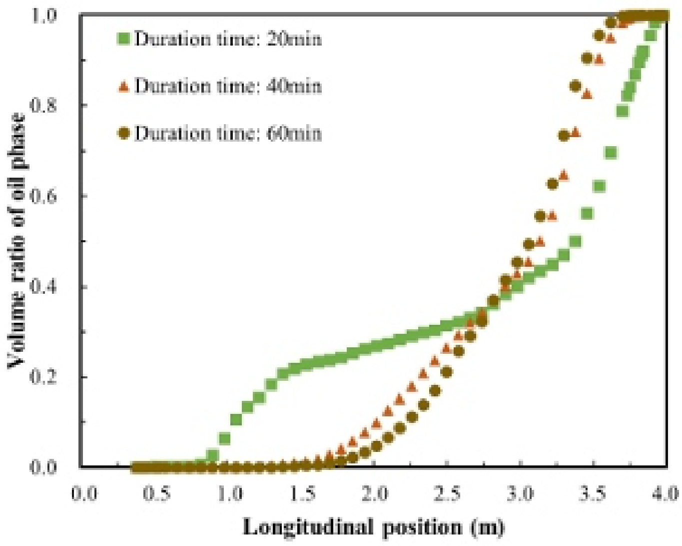

Figure 18: The volume ratio of oil phase in separator with duration time of 20 min, 40 min and 60 min.

As shown in Fig. (19a), the water content of the oil outlet increases when the water content of the mixture in the separator increases, respectively, the contained polymer concentration and flow rate are 500 mg/L and 4800 m3/d. However, the rise in water content in oil outlets is not significant, although water content has always met the technical requirements of 30%. The water content of the oil outlet decreases when the flow rate increases from 3500 m3/d to 4800 m3/d, and the water content of the oil outlet increase when the flow rate continues to increase to 6000 m3/d, respectively, when the contained polymer concentration and water content of 500 mg/L and 70%. In the separation simulation of a mixture with 30% oil content, the water content of the oil outlet also decreases first and then increases after changing the inlet flow rate, which is consistent with the simulation of this paper [15]. Although the water content of the oil outlet is lower than the technical index of 30% required by the process, the irregularity of the water content of the oil outlet cannot be ignored, and separating performance should be evaluated in combination with the removal effect of free water. The water content at the oil outlet decreases from 45.4% to 20.4% when the duration time is extended from 20min to 60min, respectively, when the contained polymer concentration and water content of 500 mg/L and 70%. The increase in duration time not only makes the water content of the oil outlet meet the requirements for dehydration, but also significantly improves the oil phase concentration of the oil outlet, and the important role of duration time is further demonstrated. The result is consistent with the description of flow-field and oil phase volume fraction distribution.

The volume fraction of water and oil extracted after the calculation is stable, and the separation efficiency of free water in the separator is calculated by Eq. (6), and the separating effect is further quantitatively characterized. As shown in Fig. (19b), the separation efficiency of free-water increased from 54.7% to 68.8% with the water content in the oil-water mixture increased, respectively, when the contained polymer concentration and flow rate are 500 mg/L and 4800 m3/d, but the increasing rate is decreased with the water content in the mixture increases. The separation efficiency of free water increased from 58.7% to 65.3% when the flow rate increased from 3500 m3/d to 4800 m3/d, respectively, when the contained polymer concentration and flow rate are 500 mg/L and 4800 m3/d. The separation efficiency of free water decreased from 65.3% to 58.9% when the flow rate continued to increase to 6000 m3/d. The separation efficiency is consistent with the qualitative description of flow-field and oil phase concentration distribution. The separating efficiency of free water increased from 35.1% to 70.9% when the duration time is extended from 20 min to 60 min, respectively, when the contained polymer concentration and flow rate are 500 mg/L and 4800 m3/d. The separation efficiency of free water and the water content of the oil outlet confirm the important effect of duration time on oil-water separation.

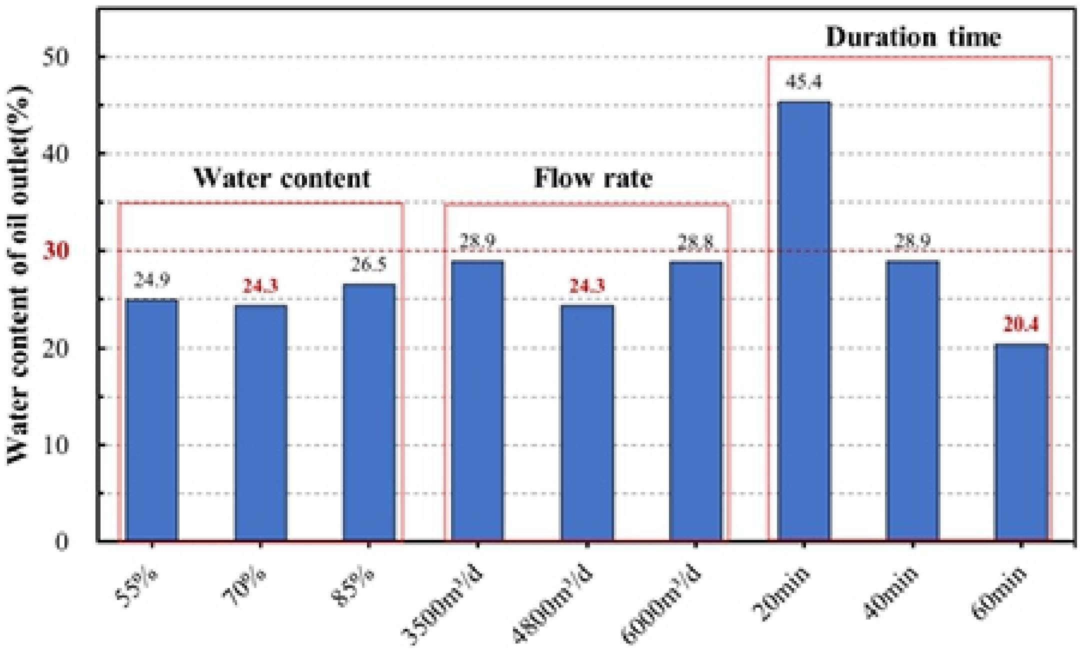

(a) Water content of oil outlet with different water content, flow rate and duration time.

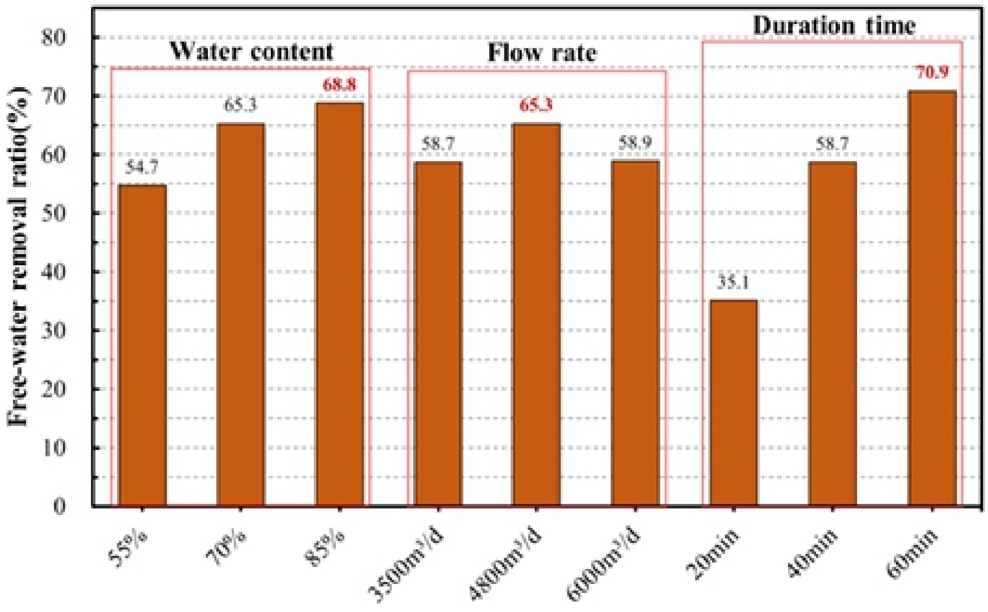

(b) Free-water removal ratio with different water content, flow rate and duration time.

Figure 19: Oil-water separation effect with different water content, flow rate and duration time.

The research of Almarouf et al. [16] and Yayla et al. [21] is consistent with the numerical simulated results in this paper. The separating efficiency of free water is positively correlated with the water content and duration time of the oil-water mixture, respectively, when the characteristics of the mixture and the specifications of the separator are similar.

4. Conclusion

The pressure, flow rate, and streamlined distribution of the oil-water mixture in a separator with coalescing plates reflect the important role of the steady flow and coalescence unit in building a stable flow field. The variation of oil phase volume fraction further confirms the oil-water separation performance of a separator with coalescing plates. In the separator, the separation efficiency of free water is positively correlated with the water content and duration time, and the effect of duration time was greater than that of water content and flow rate. When the duration time was 60 min, the water content at the oil outlet decreased to 20% and the separation efficiency of free water increased by about 71%. However, as the flow rate increased, the free-water separation efficiency first increased and then decreased. When the contained polymer concentration in the oil-water mixture is 500 mg/L and the water content is 70%, the flow rate of the free-water separation process should be no higher than 6000 m3/d.

Using mathematical methods to observe the flow-field characteristics of the oil-water mixture containing polymer in the separator can reveal the principle of action of a separator with coalescing plates, determine the influencing factors of the oil-water separation efficiency, and then improve the treatment methods and equipment parameters of the actual process to achieve efficient operation of oil-water separation. However, the variations of flow lines and oil phase volume fractions indicate that a separator with coalescing plates is not suitable for treating oil-water mixtures with higher water content. In addition, a separator with coalescing plates needs a suitable flow rate to ensure separation efficiency, which means that the separator with agglomerated plates cannot meet the demand of some high-speed production. Therefore, the structure of the coalescing plate separator can be optimized, and thus the separation efficiency of free water can be improved.

Acknowledgements

The research of this paper was supported by the National Natural Science Foundation of China (Grant No. 52074090; 52174060) and the Key Research & Development Program of Heilongjiang Province (Grant No. JD22A004). The authors also acknowledge the support of the Heilongjiang Touyan Innovation Team Program.

References

1.Yuan S, Wang Q. New progress and prospect of oilfields development technologies in China. Pet Explor Dev. 2018; 45: 698-711. https://doi.org/10.1016/S1876-3804(18)30073-9

2.Chaturvedi KR, Sharma T. Modified smart water flooding for promoting carbon dioxide utilization in shale enriched heterogeneous sandstone under surface conditions for oil recovery and storage prospects. Environ Sci Pollut R. 2022; 29: 41788-803. https://doi.org/10.1007/s11356-022-18851-6

3.Gbadamosi A, Patil S, Kamal MS, Adewunmi AA, Yusuff AS, Agi A, et al. Application of polymers for chemical enhanced oil recovery: a review. Polymers. 2022; 14(7): 1433. https://doi.org/10.3390/polym14071433

4.Tang N, Luo R, Xiao Y, Wanyan Q, Li K XJ, Zhang L, et al. Settlement experiment on insoluble particles in rock salt. Oil Gas Stor Trans. 2020; 39: 1136-41. https://doi.org/10.6047/j.issn.1000-8241.2020.10.008

5.Zhang D, Chen Z, Ren L, Meng X, Gu W. Study on stability of produced water in ASP flooding based on critical micellar theory. Polym Bull. 2022; 79: 179-92. https://doi.org/10.1007/s00289-020-03497-6

6.Xu Y, Wang H, Wang Z, Xu Z, Hong J, Sun W. Microscopic mechanism of asphaltene and resin behavior to the stability of oil-water interface. J North Petrol Univ. 2021; 45: 90-101. https://doi.org/10.3969/j.issn.2095-4107.2021.06.008

7.Wang Z, Xu Y, Gan Y, Han X, Liu W, Xin H. Micromechanism of partially hydrolyzed polyacrylamide molecule agglomeration morphology and its impact on the stability of crude oil−water interfacial film. J Petrol Sci Eng. 2022; 214: 110492. https://doi.org/10.1016/j.petrol.2022.110492

8.Pramadika H, Wastu ARR, Satiyawira B, Rosyidan C, Maulani M, Prima A, et al. Demulsification optimization process on separation of water with heavy oil. AIP Conference Proceedings 23 November 2021; 2363(1): 020029. https://doi.org/10.1063/5.0061527

9.Zhu C, Liu X, Xu Y, Liu W, Wang Z. Determination of boundary temperature and intelligent control scheme for heavy oil field gathering and transportation system. J Pipeline Sci Eng. 2021; 1: 407-18. https://doi.org/10.1016/j.jpse.2021.09.007

10.Xing L, Jiang M, Zhao L, Gao J, Liu L. Design and analysis of de-oiling coalescence hydrocyclone. Sep Sci Technol. 2022; 57: 749-67. https://doi.org/10.1080/01496395.2021.1945102

11.Luo H, Wen J, Lv C, Wang Z. Modeling of viscosity of unstable crude oil–water mixture by characterization of energy consumption and crude oil physical properties. J Petrol Sci Eng. 2022; 212: 110222. https://doi.org/10.1016/j.petrol.2022.110222

12.Mohayeji M, Farsi M, Rahimpour MR, Shariati A. Modeling and operability analysis of water separation from crude oil in an industrial gravitational coalescer. J Taiwan Inst Chem E. 2016; 60: 76-82. https://doi.org/10.1016/j.jtice.2015.10.025

13.Amakiri KT, Canon AR, Molinari M, Angelis-Dimakis A. Review of oilfield produced water treatment technologies. Chemosphere. 2022; 298: 134064. https://doi.org/10.1016/j.chemosphere.2022.134064

14.Han Y, He L, Luo X, Lü Y, Shi K, Chen J, et al. A review of the recent advances in design of corrugated plate packs applied for oil–water separation. J Ind Eng Chem. 2017; 53: 37-50. https://doi.org/10.1016/j.jiec.2017.04.029

15.Wang X, Yan Y, Xu Z. Application experiment and numerical simulation analysis of oil–water separator with two-oriented corrugated coalescence plate. J Disp Sci Technol. 2017; 38: 1509-15. https://doi.org/10.1080/01932691.2016.1259072

16.Almarouf HS, Nasser MS, Al-Marri MJ, Khraisheh M, Onaizi SA. Demulsification of stable emulsions from produced water using a phase separator with inclined parallel arc coalescing plates. J Petrol Sci Eng. 2015; 135: 16-21. https://doi.org/10.1016/j.petrol.2015.08.005

17.Kim DK, Choi G, Ko T-J, Shin S, Kim SJ. Numerical investigation of oil–water separation on a mesh-type filter. Acta Mech. 2022; 233: 104159. https://doi.org/10.1007/s00707-022-03155-0

18.Yuan S, Fan Y, Li J, Zhou S, Cao Y. Influence of droplet coalescence and breakup on the separation process in wave-plate separators. Can J Chem Eng. 2018; 96: 1627-36. https://doi.org/10.1002/cjce.23089

19.Oruç M, Yayla S. Experimental investigation of oil-in water separation using corrugated plates and *optimization of separation system. Sep Sci Technol. 2022; 57: 788-800. https://doi.org/10.1080/01496395.2021.1939377*

20.Yayla S, Ibrahim SS, Olcay AB. Numerical investigation of coalescing plate system to understand the separation of water and oil in water treatment plant of petroleum industry. Eng Appl Comp Fluid. 2017; 11: 184-92. https://doi.org/10.1080/19942060.2016.1273137

21.Yayla S, Sabah S, Olcay AB. CFD simulation of designed coalescing plates for separating water and oil in water treatment plants used in petroleum projects. Pamukkale U J Eng Sci. 2017; 23: 358-63. https://doi.org/10.5505/pajes.2016.67944

22.Liu Y, Lu H, Li Y, Xu H, Pan Z, Dai P, et al. A review of treatment technologies for produced water in offshore oil and gas fields. Sci Total Environ. 2021; 775: 145485. https://doi.org/10.1016/j.scitotenv.2021.145485

23.Wahba E. Derivation of the differential continuity equation in an introductory engineering fluid mechanics course. Int J Mech Eng Edu. 2022; 50: 538-47. https://doi.org/10.1177/03064190211014460

24.Wang Z-H, Liu X-Y, Zhang H-Q, Wang Y, Xu Y-F, Peng B-L, et al. Modeling of kinetic characteristics of alkaline-surfactant-polymerstrengthened foams decay under ultrasonic standing wave. Petrol Sci. 2022; 19: 1825-39. https://doi.org/10.1016/j.petsci.2022.04.012

25.Wang Z, Sun X, Li J, Zhou N. Influencing factors and laws of polymer-flooding produced water separation settlement with dissolved air flotation. China Petrol Mach. 2020; 48: 123-35. https://doi.org/10.16082/j.cnki.issn.1001-4578.2020.10.019

26.Zhuge X, Qi X, Wang S, Liu Y. Evaluation and improvement of the performance of a wellhead multistage bundle gas-liquid separator. Processes. 2022; 10(4): 632. https://doi.org/10.3390/pr10040632

27.Hattori H, Wada A, Yamamoto M, Yokoo H, Yasunaga K, Kanda T, et al. Experimental study of laminar-to-turbulent transition in pipe flow. Phys Fluids. 2022; 34: 1-18. https://doi.org/10.1063/5.0082624

28.Zhao J, Xi X, Dong H, Wang Z, Zhuo Z. Rheo-microscopy in situ synchronous measurement of shearing thinning behaviors of waxy crude oil. Fuel. 2022; 323: 124427. https://doi.org/10.1016/j.fuel.2022.124427

29.Pavlíček P. Local reynolds number. AIP Conference Proceedings 27 June 2019; 2118(1): 030035. https://doi.org/10.1063/1.5114763

30.Zhao ZG, Feng MQ, Liu JG, Tao YK, Wang JS, Wang L, et al. The research on new technology and separation performance of wastewater treatment for offshore field. Desalin Water Treat. 2018; 125: 116-23. https://doi.org/10.5004/dwt.2018.22093.

31.Koutsourakis N, Bartzis JG, Markatos NC. Evaluation of Reynolds stress, k-ε and RNG k-ε *turbulence models in street canyon flows using various experimental datasets. Environ Fluid Mech. 2012; 12: 379-403. https://doi.org/10.1007/s10652-012-9240-9*

32.Galbraith MC, Caplan PC, Carson HA, Park MA, Balan A, Anderson WK, et al. Verification of unstructured grid adaptation components. AIAA J. 2020; 58: 3947-62. https://doi.org/10.2514/1.J058783

33.Yu H, Zhang H, Guo Y, Tan H, Li Y, Xie G. Investigating neutron back scattering technique for the detection of oil water separation levels in horizontal gravity oil separators. J Radioanal Nucl Ch. 2018; 315: 323-30. https://doi.org/10.1007/s10967-017-5675-2

34.Feng X, Stewart S, Sartori L, Hodges K. Understanding the effect of skim oil recycle on the water/oil separation in steam assisted gravity drainage operations. J Petrol Sci Eng. 2020; 192: 107233. https://doi.org/10.1016/j.petrol.2020.107233

ISSN 2249-4278

The Electromagnetic Scattering Problem by a Cylindrical DoublyConnected Domain at Oblique Incidence: An Inverse Problem

Leonidas Mindrinos
Department of Natural Resources Development and Agricultural Engineering, Agricultural University of Athens, Athens118 55, Greece

Abstract:

In this work, we examine the inverse problem to reconstruct the inner boundary of a cylindrical doubly-connected infinitely long medium from measurements of the scattered electromagnetic wave in the far-field. We consider the integral representation of the solution to derive a non-linear system of equations for the unknown radial function. We propose an iterative scheme using linearization and regularization techniques.

Keywords: Inverse problem Electromagnetic scattering Singular integral equations

1. Introduction

Inverse scattering problems are a class of applied mathematical problems that arise in various fields, such as medical imaging, radar technology, and non-destructive testing. These problems involve the reconstruction of an unknown scatterer (its geometry and/or material properties) from the measurements of the scattered waves close or far from the medium. We refer to the textbooks [1-3] for the fundamentals and an extensive overview.

In the special case of obliquely incident scattering problems, where the incident wave is not normal (perpendicular) to the scatterer or the boundary, additional complexity is introduced. The scattering events depend on the incident angle and thus such problems pose additional theoretical and numerical challenges compared to normal incidence. The analysis of these problems often involves advanced mathematical and computational approaches to account for the increased complexity, see for example the early works [4, 5].

However, if we specify the scatterer to be infinitely long and spatial-independent in one direction then the three-dimensional problem reduces to a set of two-dimensional problems and the complexity has to do only with the boundary conditions where the tangential derivative of the fields appear. Motivated by the works of Nakamura and Wang, see for example [6, 7], we examined scattering problems for penetrable simply- and doublyconnected scatterers [8, 9].

In this work, we are interested in solving numerically the inverse problem to reconstruct the inner boundary curve of a doubly connected penetrable infinitely long cylinder with impedance-type conditions in its inner boundary. The well-posedness of the corresponding direct problem was proven by the author in [10].

We formulate the inverse problem as a system of singular boundary integral equations to be solved for the unknown density functions, see the initial work of Kress and Rundell [11]. The radial function appears non-linearly and we apply the Fréchet derivative on the integral operator. The ill-posedness is treated with Tikhonov regularization.

The paper is organized as follows: In sec_direct we formulate the direct problem and we present the necessary differential equations, boundary, and radiation conditions. The inverse problem and the equivalent system of integral equations are stated in sec_inverse where we propose also the numerical iterative scheme for its solution. In the last section, we present the numerical implementation and numerical examples justifying the applicability of the proposed method.

2. Problem Formulation

In [10] the author considered the direct scattering problem of a time-harmonic electromagnetic wave by an infinitely long, penetrable, and doubly-connected cylinder. The initial problem is stated in 3D but the properties of the medium allow for an equivalent formulation in 2D for the cross-section of the scatterer. The medium is bounded by two disjoint smooth boundaries. We impose transmission conditions on the exterior and Leontovich impedance conditions on the inner boundary.

Let Ω_1 denote the horizontal cross-section of the cylindrical scatterer, with a smooth boundary Γ, consisting of two disjoint closed curves Γ_1 (inner) and Γ_0 (outer) such that $\Gamma = \Gamma_1 \cup \Gamma_0$. The exterior domain is denoted by Ω_0.

We define the wave-number $\kappa_j^2 = \mu_j \varepsilon_j \omega^2 - \beta^2$, for $j = 0,1$ where μ_j and ε_j are the material parameters and $\beta = k_0 \cos\theta$, where $k_0 = \omega\sqrt{\mu_0 \varepsilon_0}$, for the frequency ω and $\theta \in (0,\pi)$ is the incident angle concerning the negative z −axis.

Following [6–8,10], the direct problem is governed by the Helmholtz equations

$$\begin{aligned} \Delta e^{ext} + \kappa_0^2 e^{ext} &= 0, \quad \Delta h^{ext} + \kappa_0^2 h^{ext} &&= 0, \quad in\ \Omega_0, \\ \Delta e^1 + \kappa_1^2 e^1 &= 0, \quad \Delta h^1 + \kappa_1^2 h^1 &&= 0, \quad in\ \Omega_1, \end{aligned}$$

for the exterior e^{ext}, h^{ext} and the interior e^1, h^1 electric and magnetic fields, respectively. The boundary conditions read

$$\begin{aligned} e^1 - e^{ext} &= 0, \quad on\ \Gamma_0, \\ \tilde{\mu}_1 \omega \frac{\partial h^1}{\partial n} + \beta_1 \frac{\partial e^1}{\partial \tau} - \tilde{\mu}_0 \omega \frac{\partial h^{ext}}{\partial n} - \beta_0 \frac{\partial e^{ext}}{\partial \tau} &= 0, \quad on\ \Gamma_0, \\ h^1 - h^{ext} &= 0, \quad on\ \Gamma_0, \\ \tilde{\varepsilon}_1 \omega \frac{\partial e^1}{\partial n} - \beta_1 \frac{\partial h^1}{\partial \tau} - \tilde{\varepsilon}_0 \omega \frac{\partial e^{ext}}{\partial n} + \beta_0 \frac{\partial h^{ext}}{\partial \tau} &= 0, \quad on\ \Gamma_0, \\ \tilde{\mu}_1 \omega \frac{\partial h^1}{\partial n} + \beta_1 \frac{\partial e^1}{\partial \tau} + \lambda i h^1 &= 0, \quad on\ \Gamma_1, \\ \lambda \tilde{\varepsilon}_1 \omega \frac{\partial e^1}{\partial n} - \lambda \beta_1 \frac{\partial h^1}{\partial \tau} + i e^1 &= 0, \quad on\ \Gamma_1, \end{aligned}$$

where appear both the normal and tangential derivatives of the fields. The impedance function λ is known. Here, we used

$$\tilde{\mu}_j = \frac{\mu_j}{\kappa_j^2}, \quad \tilde{\varepsilon}_j = \frac{\varepsilon_j}{\kappa_j^2}, \quad \beta_j = \frac{\beta}{\kappa_j^2}, \quad for\ j = 0,1.$$

The exterior fields are written as the sum of the scattered e^0, h^0 and incident fields e^{inc}, h^{inc}, given by

$$e^{inc}(\boldsymbol{x}) = \frac{1}{\sqrt{\varepsilon_0}} sin\,\theta\, e^{i\kappa_0(x\cos\varphi + y\sin\varphi)}, \quad h^{inc}(\boldsymbol{x}) = 0, \quad \boldsymbol{x} = (x, y), \tag{1}$$

where φ is the polar angle of the incident direction. The scattered wave satisfies also the Sommerfeld radiation condition.

The direct problem admits a unique solution [10]. In this work, we are interested in solving numerically the inverse problem to reconstruct the boundary curve Γ_1, given λ and the far-field pattern $e^\infty(\hat{\boldsymbol{x}}), h^\infty(\hat{\boldsymbol{x}})$ of the scattered field, for all $\hat{\boldsymbol{x}}$ in the unit circle.

3. The Inverse Problem

Given the far-fields, we aim to reconstruct the inner boundary of the scatterer given its material parameters and the impedance function. To do so, we present the solution of the problem using its integral representation.

Thus, we define the single- and double-layer potentials

$$(\mathcal{S}_{klj} f)(\boldsymbol{x}) = \int_{\Gamma_j} \Phi_k(\boldsymbol{x},\boldsymbol{y}) f(\boldsymbol{y}) ds(\boldsymbol{y}), \quad \boldsymbol{x} \in \Omega_l,$$

$$(\mathcal{D}_{klj} f)(\boldsymbol{x}) = \int_{\Gamma_j} \frac{\partial \Phi_k}{\partial n(\boldsymbol{y})}(\boldsymbol{x},\boldsymbol{y}) f(\boldsymbol{y}) ds(\boldsymbol{y}), \quad \boldsymbol{x} \in \Omega_l,$$

for $k, l, j = 0,1$, where Φ_k is the fundamental solution of the Helmholtz equation in R^2, and f is a continuous density function. In addition, we define the integral operators

$$(S_{klj} f)(\boldsymbol{x}) = \int_{\Gamma_j} \Phi_k(\boldsymbol{x},\boldsymbol{y}) f(\boldsymbol{y}) ds(\boldsymbol{y}), \quad \boldsymbol{x} \in \Gamma_l,$$

$$(D_{klj} f)(\boldsymbol{x}) = \int_{\Gamma_j} \frac{\partial \Phi_k}{\partial n(\boldsymbol{y})}(\boldsymbol{x},\boldsymbol{y}) f(\boldsymbol{y}) ds(\boldsymbol{y}), \quad \boldsymbol{x} \in \Gamma_l,$$

$$(NS_{klj} f)(\boldsymbol{x}) = \int_{\Gamma_j} \frac{\partial \Phi_k}{\partial n(\boldsymbol{x})}(\boldsymbol{x},\boldsymbol{y}) f(\boldsymbol{y}) ds(\boldsymbol{y}), \quad \boldsymbol{x} \in \Gamma_l,$$

$$(ND_{klj} f)(\boldsymbol{x}) = \int_{\Gamma_j} \frac{\partial^2 \Phi_k}{\partial n(\boldsymbol{x})\partial n(\boldsymbol{y})}(\boldsymbol{x},\boldsymbol{y}) f(\boldsymbol{y}) ds(\boldsymbol{y}), \quad \boldsymbol{x} \in \Gamma_l,$$

$$(TS_{klj} f)(\boldsymbol{x}) = \int_{\Gamma_j} \frac{\partial \Phi_k}{\partial \tau(\boldsymbol{x})}(\boldsymbol{x},\boldsymbol{y}) f(\boldsymbol{y}) ds(\boldsymbol{y}), \quad \boldsymbol{x} \in \Gamma_l,$$

$$(TD_{klj} f)(\boldsymbol{x}) = \int_{\Gamma_j} \frac{\partial^2 \Phi_k}{\partial \tau(\boldsymbol{x})\partial n(\boldsymbol{y})}(\boldsymbol{x},\boldsymbol{y}) f(\boldsymbol{y}) ds(\boldsymbol{y}), \quad \boldsymbol{x} \in \Gamma_l,$$

needed in the following analysis.

We apply both the direct and indirect methods and we consider a single-layer ansatz for the interior fields and a modified Green representation for the exterior fields. The exterior fields are represented through a combination of potentials where we have specified the density functions to reduce the number of unknowns.

We set

$$\begin{aligned}
e^1(\boldsymbol{x}) &= (\mathcal{S}_{110}\psi_1^e)(\boldsymbol{x}) + (\mathcal{S}_{111}\psi_2^e)(\boldsymbol{x}), && \boldsymbol{x} \in \Omega_1,\\
h^1(\boldsymbol{x}) &= (\mathcal{S}_{110}\psi_1^h)(\boldsymbol{x}) + (\mathcal{S}_{111}\psi_2^h)(\boldsymbol{x}), && \boldsymbol{x} \in \Omega_1,\\
e^0(\boldsymbol{x}) &= (\mathcal{D}_{000}\varphi_0^e)(\boldsymbol{x}) + \frac{\tilde{\varepsilon}_1}{\tilde{\varepsilon}_0}(\mathcal{S}_{000}\psi_1^e)(\boldsymbol{x}), && \boldsymbol{x} \in \Omega_0,\\
h^0(\boldsymbol{x}) &= (\mathcal{D}_{000}\varphi_0^h)(\boldsymbol{x}) + \frac{\tilde{\mu}_1}{\tilde{\mu}_0}(\mathcal{S}_{000}\psi_1^h)(\boldsymbol{x}), && \boldsymbol{x} \in \Omega_0.
\end{aligned} \tag{2}$$

Then, using the standard jump relations, we find that the fields (2) solve the boundary value problem if the densities satisfy a well-posed Fredholm-type system of integral equations. We enlarge the system with the sum of the two far-field equations, given the specific form of the scattered fields. In the end, we obtain the system

$$\boldsymbol{A\varphi} = \boldsymbol{b}, \tag{3}$$

where

$$\boldsymbol{A} = \begin{pmatrix} 1+A_{11} & 0 & 0 & A_{14} & 0 & A_{16} \\ 0 & 1+A_{22} & A_{23} & A_{24} & A_{25} & A_{26} \\ 0 & A_{32} & 1+A_{33} & 0 & A_{35} & 0 \\ A_{41} & A_{42} & 0 & 1+A_{44} & A_{45} & A_{46} \\ 0 & A_{52} & 0 & A_{54} & 1+A_{55} & A_{56} \\ 0 & A_{62} & 0 & A_{64} & A_{65} & 1+A_{66} \\ D^\infty & \frac{\tilde{\mu}_1}{\tilde{\mu}_0} S^\infty & D^\infty & \frac{\tilde{\varepsilon}_1}{\tilde{\varepsilon}_0} S^\infty & 0 & 0 \end{pmatrix},$$

and $\boldsymbol{\varphi} = (\varphi_0^e, \psi_1^h, \varphi_0^h, \psi_1^e, \psi_2^h, \psi_2^e)^T$ for the right-hand side $\boldsymbol{b} = (-2e^{inc}, 0,0, \frac{\tilde{\varepsilon}_0}{\tilde{\varepsilon}_1}\partial_n e^{inc}, 0,0, e^\infty + h^\infty)^T$. The elements (integral operators) of the matrix are given by

$$\begin{aligned}
A_{11} &= A_{33} = 2D_{000}, & A_{16} &= A_{35} = -2S_{101}, \\
A_{14} &= -2\left(S_{100} - \frac{\tilde{\varepsilon}_1}{\tilde{\varepsilon}_0} S_{000}\right), & A_{22} &= A_{44} = NS_{100} - NS_{000}, \\
A_{23} &= -\frac{\tilde{\mu}_0}{\tilde{\mu}_1} ND_{000}, & A_{24} &= \frac{\beta_1 - \beta_0}{\tilde{\mu}_1 \omega} TS_{100}, \\
A_{25} &= A_{46} = NS_{101}, & A_{26} &= \frac{\beta_1 - \beta_0}{\tilde{\mu}_1 \omega} TS_{101}, \\
A_{32} &= -2\left(S_{100} - \frac{\tilde{\mu}_1}{\tilde{\mu}_0} S_{000}\right), & A_{41} &= -\frac{\tilde{\varepsilon}_0}{\tilde{\varepsilon}_1} ND_{000}, \\
A_{42} &= \frac{\beta_0 - \beta_1}{\tilde{\varepsilon}_1 \omega} TS_{100}, & A_{45} &= \frac{\beta_0 - \beta_1}{\tilde{\varepsilon}_1 \omega} TS_{101}, \\
A_{52} &= -2NS_{110} - \frac{2i\lambda}{\tilde{\mu}_1 \omega} S_{110}, & A_{54} &= -\frac{2\beta_1}{\tilde{\mu}_1 \omega} TS_{110}, \\
A_{55} &= -2NS_{111} - \frac{2i\lambda}{\tilde{\mu}_1 \omega} S_{111}, & A_{56} &= -\frac{2\beta_1}{\tilde{\mu}_1 \omega} TS_{111}, \\
A_{62} &= -\frac{2\beta_1}{\tilde{\varepsilon}_1 \omega} TS_{110}, & A_{64} &= -2NS_{110} + \frac{2i}{\lambda \tilde{\varepsilon}_1 \omega} S_{110}, \\
A_{65} &= \frac{2\beta_1}{\tilde{\varepsilon}_1 \omega} TS_{111}, & A_{66} &= -2NS_{111} + \frac{2i}{\lambda \tilde{\mu}_1 \omega} S_{111}.
\end{aligned}$$

Here, D^∞ and S^∞ denote the far-field operators of D_{000} and S_{000}, respectively, where we replace Φ_0 with its far-field approximation.

The system (3) has to be solved for the six unknown density functions and the parametrization of the interior boundary curve. We propose to split it into two sub-systems and use the iterative scheme proposed in [12] and further applied successfully in many inverse problems, see for example [9, 13-15]. The difference here is that the far-field equation does not provide information on Γ_1, so we have to consider this equation together with the boundary equations for recovering the density functions (ill-posed problem) and solve instead one boundary equation for the unknown boundary.

Let us write (3) in a row-based form

$$\boldsymbol{A}[k]\boldsymbol{\varphi} = \boldsymbol{b}[k], \quad for\ k = 1, \dots, 7.$$

where $\boldsymbol{A'}_1[1]$ denotes the Fréchet derivative of the operator depending on Γ_1 (specified in the next section) and $\boldsymbol{q}$ the radial function (to be reconstructed). The regularization parameter is decreasing at every iteration step.

4. Numerical Examples

We assume star-like boundary curves of the form

$$\Gamma_j = r_j(t)(\cos t\,, \sin t): t \in [0,2\pi], \quad j = 0,1,$$

for a smooth radial function r_j and we consider an equidistant grid discretization $t_k = k\pi/n$, for $k = 0, \dots, 2n-1$.

The discretized form of the operators are analytically presented In [10] and they are omitted here for the sake of presentation. We apply quadrature rules to handle the singular kernels. We present only the single layer and its Fréchet derivative.

We observe that only the operator S_{101} depends (non-linearly) on Γ_1, and it is explicitly given by

$$\begin{aligned}\big(S_{101}(r_1;\phi)\big)(t) &= \int_0^{2\pi} \Phi_1\big(\boldsymbol{y}(t),\boldsymbol{x}(\tau)\big)\phi(\tau)|\boldsymbol{x}'(\tau)|d\tau \\ &= \frac{i}{4}\int_0^{2\pi} H_0^{(1)}(\kappa_1|\boldsymbol{d}(t,\tau)|)\phi(\tau)|\boldsymbol{x}'(\tau)|d\tau,\end{aligned}$$

where $\boldsymbol{d}(t,\tau) = \boldsymbol{y}(t) - \boldsymbol{x}(\tau)$, for $\boldsymbol{y} \in \Gamma_0$ and $\boldsymbol{x} \in \Gamma_1$.

We compute the Fréchet derivative by formally differentiating the kernel of the operator, resulting in

$$\Big(\big(S'_{101}(r_1;\phi)\big)(q)\Big)(t) = \int_0^{2\pi} M(t,\tau)\phi(\tau)d\tau,$$

for the update q of the radial function r_1, with kernel

$$M(t,\tau) = \frac{i\kappa_1}{4}H_1^{(1)}(\kappa_1|\boldsymbol{d}(t,\tau)|)\frac{\boldsymbol{d}(t,\tau)\cdot\boldsymbol{q}(\tau)}{|\boldsymbol{d}(t,\tau)|}|\boldsymbol{x}'(\tau)| + \frac{i}{4}H_0^{(1)}(\kappa_1|\boldsymbol{d}(t,\tau)|)\frac{\boldsymbol{x}'(\tau)\cdot\boldsymbol{q}'(\tau)}{|\boldsymbol{x}'(\tau)|}$$

Since

$$\boldsymbol{q}'(\tau) = q'(\tau)(\cos\tau\,, \sin\tau) + q(\tau)(-\sin\tau\,, \cos\tau),$$

we decompose the kernel M, to the parts applied to q and its derivative, as follows

$$\begin{aligned}M(t,\tau) = &\left(\frac{i\kappa_1}{4}H_1^{(1)}(\kappa_1|\boldsymbol{d}(t,\tau)|)\frac{\boldsymbol{d}(t,\tau)\cdot(\cos\tau\,, \sin\tau)}{|\boldsymbol{d}(t,\tau)|}|\boldsymbol{x}'(\tau)|\right. \\ &\left.+\frac{i}{4}H_0^{(1)}(\kappa_1|\boldsymbol{d}(t,\tau)|)\frac{\boldsymbol{x}'(\tau)\cdot(-\sin\tau\,, \cos\tau)}{|\boldsymbol{x}'(\tau)|}\right)q(\tau) \\ &+\frac{i}{4}H_0^{(1)}(\kappa_1|\boldsymbol{d}(t,\tau)|)\frac{\boldsymbol{x}'(\tau)\cdot(\cos\tau\,, \sin\tau)}{|\boldsymbol{x}'(\tau)|}q'(\tau).\end{aligned}$$

We approximate the updated radial function using trigonometric interpolation with $2M+1$ coefficients. We consider half collocation points concerning the direct problem and we add noise to the far-field data concerning the L^2 −norm:

$$e_\delta^\infty = e^\infty + \delta\frac{\|e^\infty\|_2}{\|u\|_2}u, \quad h_\delta^\infty = h^\infty + \delta\frac{\|h^\infty\|_2}{\|v\|_2}v,$$

for a given noise level δ, and complex-valued vectors u and v, with normally distributed random variables as components.

In the numerical example, the domain is bounded by the curves with radial functions

$$r_0 = 0.8, \quad and \quad r_1 = 0.7\sqrt{0.5\cos^2 t + 0.1\sin^2 t},$$

and we set $\lambda = 1$ for the impedance function. The material parameters are $\varepsilon_0 = \mu_0 = 1$, in the exterior domain and $\varepsilon_0 = \mu_0 = 5$, in the interior domain. We consider measurements from two incident directions and we use $n = 64$ and $M = 2$. In Fig (**1**), we present the reconstructions for $\theta = \pi/4$ and $\varphi = 0, \pi$. The boundary is initially approximated by a circle with radius 0.4. The recovered curve is obtained after 20 and 12 iterations for exact and noisy data, respectively.

We observe that the reconstructions are satisfactory and stable with respect to noise. However, they depend on the initial guess.

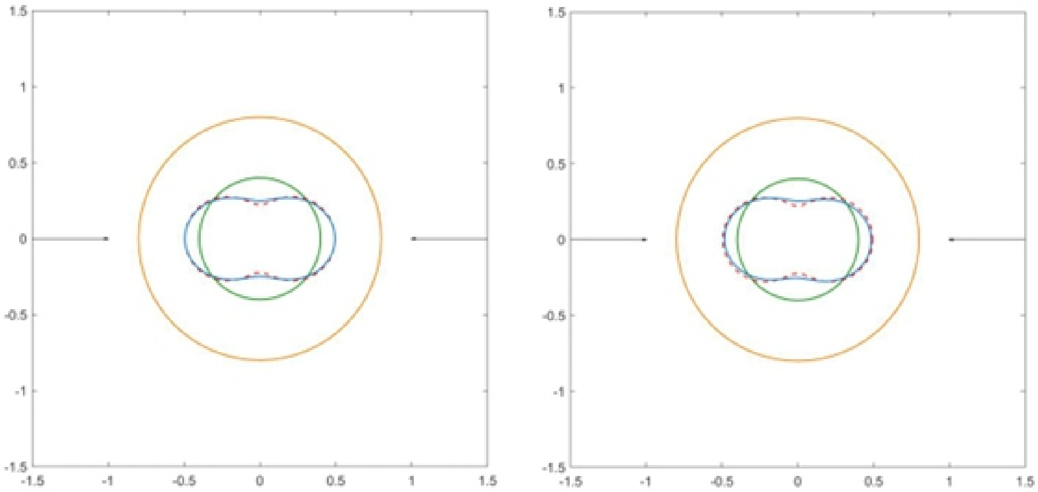

Figure 1: The reconstructed boundary curve (blue) for exact (left) and data with noise 4% (right) from two incident directions (arrows). The outer boundary (brown) and the initial guess (green) are both circles with different radii.

Funding

Not applicable

Conflict of Interest

The authors declare no conflict of interest.

References

1.Colton D. Qualitative methods in inverse scattering theory. In: Engl HW, Louis AK, Rundell W, Eds. Inverse problems in medical imaging and nondestructive testing. Vienna: Springer; 1997. https://doi.org/10.1007/978-3-7091-6521-8_4

2.Kress R. Linear integral equations. vol. 82, 3rd ed. New York, NY: Springer; 2014. https://doi.org/10.1007/978-1-4614-9593-2

3.Kress R. A collocation method for a hypersingular boundary integral equation via trigonometric differentiation. J Integral Equations Appl. 2014; 26: 197-213. https://doi.org/10.1216/JIE-2014-26-2-197

4.Yousif HA, Köhler S. Scattering by two penetrable cylinders at oblique incidence I The analytical *solution. J Opt Soc Am A. 1988; 5(7): 1085-96. https://doi.org/10.1364/JOSAA.5.001085*

5.Wait JR. Scattering of a plane wave from a circular dielectric cylinder at oblique incidence. Can J Phys. 1955; 33: 189-95. https://doi.org/10.1139/p55-024

6.Nakamura G, Wang H. The direct electromagnetic scattering problem from an imperfectly conducting cylinder at oblique incidence. J Math Anal Appl. 2013; 397: 142-55. https://doi.org/10.1016/j.jmaa.2012.07.049

7.Wang H, Nakamura G. The integral equation method for electromagnetic scattering problem at oblique incidence. Appl Num Math. 2012; 62: 860-73. https://doi.org/10.1016/j.apnum.2012.02.006

8.Gintides D, Mindrinos L. The direct scattering problem of obliquely incident electromagnetic waves by a penetrable homogeneous cylinder. J Integral Equations Appl. 2016; 28: 91-122. https://doi.org/10.1216/JIE-2016-28-1-91

9.Gintides D, Mindrinos L. The inverse electromagnetic scattering problem by a penetrable cylinder at oblique incidence. Appl Analysis. 2019; 98: 781-98. https://doi.org/10.1080/00036811.2017.1402891

10.Mindrinos L. The electromagnetic scattering problem by a cylindrical doubly connected domain at oblique incidence: the direct problem. IMA J Appl Math. 2019; 84: 292-311. https://doi.org/10.1093/imamat/hxy059

11.Kress R, Rundell W. Nonlinear integral equations and the iterative solution for an inverse boundary value problem. Inverse Probl. 2005; 21: 1207-23. https://doi.org/10.1088/0266-5611/21/4/002

12.Johansson T, Sleeman BD. Reconstruction of an acoustically sound-soft obstacle from one incident field and the far-field pattern. IMA J Appl Math. 2007; 72: 7296-112. https://doi.org/10.1093/imamat/hxl026

13.Altundag A, Kress R. On a two-dimensional inverse scattering problem for a dielectric. Appl Analysis. 2012; 91: 757-71. https://doi.org/10.1080/00036811.2011.619981

14.Chapko R, Gintides D, Mindrinos L. The inverse scattering problem by an elastic inclusion. Adv Comput Math. 2017; 44: 1-24. https://doi.org/10.1007/s10444-017-9550-z

15.Lee K-M. Inverse scattering problem from an impedance crack via a composite method. Wave Motion. 2015; 56: 43–51. https://doi.org/10.1016/j.wavemoti.2015.02.002

ISSN 2249-4278

A Conformable Inverse Problem with Constant Delay

Auwalu Sa'idu and Hikmet Koyunbakan
Department of Mathematics, Faculty of Science, Firat University, Elazig, Turkey

Abstract:

This paper aims to express the solution of an inverse Sturm-Liouville problem with constant delay using a conformable derivative operator under mixed boundary conditions. For the problem, we stated and proved the specification of the spectrum. The asymptotics of the eigenvalues of the problem was and the solutions were extended to the Regge-type boundary value problem. As such, a new result, as an extension of the classical Sturm-Liouville problem to the fractional phenomenon, has been achieved. The uniqueness theorem for the solution of the inverse problem is proved in different cases within the interval $(0,\pi)$. The results in the classical case of this problem can be obtained at $a = 1$. 2000 Mathematics Subject Classification. 34L20,34B24,34L30.

Keywords: Spectrum Constant delay Conformable derivative Fractional sturm-liouville problem

1. Introduction

As differential equations are used to model real-life problems in sciences, technology, social sciences, etc, the Sturm-Liouville equation, which is a special case of a second-order differential equation, plays a vital role in the literature both in classical and fractional cases. The fractional derivative approach is such a vital tool in which certain phenomenon, that can not be or is very difficult to analyze in the classical case, can easily be analyzed and expressed. There are many fractional derivative approaches such as Riemann-Liouville, Caputo, M-derivative, Grunwald-Letnikov, Weyl, etc, but each has its shortcomings [1-3]. Looking into those shortcomings associated with the most popular fractional differentiation approaches, Khalil, et al. [4] established a new fractional derivatives approach which turned out to be easy in evaluations and satisfied most of the properties of differentiation and named it Conformable Fractional Derivative. This new approach was criticized, affirmed, and further developed and is in use by many authors [5-9]. As this article involves an inverse problem in the Sturm-Liouville Problem (SLP) in fractional case, there are many studies on the fractional SLP that are being progressed as can be seen in [10-19].

There is an inverse problem in a parameter identification problem of partial differential equations, which involves finding the unknown parameter (usually p(x)) from some observed data from the situation under consideration in the system. Under this, many authors designed many inversion strategies that appropriately describe and many different inverse problems, details on these can be obtained from [20-25], but the inverse problem in SLP, deals with the concept of finding the potential q(x)) and the constants in the conditions in the differential SLP by using the spectral parameters. Ambarzumyan theorem gives the first results of inverse SLP [26], it says that if the spectrum of SLP under Neumann boundary conditions is $n^2, n \geq 0$, then the potential function will be zero, $q(x)) = 0$). The authors in [27, 28] gave some results, in various cases, on this theory. The inverse SLP has been under discussion for a long time by many researchers and so many results have been obtained by many authors as in [29-38].

Inverse SLP under fractional derivative operator is now one of the current research fields, researchers are crescively expanding their studies in the area and many results in different problems were obtained as detailed in [39-42]. There are differential equations with delay in various mathematical problems and applications which produces vital changes in the quality of the studies on the corresponding inverse problems of spectral analysis. The methods of transformation operator, spectral mappings, etc, are the standard methods of solving an inverse SLP without delay (differential operators), but these methods do not work for operators with delay, as such some researchers constructed new approaches for the latter general spectral theory. The authors in [43] consider the Sturm-Liouville differential equation with a large constant delay, that is $a \in \pi/2, \pi)$, and generated an effective algorithm for solving the problem, also the authors in [44] studied the nonlinear inverse problem and obtained the Properties of their spectral characteristics. Most of the studies in inverse SLP focus on the situation with function with the assumption that the potential q(x) vanishes on the corresponding subinterval but the authors [45] waived that assumption in favor of a continuously matching initial function, which leads to appearing an additional term with frozen argument in the equation, they solved the problem and proved its spectral properties, more on these problem can be found in [46-50].

The authors of [36] gave an interesting result of inverse SLP with a constant delay under a non-self-adjoint operator with a mixed boundary condition, expressing the spectral properties of the eigenvalues obtained and also, proving the uniqueness theorem. Studies and results on fractional inverse SLP are scarce, as such we intended in this paper to express the case in [36] in a fractional case under a conformable derivative operator. We obtained the result of the inverse SLP with a constant delay under a mixed boundary condition using the conformable derivative approach, expressed the corresponding spectral properties, and proved the uniqueness theorem. The corresponding classical results can be retrieved at $a = 1$.

2. Some Basic Definitions

Definition 2.1. Consider the function $h:[0,\infty) \to \mathbb{R}$, then the a^{th} order derivative of h is given

$$D_x^{\alpha} h(x) = \lim_{e \to 0} \frac{h(x + ex^{1-\alpha}) - h(x))}{e} \tag{2.1}$$

for all $x > 0$, $\alpha \in (0,1]$, that is,if h is differentiable, then $D_x^{\alpha} h(x) = x^{1-\alpha} h'(x)$.

The conformable fractional derivative is also defined for $\alpha \in (n-1, n)$ for $n \in N$ as,

Definition 2.2. Let h be an n -differentiable function at x, where $x > 0$ and $\alpha \in (n-1, n)$, then the conformable fractional derivative h of order α is defined as,

$$D_x^{\alpha} h(x) = \lim_{e \to 0} \frac{h^{\lceil \alpha \rceil - 1}(x + e x^{\lceil \alpha \rceil - \alpha}) - h^{\lceil \alpha \rceil - 1}(x)}{e} \tag{2.2}$$

Where $\lceil \alpha \rceil$ is the smallest integer greater than or equal to α.

It can be calculated by $D_x^{\alpha} h(x) = x^{\lceil \alpha \rceil - \alpha} h^{\lceil \alpha \rceil}(x)$

Definition 2.3. The integral of a function h of order α is given by

$$I_{\alpha} h(x) = \int_0^x \quad h(t) d_{\alpha} t = \int_0^x \quad t^{\alpha - 1} h(t) dt \tag{2.3}$$

for all $x > 0$.

Lemma 2.1. If the function $h: [a, \infty) \to \mathbb{R}$ is differentiable, then, we have for $x > a$ (a is any real number)

$$D_x^{\alpha} I_{\alpha} h(x) = h(x).$$

Lemma 2.2. Let the function $h: (a, b) \to \mathbb{R}$ be differentiable, then, for $x > a$,(a and b are any real numbers)

$$D_x^{\alpha} I_{\alpha} h(x) = h(x) - h(a).$$

Theorem 2.4. Let g, h be two differentiable functions, then

$$\int_a^b \quad g(x) D_x^{\alpha}(h(x))(x) d_{\alpha} x = gh|_a^b - \int_a^b \quad h(x) D_x^{\alpha}(g(x)) d_{\alpha} x. \tag{2.4}$$

3. The Main Work

We consider the fractional Sturm-Liouville problem below with conformable derivative operator

$$-D_x^{\alpha} D_x^{\alpha} y + q(x) y(x-a) = \mu y(x), \ for \quad x \in (0, \pi) \tag{3.1}$$

under the condition

$$y(0) = y^{(j)}(\pi) = 0, \quad for \ j = 0{,}1, \tag{3.2}$$

for $a \in (0, \pi)$, and $q(x) \in L(a, \pi)$. Taking μ as the spectral parameter and the potential function(complex-valued) $q(x) = 0$ for $x \in [0, a]$.

By defining an operator

$$L_{\alpha} y(x) = -D_x^{\alpha} D_x^{\alpha} y + q(x) y(x-a)$$

then (3.1) can be expressed as

$$L_{\alpha} y(x) = \mu y(x), \quad x \in (0, \pi) \tag{3.3}$$

The main work here is to recover the function $q(x)$ from the spectra of $L_{\alpha_j}(q)$, $j = 0{,}1.$, to state and prove some properties of the spectra, and also to prove the uniqueness of the results. We assumed that $\{\mu_{n_j}\}_{n \geq 1, j=0,1}$ indicates the eigenvalues of (3.3).

3.1. Existence of the Solution

Consider $N \in N$ such that $a \in \left[\frac{\pi}{N+1}, \frac{\pi}{N}\right]$ and $Q(x, \mu)$ be a solution of (3.3) under the conditions that

$$Q(0, \mu) = 0, \ D_x^{\alpha} Q(0, \mu) = 1.$$

We can then expressed $Q(x,\mu)$ as

$$Q(x,\mu)=\frac{1}{\sqrt{\mu}}sin\left(\frac{\sqrt{\mu}}{\alpha}x^{\alpha}\right)+\frac{1}{\sqrt{\mu}}\int_{0}^{x} sin\left(\frac{\sqrt{\mu}}{\alpha}(x^{\alpha}-t^{\alpha})\right)q(t)Q(t-a,\mu)d_{\alpha}t \tag{3.4}$$

clearly, $Q^{(j)}(x,\mu)$, for any x in the interval $(0,\pi)$ and $j=0{,}1$, are entire in μ of order $\frac{1}{2}$.

By the method of successive approximations, the solution of (3.4) is

$$Q(x,\mu)=Q_0(x,\mu)+Q_1(x,\mu)+\cdots+Q_N(x,\mu) \tag{3.5}$$

for which,

$$Q_0(x,\mu)=\frac{1}{\sqrt{\mu}}sin\left(\frac{\sqrt{\mu}}{\alpha}x^{\alpha}\right) \quad for \quad x\geq 0 \tag{3.6}$$

$$Q_k(x,\mu)=\frac{1}{\sqrt{\mu}}\int_{ka}^{x} sin\left(\frac{\sqrt{\mu}}{\alpha}(x^{\alpha}-t^{\alpha})\right)q(t)Q_{k-1}(t-a,\mu)d_{\alpha}t \tag{3.7}$$

for $x\geq ka$, and $Q_k(x,\mu)=0$ for $x\leq ka$.

Now, for $k\geq 1$, and from (3.7) and by Definition 2.1 we have,

$$D_x^{\alpha}Q_k(x,\mu)=\int_{ka}^{x} cos\left(\frac{\sqrt{\mu}}{\alpha}(x^{\alpha}-t^{\alpha})\right)q(t)Q_{k-1}(t-a,\mu)d_{\alpha}t \quad for\ x\geq ka. \tag{3.8}$$

From (3.7) we obtained

$$\begin{aligned} Q_1(x,\mu) &= \frac{1}{\sqrt{\mu}}\int_{a}^{x} sin\left(\frac{\sqrt{\mu}}{\alpha}(x^{\alpha}-t^{\alpha})\right)q(t)Q_0(t-a,\mu)d_{\alpha}t \\ &= \frac{1}{\mu}\int_{a}^{x} sin\left(\frac{\sqrt{\mu}}{\alpha}(x^{\alpha}-t^{\alpha})\right).sin\left(\frac{\sqrt{\mu}}{\alpha}(t^{\alpha}-a^{\alpha})\right)q(t)d_{\alpha}t \end{aligned} \tag{3.9}$$

so that

$$\begin{aligned} Q_1(x,\mu) &= -\frac{1}{2\mu}cos\left(\frac{\sqrt{\mu}}{\alpha}(x^{\alpha}-a^{\alpha})\right)\int_{a}^{x} q(t)d_{\alpha}t \\ &+\frac{1}{2\mu}\int_{a}^{x} cos\left(\frac{\sqrt{\mu}}{\alpha}(2t^{\alpha}-x^{\alpha}-a^{\alpha})\right)q(t)d_{\alpha}t \end{aligned} \tag{3.10}$$

then, we have from (3.10) that

$$\begin{aligned} D_x^{\alpha}(Q_1(x,\mu)) &= \frac{1}{2\sqrt{\mu}}sin\left(\frac{\sqrt{\mu}}{\alpha}(x^{\alpha}-a^{\alpha})\right)\int_{a}^{x} q(t)d_{\alpha}t \\ &+\frac{1}{2\sqrt{\mu}}\int_{a}^{x} sin\left(\frac{\sqrt{\mu}}{\alpha}(2t^{\alpha}-x^{\alpha}-a^{\alpha})\right)q(t)d_{\alpha}t. \end{aligned} \tag{3.11}$$

Now, from (3.8) -(3.10), it can be shown that

$$Q_k^{(j)}(x,\mu)=O\left((\sqrt{\mu})^{j-k-1}e^{\left(\frac{1}{\alpha}|Im\sqrt{\mu}|(x^{\alpha}-(ka)^{\alpha})\right)}\right) \tag{3.12}$$

3.2. The Asymptotic Formulae

Let us denote the characteristics function of $L_j(q)$ by $W_j(\mu)$, $j=0{,}1$, and $W_j(\mu)=Q^{(j)}(\pi,\mu)$. Since $Q^{(j)}(\pi,\mu)$ are entire in μ of order $\frac{1}{2}$ so also the $W_j(\mu)$.

We drived the asymptotical formulae for the SLP $L_j(q)$ for $|\sqrt{\mu}|\to\infty$ from (3.7), (3.11) and (3.12) as follows,

$$\begin{aligned} W_0(\mu) &= Q(\pi,\mu)=Q_0(\pi,\mu)+Q_1(\pi,\mu)+\cdots+Q_N(\pi,\mu) \\ &= \frac{1}{\sqrt{\mu}}sin\left(\frac{\sqrt{\mu}}{\alpha}\pi^{\alpha}\right)-\frac{1}{2\mu}cos\left(\frac{\sqrt{\mu}}{\alpha}(\pi^{\alpha}-a^{\alpha})\right)\int_{a}^{\pi} q(t)d_{\alpha}t \\ &+o\left(\mu^{-1}e^{\left(\frac{1}{\alpha}|Im\sqrt{\mu}|(\pi^{\alpha}-a^{\alpha})\right)}\right) \end{aligned} \tag{3.13}$$

so that we have

$$\begin{aligned} W_1(\mu) &= cos\left(\frac{\sqrt{\mu}}{\alpha}\pi^{\alpha}\right)+\frac{1}{2\sqrt{\mu}}sin\left(\frac{\sqrt{\mu}}{\alpha}(\pi^{\alpha}-a^{\alpha})\right)\int_{a}^{\pi} q(t)d_{\alpha}t \\ &+o\left(\mu^{-\frac{1}{2}}e^{\left(\frac{1}{\alpha}|Im\sqrt{\mu}|(\pi^{\alpha}-a^{\alpha})\right)}\right) \end{aligned} \tag{3.14}$$

The asymptotical formulae for the eigenvalues of the $L_j(q)$ for $\mu_{nj} = \rho_{nj}^2$ as $n \to \infty$ were also obtained using (3.13) and (3.14) and the method described in [37] as

$$\rho_{n_0} = \frac{\alpha n}{\pi^{\alpha-1}} + \frac{1}{2n\pi} cos\left(\frac{n}{\pi^{\alpha-1}} a^{\alpha}\right) \int_a^{\pi} q(t) d_{\alpha} t + O\left(\frac{1}{n}\right) \tag{3.15}$$

and

$$\rho_{n_1} = \frac{\alpha(n-\frac{1}{2})}{\pi^{\alpha-1}} + \frac{1}{2(n-\frac{1}{2})\pi} cos\left(\frac{n}{\pi^{\alpha-1}} a^{\alpha}\right) \int_a^{\pi} q(t) d_{\alpha} t + O\left(\frac{1}{n}\right) \tag{3.16}$$

3.3. The Specification of the Spectrum

The Specification of the Spectrum is one of the spectral properties, as for the spectrum corresponding to a problem for a Sturm-Liouville operator for the interval $(0, \infty)$, it means the complement of the set of points in a neighborhood of which the spectral function $W_j(\mu)$ is constant, as such, to affirm applying the conformable derivative operator, we obtained and proved the specification of the spectrum for the characteristics function as it follows.

Lemma 3.1. The specification of the spectrum $\{\mu_{nj}\}_{n\geq 1}$, $j = 0,1$ uniquely determines the characteristics function $W_j(\mu)$ by the formulas

$$W_0(\mu) = \frac{\pi^{3\alpha-2}}{\alpha^3} \prod_{n=1}^{\infty} \left(\frac{\mu_{n0}-\mu}{n^2}\right) \tag{3.17}$$

and

$$W_1(\mu) = \frac{\pi^{2\alpha-2}}{\alpha^2} \prod_{n=1}^{\infty} \frac{(\mu_{n1}-\mu)}{\left(n-\frac{1}{2}\right)^2} \tag{3.18}$$

Proof. Being $W_j(\mu)$ entire in μ of order $\frac{1}{2}$, then by Hadamard's factorization theorem [51], it can be uniquely determined up to a multiplicative constant by its zeros, that is

$$W_0(\mu) = C \prod_{n=1}^{\infty} \left(1 - \frac{\mu}{\mu_{n0}}\right)$$

Now, since

$$sin\, z = z \prod_{n=1}^{\infty} \left(1 - \frac{z^2}{(k\pi)^2}\right)$$

it implies that

$$\widetilde{W}_0(\mu) = \frac{sin\left(\frac{\sqrt{\mu}}{\alpha}\pi^{\alpha}\right)}{\sqrt{\mu}} = \frac{\pi^{\alpha}}{\alpha} \prod_{n=1}^{\infty} \left(1 - \frac{\mu\pi^{2\alpha-2}}{\alpha^2 n^2}\right) = \frac{\pi^{\alpha}}{\alpha} \prod_{n=1}^{\infty} \left(1 - \frac{\mu}{\left(\frac{\alpha^2}{\pi^{2\alpha-2}}\right)n^2}\right)$$

Then,

$$\frac{W_0(\mu)}{\widetilde{W}_0(\mu)} = C \frac{\alpha^3}{\pi^{3\alpha-2}} \prod_{n=1}^{\infty} \frac{n^2}{\mu_{n0}} \prod_{n=1}^{\infty} \left(1 + \frac{\mu_{n0} - \left(\frac{\alpha^2}{\pi^{2\alpha-2}}\right)n^2}{\left(\frac{\alpha^2}{\pi^{2\alpha-2}}\right)n^2 - \mu}\right)$$

Now,

$$\lim_{\mu\to-\infty} \frac{W_0(\mu)}{\widetilde{W}_0(\mu)} = 1 \text{ and } \lim_{\mu\to-\infty} \prod_{n=1}^{\infty} \left(1 + \frac{\mu_{n0} - \left(\frac{\alpha^2}{\pi^{2\alpha-2}}\right)n^2}{\left(\frac{\alpha^2}{\pi^{2\alpha-2}}\right)n^2 - \mu}\right) = 1$$

then,

$$C = \frac{\pi^{3\alpha-2}}{\alpha^3} \prod_{n=1}^{\infty} \frac{\mu_{n0}}{n^2}$$

and eventually, we reached

$$W_0(\mu) = C \prod_{n=1}^{\infty} \left(1 - \frac{\mu}{\mu_{n0}}\right) = \frac{\pi^{3\alpha-2}}{\alpha^3} \prod_{n=1}^{\infty} \left(\frac{\mu_0-\mu}{n^2}\right).$$

This completes the proof of the first case, that is for $j = 0$. The proof for the second case, $j = 1$, similarly follows.

3.4. Regge-type Boundary Value Problem

The problem considered in this work, (3.3), can also be extended to Regge-type boundary value problem $L(q)$, that is,

$$y(0) = 0, \quad D_x^\alpha y(\pi) + i\rho y(\pi) = 0.$$

In such a case, the characteristic function will be of the form;

$$S(\mu) = W_1(\mu) + i\rho W_0(\mu) \tag{3.19}$$

which is, also, entire in μ. Now from (3.5) we have

$$S(\mu) = S_0(\mu) + S_1(\mu) + \cdots + S_N(\mu) \tag{3.20}$$

where $S_k(\mu) = D_x^\alpha Q_k(\mu) + i\sqrt{\mu} Q_k(\mu)$ which implies that

$$S_0(\mu) = cos\left(\frac{\sqrt{\mu}}{\alpha}\pi^\alpha\right) + i\, sin\left(\frac{\sqrt{\mu}}{\alpha}\pi^\alpha\right) = e^{i\left(\frac{\sqrt{\mu}}{\alpha}\pi^\alpha\right)}$$

From (3.7) and (3.8) we obtained

Consider $\tilde{S}(\mu)$ as the characteristic function of $\tilde{L} = L(\tilde{q})$. It implies from (3.19) that $\tilde{S}(\mu) = e^{\frac{i\sqrt{\mu}}{\alpha}\pi^\alpha}$.

(3.21)

Theorem 4.1. If $\mu_{nj} = \tilde{\mu}_{nj}$, $\forall \;\; n \geq 1,\; for\; j = 0{,}1$, then the potential $q(x) = 0$ almost everywhere on (a, π).

Proof. From lemma 3.1 and the special infinite series, we have

(3.22)

$$W_0(\mu) = \frac{sin\left(\frac{\sqrt{\mu}}{\alpha}\pi^\alpha\right)}{\sqrt{\mu}} \text{ and } W_1(\mu) = cos\left(\frac{\sqrt{\mu}}{\alpha}\pi^\alpha\right)$$

as such, $S(\mu) = e^{\frac{i\sqrt{\mu}}{\alpha}\pi^\alpha}$. From (3.20), we can deduce that

(3.23)

$$S_1(\mu) = -S^+(\mu) \tag{4.1}$$

where, $S^+(\mu) = \sum_{k=2}^{N} \quad S_k(\mu)$, $k \geq 2$ with $S^+(\mu) = 0$, $k = 1$.

Taking $\mu_{nj} = \tilde{\mu}_{nj}$, (3.15) and (3.16) implies that $\int_a^\pi \quad q(t) d_\alpha t = 0$, then (3.22) yields

tential

$$S_1(\mu) = -\frac{1}{2i\sqrt{\mu}} e^{\left(\frac{i\sqrt{\mu}}{\alpha}(\pi^\alpha + a^\alpha)\right)} \int_a^\pi \quad q(t) e^{\left(\frac{-2i\sqrt{\mu}}{\alpha}t^\alpha\right)} d_\alpha t \tag{4.2}$$

ons. It

ed and

Let $N = 1$, i.e. $a \in [\frac{\pi}{2}, \pi]$, then $S^+(\mu) = 0$ which implies from(4.1) that $S_1(\mu) = 0$ as such, (4.2) gives, assical

esults

$$\int_a^\pi \quad q(t) e^{\left(\frac{-2i\sqrt{\mu}}{\alpha}t^\alpha\right)} d_\alpha t = 0$$

6].

To prove the uniqueness theorem, let $\{\tilde{\mu}_{nj}\}_{n\geq 1}, j = 0{,}1$, be the eigenvalues of the problems $\tilde{L}_j = L_j(\tilde{q})$ with the potential $\tilde{q}(x) = 0$, then $\tilde{\mu}_{n0} = (\frac{\alpha n}{\pi^{\alpha-1}})^2$ and $\tilde{\mu}_{n1} = (\frac{\alpha(n-\frac{1}{2})}{\pi^{\alpha-1}})^2$, for $n \geq 1$.

Consider $\tilde{S}(\mu)$ as the characteristic function of $\tilde{L} = L(\tilde{q})$. It implies from (3.19) that $\tilde{S}(\mu) = e^{\frac{i\sqrt{\mu}}{\alpha}\pi^\alpha}$.

Theorem 4.1. If $\mu_{nj} = \tilde{\mu}_{nj}$, $\forall \;\; n \geq 1,\; for\; j = 0{,}1$, then the potential $q(x) = 0$ almost everywhere on (a, π).

Proof. From lemma 3.1 and the special infinite series, we have

$$W_0(\mu) = \frac{sin\left(\frac{\sqrt{\mu}}{\alpha}\pi^\alpha\right)}{\sqrt{\mu}} \text{ and } W_1(\mu) = cos\left(\frac{\sqrt{\mu}}{\alpha}\pi^\alpha\right)$$

as such, $S(\mu) = e^{\frac{i\sqrt{\mu}}{\alpha}\pi^\alpha}$. From (3.20), we can deduce that

$$S_1(\mu) = -S^+(\mu) \tag{4.1}$$

where, $S^+(\mu)=\sum_{k=2}^{N} \quad S_k(\mu)$, $k\geq 2$ with $S^+(\mu)=0$, $k=1$.

Taking $\mu_{nj}=\tilde{\mu}_{nj}$, (3.15) and (3.16) implies that $\int_a^\pi \quad q(t)d_\alpha t=0$, then (3.22) yields

$$S_1(\mu)=-\frac{1}{2i\sqrt{\mu}}e^{\left(\frac{i\sqrt{\mu}}{\alpha}(\pi^\alpha+a^\alpha)\right)}\int_a^\pi \quad q(t)e^{\left(\frac{-2i\sqrt{\mu}}{\alpha}t^\alpha\right)}d_\alpha t \tag{4.2}$$

Let $N=1$, i.e. $a\in[\frac{\pi}{2},\pi]$, then $S^+(\mu)=0$ which implies from(4.1) that $S_1(\mu)=0$ as such, (4.2) gives,

$$\int_a^\pi \quad q(t)e^{\left(\frac{-2i\sqrt{\mu}}{\alpha}t^\alpha\right)}d_\alpha t=0$$

and the only possibility is $q(x)=0$ almost everywhere on (a,π). This completes the proof for $N=1$ and below is for $N\geq 2$.

Lemma 4.1. If the potential $q(x)=0$ almost everywhere on $(2a,\pi)$, then $q(x)=0$ almost everywhere on (a,π).

Proof. Let $q(x)=0$ almost everywhere on $(2a,\pi)$, from (3.21) $S_k(\mu)=0$ for $k\geq 2$ and hence $S^+(\mu)=0$, then from (4.1) we have $S_1(\mu)=0$ and consequently $q(x)=0$ almost everywhere on (a,π). This completes the proof of lemma 4.1.

To make it more clear, let's consider the N in two ways; odd and even. Firstly, we will assume that $N=2M+1$, i.e. N is odd, in the following.

Lemma 4.2. Let $d=0,1,3,\ldots 2M-1$. If the potential $q(x)=0$ almost everywhere on $\left(\pi-\frac{da}{2},\pi\right)$, then $q(x)=0$ almost everywhere on $\left(\pi-\frac{(d+1)a}{2},\pi\right)$.

Proof. From the fact that $\left(\pi-\frac{da}{2},\pi\right)>2a$, it follows (3.23) that

$$S_2(\mu)=O\left(\frac{1}{\mu}\int_{2a}^{\pi-\frac{da}{2}} \quad q(t)e^{\left(\frac{i\sqrt{\mu}}{\alpha}(2t^\alpha-\pi^\alpha-(2a)^\alpha)\right)}d_\alpha t\right),\ Im\sqrt{\mu}\geq 0,\ |\sqrt{\mu}|\to\infty$$

clearly, $2t-\pi-2a\in(2a-\pi,\pi-(d+2)a)$, for $\pi-(d+2)a)\geq\pi-Na$ which yields,

$$S_2(\mu)=O\left(\frac{1}{\mu}e^{\left(\frac{-i\sqrt{\mu}}{\alpha}(\pi^\alpha-((d+2)a)^\alpha)\right)}d_\alpha t\right),\ Im\sqrt{\mu}\geq 0,\ |\sqrt{\mu}|\to\infty. \tag{4.3}$$

$S_k(\mu)$ in the equation (4.3), increase less rapidly than the right-hand side when $k\geq 2$, that is,

$$S^+(\mu)=O\left(\frac{1}{\mu}e^{\left(\frac{-i\sqrt{\mu}}{\alpha}(\pi^\alpha-((d+2)a)^\alpha)\right)}d_\alpha t\right),\ Im\sqrt{\mu}\geq 0,\ |\sqrt{\mu}|\to\infty \tag{4.4}$$

it follows from (4.1), (4.2) and (4.4) that

$$e^{\left(\frac{i\sqrt{\mu}}{\alpha}(\pi^\alpha+a^\alpha)\right)}\int_a^{\pi-\frac{da}{2}} \quad q(t)e^{\left(\frac{-2i\sqrt{\mu}}{\alpha}t^\alpha\right)}d_\alpha t=O\left(\frac{1}{\sqrt{\mu}}e^{\left(\frac{-i\sqrt{\mu}}{\alpha}(\pi^\alpha-((d+2)a)^\alpha)\right)}\right),$$

$Im\sqrt{\mu}\geq 0,\ |\sqrt{\mu}|\to\infty,$

which can be expressed as

$$e^{\left(\frac{i\sqrt{\mu}}{\alpha}(2\pi^\alpha+(1-(d+2)^\alpha)a^\alpha)\right)}\int_a^{\pi-\frac{da}{2}} \quad q(t)e^{\left(\frac{-2i\sqrt{\mu}}{\alpha}t^\alpha\right)}d_\alpha t=O\left(\frac{1}{\sqrt{\mu}}\right), \tag{4.5}$$

$Im\sqrt{\mu}\geq 0,\quad |\sqrt{\mu}|\to\infty.$

Furthermore, we have

$$\int_a^{\pi-\frac{(d+1)a}{2}} \quad q(t)e^{\left(\frac{-2i\sqrt{\mu}}{\alpha}t^\alpha\right)}d_\alpha t=O\left(e^{\left(\frac{-i\sqrt{\mu}}{\alpha}(2\pi^\alpha+(1-(d+2)^\alpha)a^\alpha\right)}d_\alpha t\right), \tag{4.6}$$

$Im\sqrt{\mu}\geq 0,\quad |\sqrt{\mu}|\to\infty.$

Now, let's define the function,

$$G(\sqrt{\mu}) = e^{\left(\frac{i\sqrt{\mu}}{\alpha}(2\pi^{\alpha}+(1-(d+2)^{\alpha})a^{\alpha})\right)} \int_{\pi-\frac{(d+1)a}{2}}^{\pi-\frac{da}{2}} q(t)e^{\left(\frac{-2i\sqrt{\mu}}{\alpha}t^{\alpha}\right)} d_{\alpha}t \tag{4.7}$$

which is entirely in μ. Clearly, $G(\sqrt{\mu}) = O(1)$ for $Im\sqrt{\mu} \leq 0$, also, it follows from (4.5) and (4.6) that $G(\sqrt{\mu}) = O(1)$ for $Im\sqrt{\mu} \geq 0$. Since the function $G(\sqrt{\mu})$ is entire bounded it follows from Liouville's theorem [51] that $G(\sqrt{\mu}) = c$, where c is a constant. From $G(\sqrt{\mu}) = o(1)$ for real $\sqrt{\mu}$, $|\sqrt{\mu}| \to \infty$, then $G(\sqrt{\mu}) = 0$, hence (4.7) gives

$$\int_{\pi-\frac{(d+1)a}{2}}^{\pi-\frac{va}{2}} q(t)e^{\left(\frac{-2i\sqrt{\mu}}{\alpha}t^{\alpha}\right)} d_{\alpha}t = 0$$

which gives $q(x) = 0$ almost everywhere on $\left(\pi - \frac{(d+1)a}{2}, \pi - \frac{da}{2}\right)$ which completes the proof.

We obtained $q(x) = 0$ almost everywhere on $(\pi - Ma, \pi)$ by applying lemma 4.2 successively for $d = 0,1,3, \dots 2m - 1$.

We noted that lemma 4.2 is for the odd case. Now, let $d \geq 2M$ such that N is even.

Lemma 4.3. If the potential $q(x) = 0$ almost everywhere on $\pi - Ma, \pi$, then $q(x) = 0$ almost everywhere on $\left(\frac{(M+2)a}{2}, \pi\right)$.

Proof. If $k \geq M + 2$, we then have $\pi - Ma - ka \leq \pi - (N + 1)a \leq 0$ and hence, $S_{\mu} = 0$ for $k \geq M + 2$.

According to (3.23), for $k = 2,3,4, \dots, M + 1$,

$$S_k(\mu) = O\left((\sqrt{\mu})^{-k} \int_{ka}^{\pi-Ma} q(t)e^{\left(\frac{-i\sqrt{\mu}}{\alpha}(2t^{\alpha}-\pi^{\alpha}-(ka)^{\alpha})\right)} d_{\alpha}t\right), \tag{4.8}$$

for $Im\sqrt{\mu} \geq 0, \quad |\sqrt{\mu}| \to \infty$.

Being $2t - \pi - ka \leq 0$, it follows that

$$S_k(\mu) = O\left((\sqrt{\mu})^{-k} e^{\left(\frac{i\sqrt{\mu}}{\alpha}(\pi^{\alpha}-(ka)^{\alpha})\right)}\right), \tag{4.9}$$

for $Im\sqrt{\mu} \geq 0, \quad |\sqrt{\mu}| \to \infty, \; for \; k = 2,3,4, \dots, M + 1$ and hence

$$S^{+}(\mu) = O\left(\frac{1}{\mu} e^{\left(\frac{i\sqrt{\mu}}{\alpha}(\pi^{\alpha}-((M+1)a)^{\alpha})\right)}\right), \tag{4.10}$$

for $Im\sqrt{\mu} \geq 0, \quad |\sqrt{\mu}| \to \infty$,

As a result of (4.1), (4.2) and (4.9) we obtained

$$e^{\left(\frac{i\sqrt{\mu}}{\alpha}(\pi^{\alpha}+a^{\alpha})\right)} \int_{a}^{\pi-Ma} q(t)e^{\left(\frac{-2i\sqrt{\mu}}{\alpha}t^{\alpha}\right)} d_{\alpha}t = O\left(\frac{1}{\sqrt{\mu}} e^{\left(\frac{i\sqrt{\mu}}{\alpha}(\pi^{\alpha}-((M+1)a)^{\alpha})\right)}\right),$$

$Im\sqrt{\mu} \geq 0, \; |\sqrt{\mu}| \to \infty$ or, which is equivalent to,

$$e^{\left(\frac{i\sqrt{\mu}}{\alpha}((M+2)a)^{\alpha}\right)} \int_{a}^{\pi-Ma} q(t)e^{\left(\frac{-2i\sqrt{\mu}}{\alpha}t^{\alpha}\right)} d_{\alpha}t = O\left(\frac{1}{\sqrt{\mu}}\right), \; Im\sqrt{\mu} \geq 0, \; |\sqrt{\mu}| \to \infty \tag{4.11}$$

furthermore,

$$\int_{a}^{\frac{(M+2)a}{2}} q(t)e^{\left(\frac{-2i\sqrt{\mu}}{\alpha}t^{\alpha}\right)} d_{\alpha}t = O\left(e^{\left(\frac{-i\sqrt{\mu}}{\alpha}((M+2)a)^{\alpha}\right)}\right) \tag{4.12}$$

$Im\sqrt{\mu} \geq 0, \; |\sqrt{\mu}| \to \infty$

Let us denote

$$G^{*}(\sqrt{\mu}) = e^{\left(\frac{i\sqrt{\mu}}{\alpha}((M+2)a)^{\alpha}\right)} \int_{\frac{(M+2)a}{2}}^{\pi-Ma} q(t)e^{\left(\frac{-2i\sqrt{\mu}}{\alpha}t^{\alpha}\right)} d_{\alpha}t$$

Which is entire in μ and $G^*(\sqrt{\mu}) = O(1)$ for $Im\sqrt{\mu} \leq 0$. In view of (4.11) and (4.12), $G^*(\sqrt{\mu}) = O(1)$ for $Im\sqrt{\mu} \geq 0$. Therefore,as in the above similar case, $G^*(\sqrt{\mu}) = C$, since $G^*(\sqrt{\mu}) = o(1)$ for real $\sqrt{\mu}$, $|\sqrt{\mu}| \to \infty$, then $G^*(\sqrt{\mu}) = 0$, that is,

$$\int_{\frac{(M+2)a}{2}}^{\pi-\frac{Ma}{2}} q(t)e^{\left(\frac{-2i\sqrt{\mu}}{\alpha}t^{\alpha}\right)}d_\alpha t = 0.$$

This implies that $q(x) = 0$ almost everywhere on $\left(\frac{(M+2)a}{2}, \pi - Ma\right)$ which completes the proof.

It has been proved that $q(x) = 0$ almost everywhere on $(2a, \pi)$ for $M = 1$ or $M = 2$. According to lemma 4.1, $(x) = 0$ almost everywhere on (a, π). Therefore, theorem 4.1 is proved for $M = 1$ and $M = 2$.

Let now $M \geq 3$. Fix $d = 5,6,7,8, \ldots, M + 2$. Let $l = \frac{(d+1)}{2}$. Clearly, $l < d$.

Lemma 4.4. If the potential $q(x) = 0$ almost everywhere on $\left(\frac{da}{2}, \pi\right)$, then $q(x) = 0$ almost everywhere on $\left(\frac{la}{2}, \pi\right)$.

Proof. Considering $\frac{d}{2} - k \leq \frac{d}{2} - l \leq 0$ for $k \geq l$, we have $S_k(\mu) = 0$ for $k \geq l$. By virtue of (3.23)

$$S_k(\mu) = O\left((\sqrt{\mu})^{-k} \int_{ka}^{\frac{da}{2}} q(t)e^{\left(\frac{-i\sqrt{\mu}}{\alpha}(2t^{\alpha}-\pi^{\alpha}-(ka)^{\alpha})\right)}d_\alpha t\right), \tag{4.13}$$

for $Im\sqrt{\mu} \geq 0, \quad |\sqrt{\mu}| \to \infty, \quad k = 2,3,4, \ldots, l - 1$. Now, $2t - \pi - ka < 0$ that is, the exponent is decreasing for $Im\sqrt{\mu} > 0$, then,

$$S_k(\mu) = O\left((\sqrt{\mu})^{-k} e^{\left(\frac{i\sqrt{\mu}}{\alpha}(\pi^{\alpha}-(ka)^{\alpha})\right)}\right), \tag{4.14}$$

for $Im\sqrt{\mu} \geq 0, \quad |\sqrt{\mu}| \to \infty, \quad k = 2,3,4, \ldots, l - 1$, therefore,

$$S^+(\mu) = O\left(\frac{1}{\mu} e^{\left(\frac{i\sqrt{\mu}}{\alpha}(\pi^{\alpha}-((l-1)a)^{\alpha})\right)}\right), \; Im\sqrt{\mu} \geq 0, \quad |\sqrt{\mu}| \to \infty, \tag{4.15}$$

from (4.1), (4.2) and (4.15) we obtained

$$e^{\left(\frac{i\sqrt{\mu}}{\alpha}(la)^{\alpha}\right)} \int_0^{\frac{da}{2}} q(t)e^{\left(\frac{-2i\sqrt{\mu}}{\alpha}t^{\alpha}\right)}d_\alpha t = O\left(\frac{1}{\sqrt{\mu}}\right) \tag{4.16}$$

for $Im\sqrt{\mu} \geq 0, \quad |\sqrt{\mu}| \to \infty$. moreover,

$$\int_a^{\frac{la}{2}} q(t)e^{\left(\frac{-2i\sqrt{\mu}}{\alpha}t^{\alpha}\right)}d_\alpha t = O\left(e^{\left(\frac{-i\sqrt{\mu}}{\alpha}(la)^{\alpha}\right)}\right) \; for \; Im\sqrt{\mu} \geq 0, \; |\sqrt{\mu}| \to \infty. \tag{4.17}$$

$Im\sqrt{\mu} \geq 0, \; |\sqrt{\mu}| \to \infty$ Let us denote,

$$G^{**}(\sqrt{\mu}) = e^{\left(\frac{i\sqrt{\mu}}{\alpha}((la)^{\alpha})\right)} \int_{\frac{(la)}{2}}^{\frac{da}{2}} q(t)e^{\left(\frac{-2i\sqrt{\mu}}{\alpha}t^{\alpha}\right)}d_\alpha t$$

Which is entire in μ as well, and $G^{**}(\sqrt{\mu}) = O(1)$ for $Im\sqrt{\mu} \leq 0$. Considering (4.16) and (4.17), $G^{**}(\sqrt{\mu}) = O(1)$ for $Im\sqrt{\mu} \geq 0$. consequently $G^{**}(\sqrt{\mu}) = o(1)$ for real $\sqrt{\mu}$, $|\sqrt{\mu}| \to \infty$, therefore $G^{**}(\sqrt{\mu}) = 0$ and as a result of which $q(x) = 0$ almost everywhere on $\left(\frac{la}{2}, \frac{da}{2}\right)$. Hence lemma 4.4 is proved.

Applying the lemma 4.4 many times consecutively starting from $d = M + 2$, we obtain that the potential $q(x) = 0$ almost everywhere on $(2a, \pi)$. Therefore, due to lemma 4.1, $q(x) = 0$ almost everywhere on (a, π). Hence, this completes the proof of the theorem.

It can be seen that, with regard to our problem we proved the existence of the solution, the spectral properties, and also the uniqueness theorem in detail using the proposed fractional approach and these completes our work.

5. Conclusion

In conclusion, the method of conformable derivative, which is more accessible to the other existing fractional derivative approaches due to its satisfying properties, has been used in this work as a derivative operator with which we show and express the possibility of solving the inverse SLP with constant delay. The problem discussed is under mixed boundary conditions and in each case, a result is obtained. Also, the specifications of the respective spectrums are given affirming the solution obtained. The asymptotics of the eigenvalues were extended to the Regge-type boundary value problem and analyzed. The proof of the uniqueness theorem is similar to the one in the classical case of the problem. Similar problems with different boundary conditions can be discussed under this new fractional derivative approach with their corresponding spectral properties and this will lead to providing an entire phase of fractional SLP.

Acknowledgments

The authors are grateful to the academic colleagues and the reviewers for their ideas and reviews that improved and aided the completion and presentation of this work.

Conflict of Interest

The authors have no competing interests to declare that are relevant to the content of this article.

Funding

No funding was received for conducting this study.

References

1.Kilbas AA, Trujillo JJ, Srivastava H. Theory and applications of fractional differential equations. Elsevier 2006; 39: 52–7. https://doi.org/10.3182/20060719-3-PT-4902.00008

2.Miller KS, Ross B. An introduction to the fractional calculus and fractional differential equations. John Wiley & Sons, New York, NY, USA; 1993.

3.Ortigueira MD, Tenreiro Machado JA. What is a fractional derivative? J Comput Phys. 2015; 293: 4-13. https://doi.org/10.1016/j.jcp.2014.07.019

4.Khalil R, Al Horani M, Yousef A, Sababheh M. A new definition of fractional derivative. J Comput Appl Math. 2014; 264: 65-70. https://doi.org/10.1016/j.cam.2014.01.002

5.Abdeljawad T. On conformable fractional calculus. J Comput Appl Math. 2015; 279: 57-66. https://doi.org/10.1016/j.cam.2014.10.016

6.Atangana A, Baleanu D, Alsaedi A. New properties of conformable derivative. Open Mathematics. 2015; 13(1): 889-98. https://doi.org/10.1515/math-2015-0081

7.Abdelhakim AA, Machado JAT. A critical analysis of the conformable derivative. Nonlinear Dyn. 2019; 95: 3063-73. https://doi.org/10.1007/s11071-018-04741-5

8.Baleanu D, Fernandez A. On fractional operators and their classifications. Mathematics. 2019;

7(9): 830. https://doi.org/10.3390/math7090830

9.Tarasov VE. No nonlocality. No fractional derivative. Commun Nonlinear Sci Numer Simul. 2018; 62: 157-63. https://doi.org/10.1016/j.cnsns.2018.02.019

10.Allahverdiev BP, Tuna H, Yalçinkaya Y. Conformable fractional Sturm-Liouville equation. Math Methods Appl Sci. 2019; 42: 3508-26. https://doi.org/10.1002/mma.5595

11.Ozarslan R, Bas E, Baleanu D. Representation of solutions for Sturm–Liouville eigenvalue problems with generalized fractional derivative. Chaos. 2020; 30(3): 033137. https://doi.org/10.1063/1.5131167

12.Sadabad MK, Akbarfam AJ, Shiri B. A numerical study of eigenvalues and eigenfunctions of fractional Sturm-Liouville problems via Laplace transform. Indian J Pure Appl Math. 2020; 51: 857-68. https://doi.org/10.1007/s13226-020-0436-2

13.Rivero M, Trujillo J, Velasco M. A fractional approach to the Sturm-Liouville problem. Open Phys. 2013; 11: 1246–54. https://doi.org/10.2478/s11534-013-0216-2

14.Sa'idu A, Koyunbakan H, Transmutation of conformable sturm-liouville operator with exactly solvable potential. Filomat. 2023; 37: 338390.

15.Wang WC. Some notes on conformable fractional Sturm–Liouville problems. Bound Value Probl. 2021; 2021: 1-8. https://doi.org/10.1186/s13661-021-01581-y

16.Al-Refai M, Abdeljawad T. Fundamental results of conformable Sturm-Liouville eigenvalue problems. Complexity. 2017; 2017: 1–7. https://doi.org/10.1155/2017/3720471

17.Anderson D, Camrud E, Ulness D. On the nature of the conformable derivative and its applications to physics. J Fract Calc Appl. 2019; 10(2): 92-135.

18.Klimek M, Agrawal OP. Fractional https://doi.org/10.1016/j.camwa.2012.12.011 sturm–liouville problem. Comput Math Appl. 2013; 66: 795-812.

19.Koyunbakan H, Shah K, Abdeljawad T. Well-posedness of inverse sturm–liouville problem with fractional derivative. Qual Theory Dyn Syst. 2023; 22(1): Article 23. https://doi.org/10.1007/s12346-022-00727-2

20.Liu T, Yu J, Zheng Y, Liu C, Yang Y, Qi Y. A nonlinear multigrid method for the parameter identification problem of partial differential equations with constraints. Mathematics. 2022; 10(16): 2938. https://doi.org/10.3390/math10162938

21.Liu T, Xia K, Zheng Y, Yang Y, Qiu R, Qi Y, et al. A homotopy method for the constrained inverse problem in the multiphase porous media flow. Processes. 2022; 10(6): 1143. https://doi.org/10.3390/pr10061143

22.Liu T. Parameter estimation with the multigrid-homotopy method for a nonlinear diffusion equation. J Comput Appl Math. 2022; 413: 114393. https://doi.org/10.1016/j.cam.2022.114393

23.Liu T. Porosity reconstruction based on Biot elastic model of porous media by homotopy *perturbation method. Chaos Solitons Fractals. 2022; 158: 112007. https://doi.org/10.1016/j.chaos.2022.112007*

24.Liu T. A wavelet multiscale-homotopy method for the parameter identification problem of partial differential equations. Comput Math Appl. 2016; 71: 1519-23. https://doi.org/10.1016/j.camwa.2016.02.036

25.Liu T, Xia K, Zheng Y, Yang Y, Qiu R, Qi Y, et al. A homotopy method for the constrained inverse problem in the multiphase porous media flow. Processes. 2022; 10(6): 1143. https://doi.org/10.3390/pr10061143

26.Ambarzumian V. Über eine Frage der Eigenwerttheorie. Z. Physik 1929; 53: 690–5. https://doi.org/10.1007/BF01330827

27.Chern H-H, Law CK, Wang H-J. Extension of ambarzumyan's theorem to general boundary conditions. J Math Anal Appl. 2001; 263: 33342. https://doi.org/10.1006/jmaa.2001.7472

28.Chuanfu Y, Xiaoping Y. Ambarzumyan's theorem with eigenparameter in the boundary conditions. Acta Mathematica Scientia. 2011; 31: 1561–8. https://doi.org/10.1016/S0252-9602(11)60342-1

29.Amirov R, Ergun A, Durak S. Half-inverse problems for the quadratic pencil of the Sturm–Liouville equations with impulse. Numer Methods Partial Differ Equ. 2021; 37: 915–24. https://doi.org/10.1002/num.22559

30.Buterin SA, Shieh CT. Incomplete inverse spectral and nodal problems for differential pencils. Results Math. 2012; 62: 167-79. https://doi.org/10.1007/s00025-011-0137-6

31.Cheng YH, Law CK, Tsay J. Remarks on a new inverse nodal problem. J Math Anal Appl. 2000; 248: 145–55. https://doi.org/10.1006/jmaa.2000.6878

32.Guliyev NJ. Inverse eigenvalue problems for sturm–liouville equations with spectral parameter linearly contained in one of the boundary conditions. Inverse Probl. 2005; 21: 1315-30. https://doi.org/10.1088/0266-5611/21/4/008

33.Gulsen T, Yilmaz E, Akbarpoor S. Numerical investigation of the inverse nodal problem by chebisyhev interpolation method. Therm Sci. 2018; 22: 123–36. https://doi.org/10.2298/TSCI170612278G

34.Mosazadeh S. A new approach to uniqueness for inverse sturm--liouville problems on finite intervals. Turkish J Math. 2017; 41: 1224–34. https://doi.org/10.3906/mat-1609-38

35.Sadovnichii VA, Sultanaev YaT, Akhtyamov AM. Solvability theorems for an inverse nonself-adjoint Sturm-Liouville problem with nonseparated boundary conditions. Differ Equ. 2015; 51(6): 717-25. https://doi.org/10.1134/S0012266115060026

36.Freiling G, Yurko VA. Inverse problems for Sturm-Liouville differential operators with a constant delay. Appl Math Lett. 2012; 25: 19992004. https://doi.org/10.1016/j.aml.2012.03.026.

37.Freiling G, Yurko VA. Inverse Sturm-Liouville problems and their applications. Huntington:

NOVA Science Publishers; 2001.

38.Koyunbakan H, Mosazadeh S. Inverse nodal problem for discontinuous sturm–liouville operator by new Prüfer Substitutions. Math Sci. 2021; 15: 387–94. https://doi.org/10.1007/s40096-021-00383-8

39.Adalar İ, Ozkan AS. Inverse problems for a Fractional Sturm-Liouville operators. J Inverse Ill Posed Probl. 2020; 28: 775-82. https://doi.org/10.1515/jiip-2019-0058

40.Çakmak Y. Inverse nodal problem for a conformable fractional diffusion operator. Inverse Probl Sci Eng. 2021; 29: 1308–22. https://doi.org/10.1080/17415977.2020.1847103

41.Mortazaasl H, Jodayree Akbarfam A. Trace formula and inverse nodal problem for a conformable fractional sturm-liouville problem. Inverse Probl Sci Eng. 2020; 28: 524-55. https://doi.org/10.1080/17415977.2019.1615909

42.Sa'idu A, Koyunbakan H. Inverse fractional Sturm-Liouville problem with eigenparameter in the boundary conditions. Math Methods Appl Sci. 2022; 45: 1–10. https://doi.org/10.1002/mma.8433

43.Buterin SA, Yurko VA. An inverse spectral problem for Sturm–Liouville operators with a large constant delay. Anal Math Phys. 2019; 9: 1727. https://doi.org/10.1007/s13324-017-0176-6

44.Bondarenko N, Yurko V. An inverse problem for sturm–iiouville differential operators with deviating argument. Appl Math Lett. 2018; 83: 140–4. https://doi.org/10.1016/j.aml.2018.03.025

37

45.Buterin S, Vasilev S. An inverse sturm--liouville-type problem with constant delay and non-zero initial function. ArXiv Preprint 2023.

46.Myshkis AD. Linear differential equations with retarded argument. Moscow: Nauka; 1972.

47.Norkin S. Second order differential equations with a delay argument. Moscow: Nauka; 1965.

48.Yang CF. Inverse nodal problems for the Sturm–Liouville operator with a constant delay. J Differ Equ. 2014; 257: 1288–306. https://doi.org/10.1016/j.jde.2014.05.011

49.Yang CF. Trace and inverse problem of a discontinuous Sturm–Liouville operator with retarded argument. J Math Anal Appl. 2012; 395: 30–41. https://doi.org/10.1016/j.jmaa.2012.04.078

50.Bayramov A, Öztürk Uslu S. Computation of eigenvalues and eigenfunctions of a discontinuous boundary value problem with retarded argument. Appl Math Comput. 2007; 191: 592–600. https://doi.org/10.1016/j.amc.2007.02.118

51.Conway JB. Functions of One Complex Variable, second ed., vol. I, Springer-Verlag, New York, 1995.

ISSN 2249-4278

On the G′ /G Expansion Method Applied to (2+1)-Dimensional Asymmetric-Nizhnik-Novikov-Veselov Equation

S.M. Mabrouk and A.S. Rashed

Department of Physics and Engineering Mathematics, Faculty of Engineering, Zagazig University, AlSharqia, Egypt

Abstract:

In this paper, the G′ /G expansion method is applied to the (2+1)-dimensional Asymmetric-Nizhnik-Novikov-Veselov equation (ANNV). The motivation is creating new families of solitary waves. The system of equations has been combined in one partial differential equation (PDE) and the traveling wave variable has been applied to transform the resultant equation into an ordinary differential equation (ODE). The homogenous balance condition has been applied to determine the truncation variable of the G'/Gg expansion. Four cases are created according to the appropriate choice of the arbitrary constants relations. For each case, some new solitary wave solutions including solitons and kinks represented by trigonometric, hyperbolic, logarithmic, polynomial, and combinations of these functions.

Keywords: ANNV equation Soliton solution G'/G expansion method

1. Introduction

Mathematical models that take into account nonlinearity in the dynamics of a system are referred to as nonlinear evolution equations. These models are used to represent the change that occurs in a system over time. These equations are very important in a variety of scientific fields, including engineering, biology, and physics, among others [1-4]. In these areas, the ability to understand and analyze the behavior of nonlinear evolution equations has major consequences for the ability to forecast and regulate complex processes. The purpose of this study article is to investigate the applications of one of the well-known nonlinear evolution equations Asymmetric - Nizhnik - Novikov - Veselov equation in a variety of fields and to emphasize the significance of these equations in terms of comprehending events that occur in the real world.

The Asymmetric - Nizhnik - Novikov - Veselov equation is a two-dimensional KdV equation described by the system of equations:

$$u_x - v_y = 0 \tag{1.1a}$$

$$u_t - 3(uv)_x + u_{xxx} = 0 \tag{1.1b}$$

This system of equations first derived by Boiti *et al.* [5] is a model for an incompressible fluid where u and v are the components of the dimensionless velocity [6]. ANNV equations are also obtained from a symmetry constraint of the Kadomtsev-Petviashvili (KP) equation [7, 8]. The system of equations (1.1a) and (1.1b) has been widely investigated from various perspectives, such as the study of its Painlevé property [9], Lie symmetries [10, 11] and solutions using arbitrary exponential functions [12]. The conservation laws forms of this equation were also studied in [13] while iterative solutions based on Darboux and Bäcklund transformations were presented in [14, 15]. Its exact solution using a separation of variable approach was also considered in [16-19]. Equations (1.1a) and (1.1b) are here reduced to a single equation through the transformations; $v = \omega_x$ and $u = \omega_y$ giving;

$$\omega_{yt} + \omega_{xxxy} - 3\omega_{xy}\omega_x - 3\omega_y\omega_{xx} = 0 \tag{1.2}$$

In [20], multi-periodic wave solutions were constructed for Eq. (1.2) using Hirota's bilinear method and Riemann theta function while in [21] new solutions were obtained through a Bäcklund transformation and a modified Clarkson direct method. New exact solutions of Eq. (1.2) were obtained using Bell exponential polynomial in [22] or through a linearizing function having a Miura form in [23]. Notice that most of the quoted previous work is concerned with the similarity reduction of Eq. (1.2) while the reduction of its Lax pair is much less frequent [11]. Generally, evolution equations were heavily discussed using numerous techniques such as Lie infinitesimals and hidden symmetries [24-33], Lax pair and group method [34-38], numerical techniques [39-44], direct traveling wave methods [26, 45-51].

This research is organized as follows. Section 2 is devoted by describing the (G'/G) method. Next, the method is applied to the ANNV equation in Section 3. Number of obtained cases are described and depicted in the section 4. Finally, the paper ends with the concluding remarks.

2. Description of (G'/G) Expansion Method

The (2+1) nonlinear evolution equation represented by

$$P(u, u_t, u_x, u_y, u_{xt}, u_{yt}, u_{tt}, u_{xx}, u_{yy}, \dots\dots) = 0 \tag{2.1}$$

where $u = u(x, y, t)$ is an unknown function, P is a polynomial in u and its partial derivatives. The (G'/G) expansion method can be summarized as:

First, the PDE (2.1) is transformed into an ODE:
through introducing a traveling wave variable:

$$u(x, y, t) = u(\eta), \eta = x + y - ct \tag{2.3}$$

where c is a constant. If necessary, the ODE (2.2) can be integrated many times considering the constant of integration to be zero.

Second, the solution of the nonlinear differential equation is expressed in the form

$$u(\eta) = \sum_{i=0}^{m} a_i \left(\frac{G'}{G}\right)^i \tag{2.4}$$

where $G = G(\eta)$ satisfies the second-order linear ordinary differential equation

$$G''(\eta) + \lambda G'(\eta) + \mu G(\eta) = 0 \tag{2.5}$$

where $G' = \frac{dG}{d\eta}$, $G'' = \frac{d^2G}{d\eta^2}$, a_i , λ and μ are real constants to be determined.

The positive integer m is determined through the homogeneous balance between the orders of the highest derivatives and highly nonlinear terms as follows:

$$\begin{cases} O\left[u^r\left(\frac{d^q u}{d\eta^q}\right)^s\right] = mr + s\,(q+m) \\ O\left(\frac{d^p u}{d\eta^p}\right) = m + p \end{cases} \tag{2.6}$$

Substituting (2.4) into (2.2), using (2.5), then collecting all terms with the same order of (G'/G) and setting eac coefficient to zero yields a set of algebraic equations for a_i, c, μ and λ.

3. Mathematical Application

This section is motivated to find the explicit solutions of Eq. (1.2). First, inserting equation (2.3) into (1.2) confer

$$u^{(4)} - 6\,u'u'' - \,cu'' = 0 \tag{3.1}$$

where dashes refer to the derivatives with η. Integrating (3.1) with respect to η yields

$$u''' - 3u'^2 - cu' = 0 \tag{3.2}$$

Letting $u' = v$, yields

$$v'' - cv - 3v^2 = 0 \tag{3.3}$$

Homogeneous balance between v'' and v^2 yields $m = 2$, then substituting into (2.4) yields,

$$v(\eta) = \; a_0 + a_1\left(\frac{G'}{G}\right) + a_2\left(\frac{G'}{G}\right)^2 \tag{3.4}$$

Substituting from (3.4) using (2.5) into (3.3) yields,

$$\begin{gathered}(6a_2 - 3a_2^2)\left(\frac{G'}{G}\right)^4 + (10a_2\lambda - 6a_1a_2 + 2a_1)\left(\frac{G'}{G}\right)^3 + (3a_1\lambda + 4a_2\lambda^2 + 8a_2\mu - ca_2 - 3a_1^2 - 6a_0a_2)\left(\frac{G'}{G}\right)^2 \\ + (a_1\lambda^2 + 2a_1\mu + 6a_2\lambda\mu - ca_1 - 6a_0a_1)\left(\frac{G'}{G}\right) + (a_1\lambda\mu + 2a_2\mu^2 - ca_0 - 3a_0^2) = 0\end{gathered} \tag{3.5}$$

after collecting all terms with the same order of (G'/G) with setting each coefficient to zero obtain a set of algebraic equations for a_i, c, μ and λ.

$$\begin{cases} 6a_2 - 3a_2^2 = 0 \\ 10a_2\lambda - 6a_1a_2 + 2a_1 = 0 \\ 3a_1\lambda + 4a_2\lambda^2 + 8a_2\mu - ca_2 - 3a_1^2 - 6a_0a_2 = 0 \\ a_1\lambda^2 + 2a_1\mu + 6a_2\lambda\mu - ca_1 - 6a_0a_1 = 0 \\ a_1\lambda\mu + 2a_2\mu^2 - ca_0 - 3a_0^2 = 0 \end{cases} \tag{3.6}$$

Solving this system of equations reveal four cases.

4. Cases Study

In this section, many cases are studied according to the relations between the constants (Fig **1-4**).

Case 1

$$a_0 \;=\; 2\mu, a_1 \;=\; 2\lambda, a_2 \;=\; 2 \text{ and } c \;=\; 2\lambda \;-\; 4\mu \;=\; \alpha \tag{4.1}$$

G is found through solution of equation (2.5) by setting $\alpha \; = 2\lambda \;-\; 4\mu$

i- for $\alpha \; > \; 0$

$$v = 2\mu + 2\lambda\left[\frac{-\lambda}{2} + \frac{\sqrt{\alpha}}{2}\left(\frac{C_1\sinh\left(\frac{\sqrt{\alpha}}{2}\eta\right) + C_2 cosh\left(\frac{\sqrt{\alpha}}{2}\eta\right)}{C_1 cosh\left(\frac{\sqrt{\alpha}}{2}\eta\right) + C_2\sinh\left(\frac{\sqrt{\alpha}}{2}\eta\right)}\right)\right] + 2\left[\frac{-\lambda}{2} + \frac{\sqrt{\alpha}}{2}\left(\frac{C_1\sinh\left(\frac{\sqrt{\alpha}}{2}\eta\right) + C_2 cosh\left(\frac{\sqrt{\alpha}}{2}\eta\right)}{C_1 cosh\left(\frac{\sqrt{\alpha}}{2}\eta\right) + C_2\sinh\left(\frac{\sqrt{\alpha}}{2}\eta\right)}\right)\right]^2 \tag{4.2}$$

For $C_1 \;=\; 0$ and $C_2 \;=\; 1$

$$v_1 = 2\mu + 2\lambda\left[\frac{-\lambda}{2} + \frac{\sqrt{\alpha}}{2}\left(\coth\left(\frac{\sqrt{\alpha}}{2}\eta\right)\right)\right] + 2\left[\frac{-\lambda}{2} + \frac{\sqrt{\alpha}}{2}\left(\coth\left(\frac{\sqrt{\alpha}}{2}\eta\right)\right)\right]^2 \tag{4.3}$$

$$u_1 = 2\mu\eta - \frac{\lambda^2\eta}{2} - \sqrt{\alpha}\coth\left(\frac{\sqrt{\alpha}}{2}\eta\right) - \frac{\sqrt{\alpha}}{2}\ln\left(coth\left(\frac{\sqrt{\alpha}}{2}\eta\right) - 1\right) + \frac{\sqrt{\alpha}}{2}\ln\left(coth\left(\frac{\sqrt{\alpha}}{2}\eta\right) + 1\right) \tag{4.4}$$

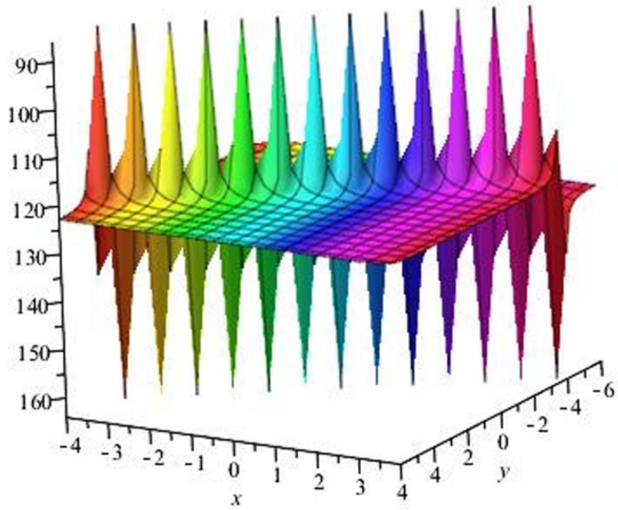

Figure 1: The soliton solution $\boldsymbol{u_1}$ for $\boldsymbol{\lambda = 3, \mu = 1, t = 10, \alpha = 5}$ and $\boldsymbol{c = 5}$.

For $C_1 = 1$ and $C_2 = 0$

$$v_2 = 2\mu + 2\lambda \left[\frac{-\lambda}{2} + \frac{\sqrt{\alpha}}{2}\left(\tanh\left(\frac{\sqrt{\alpha}}{2}\eta\right)\right)\right] + 2\left[\frac{-\lambda}{2} + \frac{\sqrt{\alpha}}{2}\left(\tanh\left(\frac{\sqrt{\alpha}}{2}\eta\right)\right)\right]^2 \tag{4.5}$$

$$u_2 = 2\mu\eta - \frac{\lambda^2\eta}{2} - \sqrt{\alpha}\tanh\left(\frac{\sqrt{\alpha}}{2}\eta\right) - \frac{\sqrt{\alpha}}{2}\ln\left(tanh\left(\frac{\sqrt{\alpha}}{2}\eta\right) - 1\right) + \frac{\sqrt{\alpha}}{2}\ln\left(tanh\left(\frac{\sqrt{\alpha}}{2}\eta\right) + 1\right) \tag{4.6}$$

ii- for $\alpha < 0$

$$v = 2\mu + 2\lambda\left[\frac{-\lambda}{2} + \frac{\sqrt{-\alpha}}{2}\left(\frac{C_1\sin\left(\frac{\sqrt{-\alpha}}{2}\eta\right) + C_2cos\left(\frac{\sqrt{-\alpha}}{2}\eta\right)}{C_1cos\left(\frac{\sqrt{-\alpha}}{2}\eta\right) + C_2\sin\left(\frac{\sqrt{-\alpha}}{2}\eta\right)}\right)\right] + 2\left[\frac{-\lambda}{2} + \frac{\sqrt{-\alpha}}{2}\left(\frac{C_1\sin\left(\frac{\sqrt{-\alpha}}{2}\eta\right) + C_2cos\left(\frac{\sqrt{-\alpha}}{2}\eta\right)}{C_1cos\left(\frac{\sqrt{-\alpha}}{2}\eta\right) + C_2\sin\left(\frac{\sqrt{-\alpha}}{2}\eta\right)}\right)\right]^2 \tag{4.7}$$

For $C_1 = 0$ and $C_2 = 1$

$$v_3 = 2\mu + 2\lambda\left[\frac{-\lambda}{2} + \frac{\sqrt{-\alpha}}{2}\left(cot\left(\frac{\sqrt{-\alpha}}{2}\eta\right)\right)\right] + 2\left[\frac{-\lambda}{2} + \frac{\sqrt{-\alpha}}{2}\left(cot\left(\frac{\sqrt{-\alpha}}{2}\eta\right)\right)\right]^2 \tag{4.8}$$

$$u_3 = 2\mu\eta - \frac{\lambda^2\eta}{2} + \frac{\alpha}{\sqrt{-\alpha}}\left(\cot\left(\frac{\sqrt{-\alpha}}{2}\eta\right)\right) - \frac{\alpha\pi}{2\sqrt{-\alpha}} + \frac{\alpha}{\sqrt{-\alpha}}\cot^{-1}\left(cot\left(\frac{\sqrt{-\alpha}}{2}\eta\right)\right) \tag{4.9}$$

For $C_1 = 1$ and $C_2 = 0$

$$v_4 = 2\mu + 2\lambda\left[\frac{-\lambda}{2} + \frac{\sqrt{-\alpha}}{2}\left(\tan\left(\frac{\sqrt{-\alpha}}{2}\eta\right)\right)\right] + 2\left[\frac{-\lambda}{2} + \frac{\sqrt{-\alpha}}{2}\left(\tan\left(\frac{\sqrt{-\alpha}}{2}\eta\right)\right)\right]^2 \tag{4.10}$$

$$u_4 = 2\mu\eta - \frac{\lambda^2\eta}{2} - \frac{\alpha}{\sqrt{-\alpha}}\left(\tan\left(\frac{\sqrt{-\alpha}}{2}\eta\right)\right) + \frac{\alpha}{\sqrt{-\alpha}}\tan^{-1}\left(tan\left(\frac{\sqrt{-\alpha}}{2}\eta\right)\right) \tag{4.11}$$

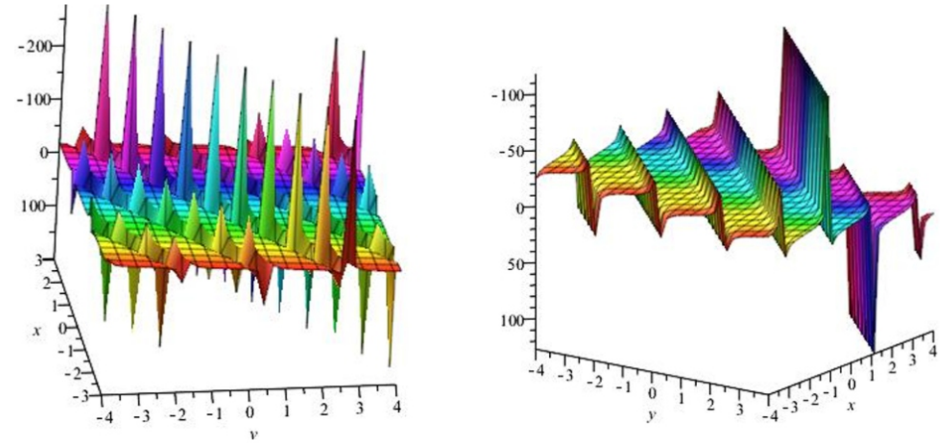

a. solution u_3 for $\boldsymbol{\lambda = 3, \mu = 4, t = 0.5, \alpha = -8}$ and $\boldsymbol{c = -8}$

b. multi kink solution u_4 for $\boldsymbol{\lambda = 3, \mu = 4, t = 0.5, \alpha = -8}$ and $\boldsymbol{c = -8}$

Figure 2: The traveling wave solutions u_3 and u_4.

Case 2

$$v = \frac{\lambda^2}{3} + \frac{2}{3}\mu + 2\lambda \left[\frac{-\lambda}{2} + \frac{\sqrt{\alpha}}{2}\left(\frac{C_1 \sinh\left(\frac{\sqrt{\alpha}}{2}\eta\right) + C_2 cosh\left(\frac{\sqrt{\alpha}}{2}\eta\right)}{C_1 cosh\left(\frac{\sqrt{\alpha}}{2}\eta\right) + C_2 \sinh\left(\frac{\sqrt{\alpha}}{2}\eta\right)}\right)\right] + 2\left[\frac{-\lambda}{2} + \frac{\sqrt{\alpha}}{2}\left(\frac{C_1 \sinh\left(\frac{\sqrt{\alpha}}{2}\eta\right) + C_2 cosh\left(\frac{\sqrt{\alpha}}{2}\eta\right)}{C_1 cosh\left(\frac{\sqrt{\alpha}}{2}\eta\right) + C_2 \sinh\left(\frac{\sqrt{\alpha}}{2}\eta\right)}\right)\right]^2 \quad (4.13)$$

For $C_1 = 0$ and $C_2 = 1$

$$v_5 = \frac{\lambda^2}{3} + \frac{2}{3}\mu + 2\lambda \left[\frac{-\lambda}{2} + \frac{\sqrt{\alpha}}{2}\left(coth\left(\frac{\sqrt{\alpha}}{2}\eta\right)\right)\right] + 2\left[\frac{-\lambda}{2} + \frac{\sqrt{\alpha}}{2}\left(coth\left(\frac{\sqrt{\alpha}}{2}\eta\right)\right)\right]^2 \quad (4.14)$$

$$u_5 = \frac{2}{3}\mu\eta - \frac{\lambda^2\eta}{6} - \sqrt{\alpha}\coth\left(\frac{\sqrt{\alpha}}{2}\eta\right) - \frac{\sqrt{\alpha}}{2}\ln\left(coth\left(\frac{\sqrt{\alpha}}{2}\eta\right) - 1\right) + \frac{\sqrt{\alpha}}{2}\ln\left(coth\left(\frac{\sqrt{\alpha}}{2}\eta\right) + 1\right) \quad (4.15)$$

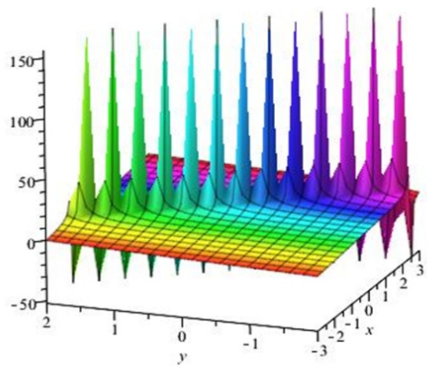

Figure 3: The soliton solution u_5 for $\boldsymbol{\lambda = 3, \mu = 1, t = 0.1, \alpha = 5}$ and $\boldsymbol{c = 5}$

For $C_1 = 1$ and $C_2 = 0$

$$v_6 = \frac{\lambda^2}{3} + \frac{2}{3}\mu + 2\lambda \left[\frac{-\lambda}{2} + \frac{\sqrt{\alpha}}{2}\left(\tanh\left(\frac{\sqrt{\alpha}}{2}\eta\right)\right)\right] + 2\left[\frac{-\lambda}{2} + \frac{\sqrt{\alpha}}{2}\left(\tanh\left(\frac{\sqrt{\alpha}}{2}\eta\right)\right)\right]^2 \quad (4.16)$$

$$u_6 = \frac{2}{3}\mu\eta - \frac{\lambda^2\eta}{6} - \sqrt{\alpha}\tanh\left(\frac{\sqrt{\alpha}}{2}\eta\right) - \frac{\sqrt{\alpha}}{2}\ln\left(tanh\left(\frac{\sqrt{\alpha}}{2}\eta\right) - 1\right) + \frac{\sqrt{\alpha}}{2}\ln\left(tanh\left(\frac{\sqrt{\alpha}}{2}\eta\right) + 1\right) \quad (4.17)$$

ii- for $\alpha < 0$

$$v=\frac{\lambda^2}{3}+\frac{2}{3}\mu+2\lambda\left[\frac{-\lambda}{2}+\frac{\sqrt{-\alpha}}{2}\left(\frac{C_1\sin\left(\frac{\sqrt{-\alpha}}{2}\eta\right)+C_2cos\left(\frac{\sqrt{-\alpha}}{2}\eta\right)}{C_1cos\left(\frac{\sqrt{-\alpha}}{2}\eta\right)+C_2\sin\left(\frac{\sqrt{-\alpha}}{2}\eta\right)}\right)\right]+2\left[\frac{-\lambda}{2}+\frac{\sqrt{-\alpha}}{2}\left(\frac{C_1\sin\left(\frac{\sqrt{-\alpha}}{2}\eta\right)+C_2cos\left(\frac{\sqrt{-\alpha}}{2}\eta\right)}{C_1cos\left(\frac{\sqrt{-\alpha}}{2}\eta\right)+C_2\sin\left(\frac{\sqrt{-\alpha}}{2}\eta\right)}\right)\right]^2 \tag{4.18}$$

For $C_1 = 0$ and $C_2 = 1$

$$v_7=\frac{\lambda^2}{3}+\frac{2}{3}\mu+2\lambda\left[\frac{-\lambda}{2}+\frac{\sqrt{-\alpha}}{2}\left(cot\left(\frac{\sqrt{-\alpha}}{2}\eta\right)\right)\right]+2\left[\frac{-\lambda}{2}+\frac{\sqrt{-\alpha}}{2}\left(cot\left(\frac{\sqrt{-\alpha}}{2}\eta\right)\right)\right]^2 \tag{4.19}$$

$$u_7=\frac{2}{3}\mu\eta-\frac{\lambda^2\eta}{6}+\frac{\alpha}{\sqrt{-\alpha}}\left(\cot\left(\frac{\sqrt{-\alpha}}{2}\eta\right)\right)-\frac{\alpha\pi}{2\sqrt{-\alpha}}+\frac{\alpha}{\sqrt{-\alpha}}\cot^{-1}\left(cot\left(\frac{\sqrt{-\alpha}}{2}\eta\right)\right) \tag{4.20}$$

For $C_1 = 1$ and $C_2 = 0$

$$v_8=\frac{\lambda^2}{3}+\frac{2}{3}\mu+2\lambda\left[\frac{-\lambda}{2}+\frac{\sqrt{-\alpha}}{2}\left(\tan\left(\frac{\sqrt{-\alpha}}{2}\eta\right)\right)\right]+2\left[\frac{-\lambda}{2}+\frac{\sqrt{-\alpha}}{2}\left(\tan\left(\frac{\sqrt{-\alpha}}{2}\eta\right)\right)\right]^2 \tag{4.21}$$

$$u_8=\frac{2}{3}\mu\eta-\frac{\lambda^2\eta}{6}+\frac{\alpha}{\sqrt{-\alpha}}\left(\tan\left(\frac{\sqrt{-\alpha}}{2}\eta\right)\right)+\frac{\alpha}{\sqrt{-\alpha}}\tan^{-1}\left(tan\left(\frac{\sqrt{-\alpha}}{2}\eta\right)\right) \tag{4.22}$$

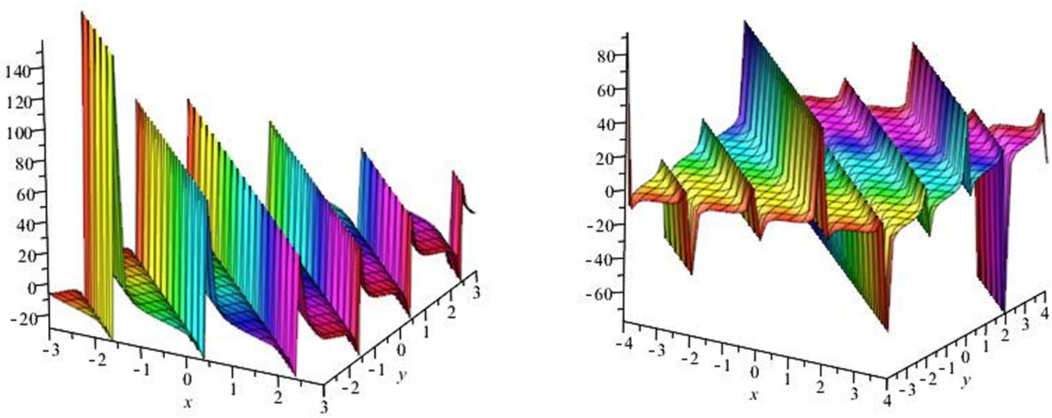

a. Descending kink solution u_7 for $\boldsymbol{\lambda = 3}$, $\boldsymbol{\mu = 4, t = 0.5, \alpha = -8}$ and $\boldsymbol{c = -8}$

b. Multi kink solution u_8 for $\boldsymbol{\lambda = 3}$, $\boldsymbol{\mu = 4, t = 0.5, \alpha = -8}$ and $\boldsymbol{c = -8}$

Figure 4: The solution u_5 for $\boldsymbol{\lambda = 3, \mu = 1, t = 0.1, \alpha = 5}$ and $\boldsymbol{c = 5}$

Case 3

$$a_0=\frac{1}{6}\left(\lambda^2+2\mu-\sqrt{(\lambda^2-2\mu)^2-4\lambda^2\mu}\right),\ a_1=\lambda,\ a_2=0 \text{ and } c=\sqrt{(\lambda^2-2\mu)^2-4\lambda^2\mu} \tag{4.23}$$

i- for $\alpha > 0$

$$v=\frac{1}{6}\left(\lambda^2+2\mu-\sqrt{(\lambda^2-2\mu)^2-4\lambda^2\mu}\right)+\lambda\left[\frac{-\lambda}{2}+\frac{\sqrt{\alpha}}{2}\left(\frac{C_1\sinh\left(\frac{\sqrt{\alpha}}{2}\eta\right)+C_2cosh\left(\frac{\sqrt{\alpha}}{2}\eta\right)}{C_1cosh\left(\frac{\sqrt{\alpha}}{2}\eta\right)+C_2\sinh\left(\frac{\sqrt{\alpha}}{2}\eta\right)}\right)\right] \tag{4.24}$$

For $C_1 = 0$ and $C_2 = 1$

$$v_9=\frac{1}{6}\left(\lambda^2+2\mu-\sqrt{(\lambda^2-2\mu)^2-4\lambda^2\mu}\right)+\lambda\left[\frac{-\lambda}{2}+\frac{\sqrt{\alpha}}{2}\left(coth\left(\frac{\sqrt{\alpha}}{2}\eta\right)\right)\right] \tag{4.25}$$

$$u_9=\left(-\frac{1}{3}\lambda^2+\frac{1}{3}\mu-\frac{1}{6}\sqrt{(\lambda^2-2\mu)^2-4\lambda^2\mu}\right)\eta-\frac{\lambda}{2}\ln\left(coth\left(\frac{\sqrt{\alpha}}{2}\eta\right)-1\right)-\frac{\lambda}{2}\ln\left(coth\left(\frac{\sqrt{\alpha}}{2}\eta\right)+1\right) \tag{4.26}$$

For $C_1 = 1$ and $C_2 = 0$

$$v_{10}=\frac{1}{6}\left(\lambda^2+2\mu-\sqrt{(\lambda^2-2\mu)^2-4\lambda^2\mu}\right)+\lambda\left[\frac{-\lambda}{2}+\frac{\sqrt{\alpha}}{2}\left(\tanh\left(\frac{\sqrt{\alpha}}{2}\eta\right)\right)\right] \tag{4.27}$$

$$u_{10}=\left(-\frac{1}{3}\lambda^2+\frac{1}{3}\mu-\frac{1}{6}\sqrt{(\lambda^2-2\mu)^2-4\lambda^2\mu}\right)\eta-\frac{\lambda}{2}\ln\left(tanh\left(\frac{\sqrt{\alpha}}{2}\eta\right)-1\right)-\frac{\lambda}{2}\ln\left(tanh\left(\frac{\sqrt{\alpha}}{2}\eta\right)+1\right) \tag{4.28}$$

ii- for $\alpha < 0$

$$v = \frac{1}{6}\left(\lambda^2 + 2\mu - \sqrt{(\lambda^2 - 2\mu)^2 - 4\lambda^2\mu}\right) + \lambda\left[\frac{-\lambda}{2} + \frac{\sqrt{-\alpha}}{2}\left(\frac{C_1 \sin\left(\frac{\sqrt{-\alpha}}{2}\eta\right) + C_2 cos\left(\frac{\sqrt{-\alpha}}{2}\eta\right)}{C_1 cos\left(\frac{\sqrt{-\alpha}}{2}\eta\right) + C_2 \sin\left(\frac{\sqrt{-\alpha}}{2}\eta\right)}\right)\right] \tag{4.29}$$

$C_1 = 0$ and $C_2 = 1$

$$v_{11} = \frac{1}{6}\left(\lambda^2 + 2\mu - \sqrt{(\lambda^2 - 2\mu)^2 - 4\lambda^2\mu}\right) + \lambda\left[\frac{-\lambda}{2} + \frac{\sqrt{-\alpha}}{2}\left(cot\left(\frac{\sqrt{-\alpha}}{2}\eta\right)\right)\right] \tag{4.30}$$

$$u_{11} = \left(-\frac{1}{3}\lambda^2 + \frac{1}{3}\mu - \frac{1}{6}\sqrt{(\lambda^2 - 2\mu)^2 - 4\lambda^2\mu}\right)\eta - \frac{\lambda}{2}\ln\left(\left(cot\left(\frac{\sqrt{-\alpha}}{2}\eta\right)\right)^2 + 1\right) \tag{4.31}$$

For $C_1 = 1$ and $C_2 = 0$

$$v_{12} = \frac{1}{6}\left(\lambda^2 + 2\mu - \sqrt{(\lambda^2 - 2\mu)^2 - 4\lambda^2\mu}\right) + \lambda\left[\frac{-\lambda}{2} + \frac{\sqrt{-\alpha}}{2}\left(\tan\left(\frac{\sqrt{-\alpha}}{2}\eta\right)\right)\right] \tag{4.32}$$

$$u_{12} = \left(-\frac{1}{3}\lambda^2 + \frac{1}{3}\mu - \frac{1}{6}\sqrt{(\lambda^2 - 2\mu)^2 - 4\lambda^2\mu}\right)\eta + \frac{\lambda}{2}\ln\left(\left(tan\left(\frac{\sqrt{-\alpha}}{2}\eta\right)\right)^2 + 1\right) \tag{4.33}$$

Case 4

$$a_0 = \frac{1}{6}\left(\lambda^2 + 2\mu + \sqrt{(\lambda^2 - 2\mu)^2 - 4\lambda^2\mu}\right), a_1 = \lambda\,, a_2 = 0 \text{ and } c = \sqrt{(\lambda^2 - 2\mu)^2 - 4\lambda^2\mu} \tag{4.34}$$

i- for $\alpha > 0$

$$v = \frac{1}{6}\left(\lambda^2 + 2\mu + \sqrt{(\lambda^2 - 2\mu)^2 - 4\lambda^2\mu}\right) + \lambda\left[\frac{-\lambda}{2} + \frac{\sqrt{\alpha}}{2}\left(\frac{C_1 \sinh\left(\frac{\sqrt{\alpha}}{2}\eta\right) + C_2 cosh\left(\frac{\sqrt{\alpha}}{2}\eta\right)}{C_1 cosh\left(\frac{\sqrt{\alpha}}{2}\eta\right) + C_2 \sinh\left(\frac{\sqrt{\alpha}}{2}\eta\right)}\right)\right] \tag{4.35}$$

For $C_1 = 0$ and $C_2 = 1$

$$v_{13} = \frac{1}{6}\left(\lambda^2 + 2\mu + \sqrt{(\lambda^2 - 2\mu)^2 - 4\lambda^2\mu}\right) + \lambda\left[\frac{-\lambda}{2} + \frac{\sqrt{\alpha}}{2}\left(coth\left(\frac{\sqrt{\alpha}}{2}\eta\right)\right)\right] \tag{4.36}$$

$$u_{13} = \left(-\frac{1}{3}\lambda^2 + \frac{1}{3}\mu + \frac{1}{6}\sqrt{(\lambda^2 - 2\mu)^2 - 4\lambda^2\mu}\right)\eta - \frac{\lambda}{2}\ln\left(coth\left(\frac{\sqrt{\alpha}}{2}\eta\right) - 1\right) - \frac{\lambda}{2}\ln\left(coth\left(\frac{\sqrt{\alpha}}{2}\eta\right) + 1\right) \tag{4.37}$$

For $C_1 = 1$ and $C_2 = 0$

$$v_{14} = \frac{1}{6}\left(\lambda^2 + 2\mu + \sqrt{(\lambda^2 - 2\mu)^2 - 4\lambda^2\mu}\right) + \lambda\left[\frac{-\lambda}{2} + \frac{\sqrt{\alpha}}{2}\left(\tanh\left(\frac{\sqrt{\alpha}}{2}\eta\right)\right)\right] \tag{4.38}$$

$$u_{14} = \left(-\frac{1}{3}\lambda^2 + \frac{1}{3}\mu + \frac{1}{6}\sqrt{(\lambda^2 - 2\mu)^2 - 4\lambda^2\mu}\right)\eta - \frac{\lambda}{2}\ln\left(tanh\left(\frac{\sqrt{\alpha}}{2}\eta\right) - 1\right) - \frac{\lambda}{2}\ln\left(tanh\left(\frac{\sqrt{\alpha}}{2}\eta\right) + 1\right) \tag{4.39}$$

ii- for $\alpha < 0$

$$v = \frac{1}{6}\left(\lambda^2 + 2\mu + \sqrt{(\lambda^2 - 2\mu)^2 - 4\lambda^2\mu}\right) + \lambda\left[\frac{-\lambda}{2} + \frac{\sqrt{-\alpha}}{2}\left(\frac{C_1 \sin\left(\frac{\sqrt{-\alpha}}{2}\eta\right) + C_2 cos\left(\frac{\sqrt{-\alpha}}{2}\eta\right)}{C_1 cos\left(\frac{\sqrt{-\alpha}}{2}\eta\right) + C_2 \sin\left(\frac{\sqrt{-\alpha}}{2}\eta\right)}\right)\right] \tag{4.40}$$

For $C_1 = 0$ and $C_2 = 1$

$$v_{16} = \frac{1}{6}\left(\lambda^2 + 2\mu + \sqrt{(\lambda^2 - 2\mu)^2 - 4\lambda^2\mu}\right) + \lambda\left[\frac{-\lambda}{2} + \frac{\sqrt{-\alpha}}{2}\left(\tan\left(\frac{\sqrt{-\alpha}}{2}\eta\right)\right)\right] \tag{4.43}$$

$$u_{16} = \left(-\frac{1}{3}\lambda^2 + \frac{1}{3}\mu + \frac{1}{6}\sqrt{(\lambda^2 - 2\mu)^2 - 4\lambda^2\mu}\right)\eta + \frac{\lambda}{2}\ln\left(\left(tan\left(\frac{\sqrt{-\alpha}}{2}\eta\right)\right)^2 + 1\right) \tag{4.44}$$

5. Conclusions

Solitary waves of the ANNV equation in its (2+1)-dimensional form have been investigated by exploiting the G′ /G method. This method had the ability to create new forms of solitary waves after getting the homogenous balance required for this method. Four cases were formulated according to the appropriate choice of the relations between the arbitrary constants. The solutions included trigonometric, hyperbolic, logarithmic, polynomial, and combinations of these functions. The attained soliton and kink solutions are very useful in describing the behavior of the solitary wave in different engineering and physical applications including plasma explosions and ocean waves.

Conflict of Interest

The authors have no competing interests to declare that are relevant to the content of this article.

Funding

No funding was received for conducting this study.

References

1.Columbu A, Frassu S, Viglialoro G. Refined criteria toward boundedness in an attraction–repulsion chemotaxis system with nonlinear productions. Appl Anal. 2023: 1-17. https://doi.org/10.1080/00036811.2023.2187789

2.Li T, Frassu S, Viglialoro G. Combining effects ensuring boundedness in an attraction–repulsion chemotaxis model with production and consumption. Zeitschrift Für Angewandte Mathematik Und Physik. 2023; 74: Article number 109. https://doi.org/10.1007/s00033-02301976-0

3.Li T, Pintus N, Viglialoro G. Properties of solutions to porous medium problems with different sources and boundary conditions. Zeitschrift Für Angewandte Mathematik Und Physik. 2019; 70: Article number 86. https://doi.org/10.1007/s00033-019-1130-2

4.Li T, Viglialoro G. Boundedness for a nonlocal reaction chemotaxis model even in the attraction-dominated regime. Differential and Integral Equations. 2021; 34: 315-36. https://doi.org/10.57262/die034-0506-315

5.Boiti M, Leon JJ-P, Manna M, Pempinelli F. On the spectral transform of a Korteweg-de Vries equation in two spatial dimensions. Inverse Probl. 1986; 2: 271-9. https://doi.org/10.1088/0266-5611/2/3/005

6.Estévez PG, Leble SB. A kdv equation in 2+1 dimensions: Painlevé analysis, solutions, and similarity reductions. Acta Appl Math. 1995; 39: 277-94. https://doi.org/10.1007/BF00994637

7.Lou S-Y. (2+1)-Dimensional Integrable Models from the Constraints of the KP Equation. Commun

Theor Phys. 1997; 27: 249-52. https://doi.org/10.1088/0253-6102/27/2/249

8.Lou S-Y, Hu X-B. Infinitely many Lax pairs and symmetry constraints of the KP equation. J Math Phys. 1997; 38: 6401-27. https://doi.org/10.1063/1.532219

9.Clarkson PA, Mansfield EL. On a shallow water wave equation. Nonlinearity. 1994; 7: 975-1000. https://doi.org/10.1088/09517715/7/3/012

10.Li-Hua Z, Xi-Qiang L, Cheng-Lin B. Symmetry, reductions and new exact solutions of ANNV equation through lax pair. Commun Theor Phys. 2008; 50: 1-6. https://doi.org/10.1088/0253-6102/50/1/01

11.Ma H-C, Lou S-Y. Finite symmetry transformation groups and exact solutions of lax integrable systems. Commun Theor Phys. 2005; 44: 193-6. https://doi.org/10.1088/6102/44/2/193

12.Lü Z-S. Special bi-solitons for asymmetric nizhnik-novikov-veselov equation. Commun Theor Phys. 2011; 55: 85-8. https://doi.org/10.1088/0253-6102/55/1/17

13.Ling W, Zhong-Zhou D, Xi-Qiang L. Symmetry reductions, exact solutions and conservation laws of asymmetric nizhnik-novikov-veselov equation. Commun Theor Phys. 2008; 49: 1-8. https://doi.org/10.1088/0253-6102/49/1/01

14.Yu G-F, Tam H-W. A vector asymmetrical nnv equation: Soliton solutions, bilinear bäcklund transformation and lax pair. J Math Anal Appl. 2008; 344: 593-600. https://doi.org/10.1016/j.jmaa.2008.02.057

15.Bai C-L, Zhao H. The study of soliton fission and fusion in (2+1)-dimensional nonlinear system. Eur Phys J D. 2006; 39: 93-9. https://doi.org/10.1140/epjd/e2006-00080-8

16.Hang-Yu R, Zhi-Fang L. Interaction between line soliton and algebraic soliton for asymmetric nizhnik novikov-veselov-equation. Commun Theor Phys. 2008; 49: 1547-52. https://doi.org/10.1088/0253-6102/49/6/41

17.Ruan H, Chen Y. Interaction between a line soliton and a y-periodic soliton in the (2+1)-dimensional nizhnik-novikov-veselov equation. Zeitschrift Für Naturforschung A. 2002; 57: 948-54. https://doi.org/10.1515/zna-2002-1207

18.Qian X, Lou S, Hu X. Variable separation approach for a differential-difference asymmetric nizhnik-novikov-veselov equation. Zeitschrift Für Naturforschung A. 2004; 59: 645-58. https://doi.org/10.1515/zna-2004-1005

19.Lou SY, Ruan HY. Revisitation of the localized excitations of the (2 + 1)-dimensional KdV equation. J Phys A Math Gen. 2001; 34: 305. https://doi.org/10.1088/0305-4470/34/2/307

20.Lin L. Quasi-periodic waves and asymptotic property for boiti-leon-manna-pempinelli equation. Commun Theor Phys. 2010; 54: 208-14. https://doi.org/10.1088/0253-6102/54/2/02

21.Li Y, Li D. New exact solutions for the (2+1)-dimensional Boiti-Leon-Manna-Pempinelli equation. Appl Math Sci. 2012; 6(9-12): 579-87.

22.Luo L. New exact solutions and bäcklund transformation for boiti-leon-manna-pempinelli equation. Phys Lett A. 2011; 375: 1059-63. https://doi.org/10.1016/j.physleta.2011.01.009

23.Song-Hua M, Jian-Ping F. Multi dromion-solitoff and fractal excitations for (2+1)-dimensional boiti-leon-manna-pempinelli system. Commun Theor Phys. 2009; 52: 641-5. https://doi.org/10.1088/0253-6102/52/4/18

24.Rashed AS, Kassem MM. Hidden symmetries and exact solutions of integro-differential Jaulent–Miodek evolution equation. Appl Math Comput. 2014; 247: 1141-55. https://doi.org/10.1016/j.amc.2014.09.025

25.Kassem MM, Rashed AS. N-solitons and cuspon waves solutions of (2 + 1)-dimensional Broer–Kaup–Kupershmidt equations via hidden symmetries of Lie optimal system. Chinese J Phys. 2019; 57: 90-104. https://doi.org/10.1016/j.cjph.2018.12.007

26.Mabrouk SM, Rashed AS. N-Solitons, kink and periodic wave solutions for (3 + 1)-dimensional Hirota bilinear equation using three distinct techniques. Chinese J Phys. 2019; 60: 48-60. https://doi.org/10.1016/j.cjph.2019.02.032

27.Rashed AS. Analysis of (3+1)-dimensional unsteady gas flow using optimal system of lie symmetries. Math Comput Simul. 2019; 156: 32746. https://doi.org/10.1016/j.matcom.2018.08.008

28.Saleh R, Rashed AS. New exact solutions of (3 + 1)-dimensional generalized Kadomtsev-Petviashvili equation using a combination of lie symmetry and singular manifold methods. Math Methods Appl Sci. 2020; 43: 2045-55. https://doi.org/10.1002/mma.6031

29.Saleh R, Rashed AS, Wazwaz A-M. Plasma-waves evolution and propagation modeled by sixth order Ramani and coupled Ramani equations using symmetry methods. Phys Scr. 2021; 96: 085213. https://doi.org/10.1088/1402-4896/ac0075

30.Rashed AS. Interaction of two long waves in shallow water using Hirota-Satsuma model and similarity transformations. Delta University Sci J. 2022; 5: 93-101. https://doi.org/10.21608/dusj.2022.233925

31.Rashed AS, Mabrouk SM, Wazwaz A-M. Forward scattering for non-linear wave propagation in (3 + 1)-dimensional Jimbo-Miwa equation using singular manifold and group transformation methods. Waves Random Complex Media. 2022; 32: 663-75. https://doi.org/10.1080/17455030.2020.1795303

32.Rashed AS, Inc M, Saleh R. Extensive novel waves evolution of three-dimensional Yu–Toda–Sasa–Fukuyama equation compatible with plasma and electromagnetic applications. Mod Phys Lett B. 2023; 37: 22501950. https://doi.org/10.1142/S0217984922501950

33.Rashed AS, Mostafa ANM, Wazwaz AM, Mabrouk SM. Dynamical behavior and soliton solutions of the jumarie's space-time fractional modified benjamin-bona-mahony equation in plasma physics. Rom Rep Phys. 2023; 75: Article no.104.

34.Mabrouk SM, Rashed AS. Analysis of (3 + 1)-dimensional boiti - leon -manna-pempinelli equation *via lax pair investigation and group transformation method. Comput Math Appl. 2017; 74: 2546-56. https://doi.org/10.1016/j.camwa.2017.07.033*

35.Shang Y. Bäcklund transformation, Lax pairs and explicit exact solutions for the shallow water waves equation. Appl Math Comput. 2007; 187: 1286-97. https://doi.org/10.1016/j.amc.2006.09.038

36.He Y, Tam H-W. Bilinear backlund transformation and lax pair for a coupled ramani equation. J Math Anal Appl. 2009; 357: 132-6. https://doi.org/10.1016/j.jmaa.2009.04.006

37.Cheng-Lin B. Extended homogeneous balance method and lax pairs, backlund transformation. Commun Theor Phys. 2002; 37: 645-8. https://doi.org/10.1088/0253-6102/37/6/645

38.Mabrouk S, Kassem M. Group similarity solutions of (2 + 1) boiti-leon-manna-pempinelli lax pair. Ain Shams Eng J. 2014; 5: 227-35. https://doi.org/10.1016/j.asej.2013.06.004

39.Mohamed NA, Rashed AS, Melaibari A, Sedighi HM, Eltaher MA. Effective numerical technique applied for Burgers' equation of (1 + 1)-, (2 + 1)-dimensional, and coupled forms. Math Methods Appl Sci. 2021; 44: 10135-53. https://doi.org/10.1002/mma.7395

40.Arora G, Joshi V. A computational approach using modified trigonometric cubic B-spline for numerical solution of Burgers' equation in one and two dimensions. Alex Eng J. 2018; 57: 1087-98. https://doi.org/10.1016/j.aej.2017.02.017

41.Biazar J, Aminikhah H. Exact and numerical solutions for non-linear Burger's equation by VIM. Math Comput Model. 2009; 49: 1394-400. https://doi.org/10.1016/j.mcm.2008.12.006

42.Shi F, Zheng H, Cao Y, Li J, Zhao R. A fast numerical method for solving coupled burgers' equations fast numerical method, Numer. Numer Methods Partial Differ Equ. 2017; 33: 1823-38. https://doi.org/10.1002/num.22160

43.Fang J, Nadeem M, Habib M, Akgül A. Numerical investigation of nonlinear shock wave equations with fractional order in propagating disturbance. Symmetry. 2022; 14(6), 1179. https://doi.org/10.3390/sym14061179

44.Kaya D, El-Sayed SM. A numerical method for solving jaulent-miodek equation. Phys Lett A. 2003; 318: 345-53. https://doi.org/10.1016/j.physleta.2003.08.033

45.Wazwaz A-M. The tanh and the sine–cosine methods for a reliable treatment of the modified equal width equation and its variants. Commun Nonlinear Sci Numer Simul. 2006; 11: 148-60. https://doi.org/10.1016/j.cnsns.2004.07.001

46.Wazwaz A-M. The sine–cosine and the tanh methods: Reliable tools for analytic treatment of nonlinear dispersive equations. Appl Math Comput. 2006; 173: 150-64. https://doi.org/10.1016/j.amc.2005.02.047

47.Wazwaz A-M. Multiple-soliton solutions for the KP equation by Hirota's bilinear method and by the tanh–coth method. Appl Math Comput. 2007; 190: 633-40. https://doi.org/10.1016/j.amc.2007.01.056

48.Wazwaz A-M. The tanh–coth method for solitons and kink solutions for nonlinear parabolic *equations. Appl Math Comput. 2007; 188: 1467-75. https://doi.org/10.1016/j.amc.2006.11.013*

49.Wazwaz A-M. The tanh-coth and the sine-cosine methods for kinks, solitons, and periodic solutions for the pochhammer-chree equations. Appl Math Comput. 2008; 195: 24-33. https://doi.org/10.1016/j.amc.2007.04.066

50.Darvishi MT, Najafi M. A modification of extended homoclinic test approach to solve the (3+1)-dimensional potential-ytsf equation. Chin Phys Lett. 2011; 28: 040202. https://doi.org/10.1088/0256-307X/28/4/040202

51.Darvishi MT, Najafi M, Najafi M. Application of multiple exp-function method to obtain multi-soliton solutions of (2 + 1)- and (3 + 1)dimensional breaking soliton equations. Am J Comput Appl Math. 2012; 1: 41-7. https://doi.org/10.5923/j.ajcam.20110102.08

ISSN 2249-4278

Fuzzy Rough Subgroups on Approximation Space

Nurettin Bağırmaz
Mardin Artuklu University, Mardin, Turkey

Abstract:

Fuzzy rough sets are a mathematical concept that combines fuzzy sets and rough sets to deal with uncertainty and incompleteness in data and information. In this study, different from the definition of Dubois and Prade (1990), the fuzzy rough set is defined within the framework of the rough group concept defined by Biswas and Nanda (1994), and some of its algebraic properties are discussed. Then, the concepts of fuzzy rough subgroup and fuzzy rough normal subgroup are introduced in the rough group. In addition, some basic features and examples of these concepts are given.

Keywords: Rough group Rough subgroup Fuzzy subgroups Approximation space Fuzzy rough subgroup

1. Introduction

To deal with vagueness, rough sets, and fuzzy sets are two efficient set theories. Both are generalizations of classical sets but have different viewpoints and applications.

Fuzzy sets are first introduced by Lotfi Zadeh [1], allowing objects to belong to a set or relation to a given degree, this is called the degree of membership. Fuzzy sets have been applied to various domains, such as logic, control, decision-making, and artificial intelligence. Fuzzy sets allow us to represent linguistic terms such as "a lot", "more or less" or "about" with a numerical value. Fuzzy sets have been applied to various mathematical fields. For example, fuzzy subgroups were defined and established by Rosenfeld [2]. Then many authors have studied it [3, 4].

Rough sets introduced by Polish computer scientist Z. Pawlak in [5], provide approximations of concepts in the presence of missing information. Although it is a generalization of classical sets, it uses a pair of sets to approximate the original set. The lower approximation includes objects that belong to the set, while the upper approximation includes objects that probably belong to the set. At the same time, some researchers have applied this theory to algebraic structures as well. Some algebraic properties of rough sets were explored by Iwinski [6]. In [7], Kuroki and Wang introduced the upper and lower approximations together with normal subgroups in a group. Then, some features of upper and lower approximations were studied according to normal subgroups [8-12]. On the other hand, in [13] definitions of the notation of rough subgroups and rough groups are given by using only the upper approximation. Miao et al. developed the rough group and rough subgroup definitions and offered some new characteristics [14]. In [15], the notation of rough semigroup is introduced. Also, Bağırmaz et al. defined the concept of the topological rough group [16]. Li et al, separation axioms of topological rough groups are discussed in [17].

On the other hand, some researchers have tried to reduce the limitations of equivalence relations in Pawlak rough sets in practice. Therefore, many researchers have proposed some general models [18-21]. Later, combining rough sets with fuzzy sets, Dubois and Prade [21] introduced the concepts of rough fuzzy sets and rough fuzzy sets. From this point of view, some researchers have applied this idea to other areas of mathematics [22-24].

This study is regulated as follows. In section 2, basic notations of fuzzy subgroups and rough groups are given. In section 3, fuzzy rough subset and (normal) subgroup definitions were made and some important features were proved.

2. Preliminaries

This section is dedicated to present some definitions and propositions that will form the basis for subsequent chapters.

Definition 2.1. [5] Assume U be a non-empty finite set called universe and R be an equivalence relation on U. Then (U, R) is called an approximation space.

Definition 2.2. [5] Assume U be a universe and R be an equivalence relation on U. We denote the equivalence class of object x in R by $[x]_R$.

Definition 2.3. [5] Assume (U, R) be an approximation space and X be a subset of U. The sets

(i) $\overline{X} = \{x|[x]_R \cap X \neq \emptyset\}$,

(ii) $\underline{X} = \{x|[x]_R \subseteq X\}$,

are called upper approximation and lower approximation of X in (U,R), respectively.

For example, suppose that (U,R) is an approximation space, where $U = \{a, b, c, d, e, f\}$ and an equivalence relation R with the following equivalence classes:

$$C_1 = \{a, b\}, \quad C_2 = \{c, e, f\}, \qquad C_3 = \{d\}.$$

Let $A = \{a, b, e\}$. Then $\underline{A} = \{a, b\}$ and $\overline{A} = \{a, b, c, e, f\}$.

Let U be a universe and "*" a binary operation defined on U. From now on, ab will be used instead of a*b, for all $a, b \in U$, and U denote a universe set in (U,R).

Definition 2.4. [13] Assume (U,R) be an approximation space and $G \subseteq U$. Then, G is called a rough group if the following properties are satisfied:

(i) $\forall a, b \in G, ab \in \overline{G}$,

(ii) Associativity property holds in $\overline{G}$

(iii) $\exists e \in \overline{G}$, $\forall a \in G$ such that $ae = ea = a$, where e is called the rough identity element of rough group G.

(iv) $\forall a \in G, \exists b \in G$ such that $ab = ba = e$, where b is called the rough inverse element of a in G, it is denoted by

Definition 2.5. [13] Assume G be a rough group and $H \subseteq G$. H is called a rough subgroup of G if H is a rough group.

Remark 2.6. [13] Assume G be a rough group. Then, G has only one rough subgroup, which is itself. A necessary and sufficient condition for {e} to be a trivial rough subgroup of G is $e \in G$.

Proposition 2.7. [13] Assume G be a rough group and $H \subseteq G$. A necessary and sufficient condition for H to be a rough subgroup is that:

(i) $\forall a, b \in H, ab \in \overline{H}$,

(ii) $\forall a \in H, a^{-1} \in H$.

Definition 2.8. [1] Assume U be a non-empty set. A fuzzy subset φ of U is a map $\phi: U \rightarrow [0,1]$.

Definition 2.9. [3] A fuzzy set φ of a group G is called a fuzzy subgroup if, for all $a, b \in G$,

(i) $\phi(ab) \geq \min\{\phi(a), \phi(b)\}$,

(ii) $\phi(a^{-1}) \geq \phi(a)$.

It is well known that a fuzzy subgroup G satisfies $\phi(a) \leq \phi(e)$ and $\phi(a^{-1}) = \phi(a)$ for all $a \in G$.

3. Fuzzy rough subgroups

In this part, a fuzzy rough (sub) set and a fuzzy rough (normal) subgroup of rough groups are defined. In addition, some important properties were proved and an example was given.

Definition 3.1. Assume G be a non-empty subset of U. A fuzzy rough set φ of $\overline{G}$ is a map $\varphi : \overline{G} \rightarrow [0,1]$.

Definition 3.2. Assume G be a non-empty subset of U. Let $\varphi : \overline{G} \rightarrow [0,1]$ is a map defined as

$$\phi(a) = \begin{cases} g_1, & a \in G, \\ g_2, & a \in \overline{G} \setminus G, 0 \leq g_1 \leq g_2 \leq 1 \end{cases}$$

where $g_1, g_2 \in [0,1]$. The set φ is known as fuzzy rough subset of $\overline{G}$.

Definition 3.3. Assume G be rough group over U. A fuzzy rough subset φ of $\overline{G}$ is named a fuzzy rough subgroup of G if, for all $a, b \in G$,

(i) $\phi(ab) \geq \min\{\phi(a), \phi(b)\}$,

(ii) $\phi(a^{-1}) \geq \phi(a)$.

Proposition 3.4. Assume G be a rough group over U. If ϕ is a fuzzy rough subgroup of G, then:

(i) $\phi(e) \geq \phi(a), \forall a \in G$,

(ii) $\phi(a^{-1}) = \phi(a), \forall a \in G$,

where e is the identity element of G.

Proof. (i) Suppose that φ be a fuzzy rough subgroup of G, then $\phi(e) = \mu(aa^{-1}) \geq \min\{\phi(a), \phi(a^{-1})\} = \phi(a)$ for all $a \in G$. Thus $\phi(e) \geq \phi(a)$.

(ii) Suppose that φ be a fuzzy rough subgroup of G, then $\phi(a) = \phi((a^{-1})^{-1}) \geq \phi(a^{-1}) \geq \phi(a)$ for all $a \in G$. Hence $\phi(a^{-1}) = \phi(a)$.

Definition 3.5. Assume G be a rough group over U. A fuzzy rough subgroup ϕ of G is named a fuzzy rough normal subgroup of G if

$\phi(ab) = \phi(ba)$ for all $a, b \in G$.

Example 3.6. Suppose that $U = \{a, b, c, d, e\}$ be a universe set with the following multiplication table:

$(\cdot)$	a	b	c	d	e
a	a	b	c	d	e
b	b	a	c	b	b
c	c	c	c	a	e
d	d	c	a	d	c
e	e	d	b	c	e

A classification of U is $U/R = \{C_1, C_2, C_3\}$, where

$$C_1 = \{a, b\},$$

$$C_2 = \{c, d\},$$

$$C_3 = \{e\}.$$

Let $G = \{b, c, d\}$, then $\overline{G} = \{a, b, c, d\}$. From Definition 2.4 , $G \subseteq U$ is a rough group.

For $\overline{G}$ define $\phi(a) = 1,\ \phi(b) = \frac{1}{2},\ \phi(c) = \phi(d) = \frac{1}{3}$. Then, from Definition 3.3, ϕ is a fuzzy rough subgroup of G.

Proposition 3.7. Assume G be a group over U. If φ is a fuzzy (normal) subgroup of G, then ϕ is a fuzzy rough (normal) subgroup of G.

Proof. Suppose that G be a group. Then $a, b \in G,\ ab \in G$. Since $G \subseteq \overline{G}, ab \in \overline{G}$. On the other hand, since ϕ is a fuzzy subgroup of G, then from Definition 3.3 we get ϕ is a fuzzy rough subgroup of G.

Similarly, since ϕ is a fuzzy normal subgroup of G, then from Definition 3.5 we conclude ϕ is a fuzzy rough normal subgroup of G.

Remark 3.8. Assume G be a group over U. Obviously, G is also a rough group over U.

Lemma 3.9. Assume G be a rough group over U and $G = \overline{G}$. Then G is a group.

Proof. This is easily obtained from Proposition 19 [16].

Proposition 3.10. Assume G be a rough group over U and $G = \overline{G}$. If ϕ is a fuzzy rough subgroup of G, then ϕ is a fuzzy subgroup of G.

Proof. Suppose that G be a rough group and $G = \overline{G}$. Then, from Lemma 3.9 we get G is a group. Thus $a, b \in G$, $ab \in G$, and so $\phi: G \to [0,1]$ is a fuzzy subset of G. Since ϕ is a fuzzy rough subgroup of G, then from Definition 3.3 we conclude ϕ is a fuzzy subgroup of G.

4. Conclusion

In this study, in the context of group theory a bridge has been established between fuzzy sets and rough sets. Fuzzy rough (sub) set, fuzzy rough (normal) subgroups have introduced. In addition, important and basic properties of these concepts were examined.

Conflict of Interest

The author declares no conflict of interest.

Funding

Not applicable.

References

1.Zadeh LA. Fuzzy sets. Inf Control1965; 8: 338-53. https://doi.org/10.1016/S0019-9958(65)90241-X

2.Rosenfeld A. Fuzzy groups. J Math Anal Appl. 971; 35: 512-7. https://doi.org/10.1016/0022-247X(71)90199-5

3.Das PS. Fuzzy groups and level subgroups. J Math Anal Appl. 1981; 84: 264-9. https://doi.org/10.1016/0022-247X(81)90164-5

4.Anthony JM, Sherwood H. A characterization of fuzzy subgroups. Fuzzy Sets Syst. 1982; 7: 297-305. https://doi.org/10.1016/01650114(82)90057-4

5.Pawlak Z. Rough sets. Int J Comput Inform Sci. 1982; 11: 341-56. https://doi.org/10.1007/BF01001956

6.Iwinski T. Algebraic approach to rough sets. Bull Polish Acad Sci Math. 1987; 35: 673-83.

7.Kuroki N, Wang PP. The lower and upper approximations in a fuzzy group. Inf Sci. 1996; 90: 203-20. https://doi.org/10.1016/00200255(95)00282-0

8.Cheng W, Mo Z-W, Wang J. Notes on "the lower and upper approximations in a fuzzy group" and "rough ideals in semigroups." Inf Sci. 2007; 177: 5134-40. https://doi.org/10.1016/j.ins.2006.12.006

9.Li F, Zhang Z. The homomorphisms and operations of rough groups. Sci World J. 2014; 2014: 1-6. https://doi.org/10.1155/2014/507972

10.Wang Z, Shu L. The lower and upper approximations in a group. Int J Math Comput Sci. 2012; 6: 158-62.

11.Wang C, Chen D. A short note on some properties of rough groups. Comput Math Appl. 2010; 59: 431-6. https://doi.org/10.1016/j.camwa.2009.06.024

12.Wang C, Chen D, Hu Q. On rough approximations of groups. Int J Mach Learn Cyber. 2013; 4: 445-9. https://doi.org/10.1007/s13042-0120108-6

13.Biswas R, Nanda S. Rough groups and rough subgroups. Bull Polish Acad Sci Math. 1994; 42: 251-4.

14.Miao D, Han S, Li D, Sun L. Rough Group, Rough Subgroup and Their Properties. In: Ślęzak D, Wang G, Szczuka M, Düntsch I, Yao Y, Eds., Rough Sets, Fuzzy Sets, Data Mining, and Granular Computing. vol. 3641. Berlin, Heidelberg: Springer; 2005. https://doi.org/10.1007/11548669

15.Bagirmaz N, Ozcan AF. Rough semigroups on approximation spaces. Int J Algebra. 2015; 9: 339-50. https://doi.org/10.12988/ija.2015.5742

16.Bağırmaz N, İçen İ, Özcan AF. Topological rough groups. Topol Algebra Appl. 2016; 4: 31-8.

https://doi.org/10.1515/taa-2016-0004

17.Li P-Y, Liu W-L, Mou L, Guo Z-F. On separation axioms of topological rough groups. Soft Comput. 2023; 27: 57-61. https://doi.org/10.1007/s00500-022-07521-x

18.Pei D. A generalized model of fuzzy rough sets. Int J Gen Syst. 2005; 34: 603-13. https://doi.org/10.1080/03081070500096010

19.Liu G, Zhu W. The algebraic structures of generalized rough set theory. Inf Sci. 2008; 178: 4105-13. https://doi.org/10.1016/j.ins.2008.06.021

20.Kondo M. On the structure of generalized rough sets. Information Sciences. 2006; 176: 589-600. https://doi.org/10.1016/j.ins.2005.01.001

21.Dubois D, Prade H. Rough fuzzy sets and fuzzy rough sets. Int J General Syst. 1990; 17: 191-209. https://doi.org/10.1080/03081079008935107

22.Radzikowska AM, Kerre EE. A comparative study of fuzzy rough sets. Fuzzy Sets Syst. 2002; 126: 137-55. https://doi.org/10.1016/S01650114(01)00032-X

23.Zhan J, Liu Q. Rough fuzzy (fuzzy rough) strong H-ideals of hemirings. Ital J Pure Appl Math. 2015: 483-96.

24.Pan W, Zhan J. Rough fuzzy groups and rough soft groups. Rough fuzzy (fuzzy rough) strong H-ideals of hemirings. Ital J Pure Appl Math. 2016; 36: 617-28.

Instructions for Authors

Essentials for Publishing in this Journal

1 Submitted articles should not have been previously published or be currently under consideration for publication elsewhere.

2 Conference papers may only be submitted if the paper has been completely re-written (taken to mean more than 50%) and the author has cleared any necessary permission with the copyright owner if it has been previously copyrighted.

3 All our articles are refereed through a double-blind process.

4 All authors must declare they have read and agreed to the content of the submitted article and must sign a declaration correspond to the originality of the article.

Submission Process

All articles for this journal must be submitted using our online submissions system. http://enrichedpub.com/ . Please use the Submit Your Article link in the Author Service area.

Manuscript Guidelines

The instructions to authors about the article preparation for publication in the Manuscripts are submitted online, through the e-Ur (Electronic editing) system, developed by **Enriched Publications Pvt. Ltd**. The article should contain the abstract with keywords, introduction, body, conclusion, references and the summary in English language (without heading and subheading enumeration). The article length should not exceed 16 pages of A4 paper format.

Title

The title should be informative. It is in both Journal's and author's best interest to use terms suitable. For indexing and word search. If there are no such terms in the title, the author is strongly advised to add a subtitle. The title should be given in English as well. The titles precede the abstract and the summary in an appropriate language.

Letterhead Title

The letterhead title is given at a top of each page for easier identification of article copies in an Electronic form in particular. It contains the author's surname and first name initial .article title, journal title and collation (year, volume, and issue, first and last page). The journal and article titles can be given in a shortened form.

Author's Name

Full name(s) of author(s) should be used. It is advisable to give the middle initial. Names are given in their original form.

Contact Details

The postal address or the e-mail address of the author (usually of the first one if there are more Authors) is given in the footnote at the bottom of the first page.

Type of Articles

Classification of articles is a duty of the editorial staff and is of special importance. Referees and the members of the editorial staff, or section editors, can propose a category, but the editor-in-chief has the sole responsibility for their classification. Journal articles are classified as follows:

Scientific articles:

1. Original scientific paper (giving the previously unpublished results of the author's own research based on management methods).
2. Survey paper (giving an original, detailed and critical view of a research problem or an area to which the author has made a contribution visible through his self-citation);
3. Short or preliminary communication (original management paper of full format but of a smaller extent or of a preliminary character);
4. Scientific critique or forum (discussion on a particular scientific topic, based exclusively on management argumentation) and commentaries. Exceptionally, in particular areas, a scientific paper in the Journal can be in a form of a monograph or a critical edition of scientific data (historical, archival, lexicographic, bibliographic, data survey, etc.) which were unknown or hardly accessible for scientific research.

Professional articles:

1. Professional paper (contribution offering experience useful for improvement of professional practice but not necessarily based on scientific methods);
2. Informative contribution (editorial, commentary, etc.);
3. Review (of a book, software, case study, scientific event, etc.)

Language

The article should be in English. The grammar and style of the article should be of good quality. The systematized text should be without abbreviations (except standard ones). All measurements must be in SI units. The sequence of formulae is denoted in Arabic numerals in parentheses on the right-hand side.

Abstract and Summary

An abstract is a concise informative presentation of the article content for fast and accurate Evaluation of its relevance. It is both in the Editorial Office's and the author's best interest for an abstract to contain terms often used for indexing and article search. The abstract describes the purpose of the study and the methods, outlines the findings and state the conclusions. A 100- to 250-Word abstract should be placed between the title and the keywords with the body text to follow. Besides an abstract are advised to have a summary in English, at the end of the article, after the Reference list. The summary should be structured and long up to 1/10 of the article length (it is more extensive than the abstract).

Keywords

Keywords are terms or phrases showing adequately the article content for indexing and search purposes. They should be allocated heaving in mind widely accepted international sources (index, dictionary or thesaurus), such as the Web of Science keyword list for science in general. The higher their usage frequency is the better. Up to 10 keywords immediately follow the abstract and the summary, in respective languages.

Acknowledgements

The name and the number of the project or programmed within which the article was realized is given in a separate note at the bottom of the first page together with the name of the institution which financially supported the project or programmed.

Tables and Illustrations

All the captions should be in the original language as well as in English, together with the texts in illustrations if possible. Tables are typed in the same style as the text and are denoted by numerals at the top. Photographs and drawings, placed appropriately in the text, should be clear, precise and suitable for reproduction. Drawings should be created in Word or Corel.

Citation in the Text

Citation in the text must be uniform. When citing references in the text, use the reference number set in square brackets from the Reference list at the end of the article.

Footnotes

Footnotes are given at the bottom of the page with the text they refer to. They can contain less relevant details, additional explanations or used sources (e.g. scientific material, manuals). They cannot replace the cited literature.
The article should be accompanied with a cover letter with the information about the author(s): surname, middle initial, first name, and citizen personal number, rank, title, e-mail address, and affiliation address, home address including municipality, phone number in the office and at home (or a mobile phone number). The cover letter should state the type of the article and tell which illustrations are original and which are not.

Note